

https://dspace.org/

Characterization of LYTM domain containing proteins in mycobacterium smegmatis

Shaku, Tube Moagi

2017

http://hdl.handle.net/10539/23164

Downloaded from a DSpace repository. https://dspace.org/

Characterization of LytM domain containing proteins in *Mycobacterium smegmatis*

Tube Moagi Shaku (1099419)

A dissertation submitted to the Faculty of Health Science, University of the Witwatersrand, Johannesburg, in fulfillment of the requirements for the degree of Master of Science in Medicine.

2017

Declaration

I, Tube Moagi Shaku, declare that this Dissertation is my own, unaided work. It is being submitted for the Degree of Master of Science in Medicine in the University of the Witwatersrand, Johannesburg. It has not been submitted before for any degree or examination at this or any other University.

_____ _____

(Tube Moagi Shaku) Date

Dedication

I dedicate this work to my family and friends.

Presentations from this study

Conference	Molecular Biosciences Research Thrust Research Day
Presentation	Poster presentation
Year	2015

Conference	Wits Research Day and Postgraduate Expo
Presentation	Oral presentation
Year	2016

Conference	Molecular Biosciences Research Thrust Research Day
Presentation	Poster presentation
Year	2016

Abstract

Mycobacterium tuberculosis assembles a complex cell wall consisting of mycolic acids, arabinogalactan and peptidoglycan layers. The peptidoglycan is important for structural maintenance and osmotic protection of the cell. Beta-lactam antibiotics, such as penicillin, perturb biogenesis of cross-linked peptidoglycan by inhibition of penicillin-binding proteins and cause cell death. As a result, penicillin-binding proteins have been extensively used in antimicrobial development. However, penicillin insensitive enzymes involved in peptidoglycan biogenesis such as amidases, transglycosylases and endopeptidases remain to be exploited for anti-TB drug development, a field that urgently requires new drugs in light of the rapid emergence of drug resistant strains. In this study, we functionally characterize a novel class of LytM domain containing peptidoglycan endopeptidases (also known as M23 peptidases) in mycobacteria. Bio-informatics tools were used to identify LytM domain-containing homologues in *Mycobacterium smegmatis,* designated MepB1-MepB4. These were deleted using standard allelic exchange mutagenesis and recombination techniques and the resulting mutants were assessed for cell wall related defects. We found that mycobacterial LytM endopeptidases have important roles in bacterial growth as demonstrated by delayed cell growth kinetics in a Δ*mepB1* deletion mutant. We noted no growth defects in Δ*mepB2* and Δ*mepB3* single deletion mutants but observed defective cell division in a Δ*mepB2* Δ*mepB3* double deletion mutant. In this double mutant, spatial localization of new cell wall biosynthesis revealed the inability to degrade the septal bridge joining two daughter cells, pointing to a critical role for these enzymes in cell separation. MepB1 is sequestered from the peptidoglycan by cytosolic localization and its absence causes a septal and polar buldging phenotype. To further investigate the biological roles of these putative peptidoglycan endopeptidases, protein interaction studies were conducted using the bacterial two-hybrid mycobacterial protein fragment complementation assay. This analysis identified FtsX, a key cell division protein, as an interacting partner for both MepB2 and MepB3, thus identifying these proteins as novel components of the mycobacterial divisome. Collectively, these observations provide the first insight into a new group of potential drug targets for tuberculosis disease and notably enhance the overall understanding of peptidoglycan turnover, which is of general revelevance in bacterial pathogens.

Acknowledgements

I thank my supervisor Prof. Bavesh Kana and my co-supervisor Dr Melissa Chengalroyen for thoughtful discussions about this project and for the technical expertise I learned from them.

To my financial sponsors (the National Research Foundation [NRF], University of the Witwatersrand and the Belgium Technical Cooperation [BTC]), I would like to say thank you for the support

I would also like to thank the Centre for Imaging and Analysis at the University of Cape Town for allowing me to use their Scanning and Transmission electron microscopes.

To my friends, collegues and the management team of the CBTBR, I would like to express my greatest gratitude.

Contents

Declaration i

Dedication ii

Presentations from this study iii

Abstract iv

Acknowledgements v

List of figures: xii

List of tables: xv

Nomenclature: xvi

1. Introduction 1

1.1. Tuberculosis 1

1.2. TB infection, transmission and treatment 2

1.3. The mycobacterial cell wall 3

1.4. Drug resistance, dormancy and drug tolerance 4

1.4.1. Genetic drug resistance 4

1.4.2. Dormancy 5

1.4.3. Drug tolerance 5

1.5. Mycobacterial PG biosynthesis 6

1.6. Cytoplasmic biosynthesis and translocation of lipid II 6

1.6.1. Periplasmic incorporation of lipid II into the cross-linked PG 8

1.7. Mycobacterial cell division 10

1.8. Targeting mycobacterial PG biosynthesis 12

1.9. Mycobacterial PG remodelling 12

1.10. Glycosidases 13

1.11. Peptidases 13

1.12. LytM domain containing peptidases (M23 peptidases) 14

1.13. Structure, substrate specificity and catalytic activity of M23 metallopeptidases 14
1.13.1. Structural diversity in M23 peptidases 17
1.14. Functional diversity of M23 peptidases 18
1.14.1. The role of M23 peptidases in cell division as regulatory factors 18
1.14.2. M23 peptidases in cell growth 20
1.14.3. M23 peptidases in bacterial virulence and pathogenesis 21
1.14.4. M23 peptidases in cell shape determination 22
1.14.5. M23 peptidases in sporulation 23
1.15. Hypothesis 26
1.16. Aims and objectives of this study 26
1.16.1. Aims 26
1.16.2. Specific objectives 26
2. Materials and methods 27
2.1. Bio-informatics and software used 27
2.1.1. Databases used to obtain genomic DNA and protein sequences of interest 27
2.1.2. NCBI BLAST 28
2.1.3. pFam database 28
2.1.4. SignalP 4.1 Server 28
2.1.5. Clustal Omega 29
2.1.6. iTOL version 3 29
2.1.7. I-TASSER 29
2.1.8. PyMOL 29
2.1.9. Fiji 29
2.1.10. STRING 29
2.1.11. GraphPad prism 6 30
2.1.12. FATCAT 30
2.2. Bacterial strains and plasmids created and/or used 30

2.3. Bacterial growth conditions 35
2.3.1. Growth conditions for *E. coli* DH5α and derivative strains 35
2.3.2. Growth conditions for *M. smegmatis* mc^2155 and derivative strains 35
2.4. DNA extractions 36
2.4.1. *M. smegmatis* mc^2155 chromosomal DNA extractions 36
2.4.1.1. Small scale chromosomal DNA extraction 36
2.4.1.2. Large scale chromosomal DNA extraction 36
2.4.2. Plasmid DNA extraction from *E. coli* DH5α 37
2.4.2.1. Small scale plasmid DNA extraction from *E. coli* DH5α 37
2.4.2.2. Large scale plasmid DNA extraction from *E. coli* DH5α 37
2.5. DNA manipulations 38
2.5.1. DNA amplification 38
2.5.1.1. Designing PCR primers 38
2.5.1.2. Polymerase Chain Reaction (PCR) 39
2.5.1.2.1. Phusion High-Fidelity DNA polymerase reaction 39
2.5.1.2.2. Roche FastStart Taq DNA polymerase reaction 39
2.5.2. DNA purification by sodium acetate precipitation 40
2.5.3. Restriction digestions 40
2.5.4. Agarose gel electrophoresis 40
2.5.5. DNA fragment purification 41
2.5.6. Dephosphorylation and phosphorylation of DNA 41
2.5.7. DNA ligation 41
2.5.8. DNA sequencing 42
2.5.9. Southern blotting 42
2.5.9.1. Synthesis of the DNA probe 42
2.5.9.2. Electro-blotting 43
2.5.9.3. Hybridization 43

2.5.9.4. Immunological detection 44
2.6. Bacterial transformations 44
2.6.1. Preparation of chemically competent *E. coli* DH5α cells 44
2.6.2. Transformation of chemically competent *E. coli* DH5α cells 45
2.6.3. Preparation of electro-competent mc^2155 or derivative strains 45
2.6.4. Electroporation of plasmids into *M. smegmatis* 45
2.6.5. Generation of *M. smegmatis* mutant strains 46
2.6.5.1. Two-step allelic exchange homologous recombination method for generation of *M. smegmatis* mutant strains 46
2.6.5.2. Generation of *M. smegmatis* mc^2155 mutant strains by the mycobacterial recombineering method 48
2.6.6. Generation of complemented *M. smegmatis* strains 50
2.7. Localization of proteins of interest 50
2.8. Analysis of protein-protein interacting partners 51
2.9. Phenotypic analysis of *M. smegmatis* mc^2155 mutant strains 52
2.9.1. Growth rate analysis 52
2.9.2. Antibiotics and lysozyme MIC determination 52
2.9.3. Fluorescence microscopy 53
2.9.3.1. Fluorescent BODIPY Vancomycin staining 53
2.9.3.2. Click chemistry D-alanine analogue staining 53
2.9.3.3. DMN-Trehalose staining 54
2.9.3.4. Membrane and DNA staining with the FM4/64 and the DAPI stains, respectively 55
2.9.4. Scanning electron microscopy (SEM) 55
2.10. Morphological analysis of the mutant strains through flow cytometry 56
2.11. Time-lapse microscopy 56
3. Results 57
3.1. Identification of mycobacterial LytM domain containing proteins (M23 peptidases) and bio-informatic analysis 57

3.2. Generation of *M. smegmatis* mutant strains lacking the genes *mepB1*, *mepB2* and *mepB3*, individually and in combination 62

3.2.1. Construction of plasmids used for deletion of the *mepB1*, *mepB2* and *mepB3* genes 62

3.2.1.1. Construction of the *mepB1* gene deletion plasmid 62

3.2.1.2. Construction of the *mepB2* gene deletion plasmid 64

3.2.1.3. Construction of the *mepB3* gene deletion plasmid 67

3.2.2. Generation of the Δ*mepB1*, Δ*mepB*2 and Δ*mepB*3 deletion mutants 67

3.2.2.1. Generation of the Δ*mepB1* deletion mutant 67

3.2.3. Generation of the Δ*mepB1*, Δ*mepB*2 and Δ*mepB*3 deletion mutants 69

3.2.3.1. Generation of the Δ*mepB1* deletion mutant 69

3.2.3.2. Generation of the Δ*mepB2* deletion mutant 70

3.2.3.3. Generation of the Δ*mepB*3 deletion mutant 72

3.2.3.4. Generation of a Δ*mepB2* Δ*mepB*3 double deletion mutant 74

3.2.4. Genetic complementation of the Δ*mepB2* and Δ*mepB3* deletion mutants 76

3.2.4.1. Construction of the *mepB2* complementation plasmid 76

3.2.4.2. Construction of the *mepB3* complementation plasmid 78

3.2.5. Complementation of the Δ*mepB2* mutant 78

3.2.6. Complementation of the Δ*mepB3* mutant 78

3.3. The role of MepB1, MepB2 and MepB3 in cell growth 80

3.4. Flow cytometry analysis of the Δ*mepB2*, Δ*mepB3* mutants and the Δ*mepB2* Δ*mepB3* double mutant. 80

3.5. Microscopic analysis of the Δ*mepB1*, Δ*mepB2*, Δ*mepB*3 and the Δ*mepB2* Δ*mepB3* strains. 83

3.6. Localization of DivIVA-GFP and FtsZ-GFP in Δ*mepB2* Δ*mepB3* mutant 87

3.7. Time-lapse microscopic analysis of the Δ*mepB2* Δ*mepB3* mutant. 89

3.8. Time-lapse microscopic analysis of the localization of DivIVA-GFP in the Δ*mepB2* Δ*mepB3* mutant 90

3.9. The Δ*mepB2* Δ*mepB3* mutant is hypersensitive to lysozyme 91
3.10. MepB2 and MepB3 are components of the mycobacterial divisome 92
3.11. Construction of the M-PFC plasmids for analysis of FtsX - MepB interactions 93
3.12. M-PFC assay for analysis of FtsX, MepB2 and MepB3 interactions 96
4. Discussion 102
4.1. Limitations 108
4.2. Future studies 108
4.3. Concluding remarks 109
5. Appendices 110
6. References 117

List of figures:

Figure 1.1: Estimated new TB incidence rates

Figure 1.2: Schematic representation of the basic components of the mycobacterial cell wall

Figure 1.3: Schematic representation of the peptidoglycan biosynthesis pathway

Figure 1.4: Schematic representation of the cleavage sites of peptidoglycan hydrolases and the different PG cross-linkages

Figure 1.5: Schematic representation of mycobacterial polar growth and cell division

Figure 1.6: Phylogenetic tree of mycobacterial peptidoglycan remodelling enzymes

Figure 1.7: M23 peptidase structure

Figure 1.8: Comparison of the different M23 domain active sites

Figure 1.9: Proposed hydrolysis reaction of the 4,3 peptidoglycan cross-link by catalytically active M23 proteins

Figure 1.10: Surface view of autoinhibited cell separation amidases

Figure 2.1: Schematic representation of the two step, allelic exchange homologous recombination

Figure 2.2: Flow diagram depiction of the process of generating a gene deletion mutant by the two step, allelic exchange homologous recombination method

Figure 2.3: Schematic representation of the the mycobacterial recombineering method

Figure 2.4: Schematic diagram illustrating the M-PFC assay principle

Figure 2.5: Schematic diagram illustrating the DMN-Trehalose staining process

Figure 3.1: Phylogenetic analysis of M23 peptidases

Figure 3.2: Predicted tertiary structures and schematic representation of the domain organization of MepB1, MepB2 and MepB3

Figure 3.3: Alignment of the M23 domain from different M23 peptidases

Figure 3.4: Flow diagram for the study of mycobacterial M23 proteins

Figure 3.5: Schematic diagram illustrating the construction of the *mepB1* gene deletion plasmid

Figure 3.6: Restriction profile of pGEM+5526::*hyg*

Figure 3.7: Schematic diagram illustrating the construction of the *mepB2* deletion plasmid

Figure 3.8: Restriction profile of p0247KO+*aadA*

Figure 3.9: Schematic diagram illustrating the construction of the *mepB3* deletion plasmid

Figure 3.10: Restriction profile of p1192KO

Figure 3.11: Deletion of the *mepB1* gene

Figure 3.12: Deletion of the *mepB2* gene

Figure 3.13: Southern blot analysis of the Δ*mepB2* mutant

Figure 3.14: Deletion of the *mepB3* gene

Figure 3.15: Southern blot analysis of the Δ*mepB3* mutant

Figure 3.16: MepB2 and MepB3 show structural similarity

Figure 3.17: Construction and restriction profiling of pMV306H+0247

Figure 3.18: Construction and restriction profiling of pTweety+1192

Figure 3.19: Loss of MepB1 causes delayed growth kinetics

Figure 3.20: Flow cytometry analysis of the morphology of Δ*mepB2* and Δ*mepB3* in comparison to mc^2155 and the complemented strains

Figure 3.21: Loss of MepB2 and MepB3 collectively affects cell morphology

Figure 3.22: Loss of MepB1 causes cell septum and cell pole buldging

Figure 3.23: Microscopic analysis of the DMN-trehalose stained Δ*mepB2* Δ*mepB3* mutant

Figure 3.24: DNA staining of the Δ*mepB2* Δ*mepB3* mutant reveals multiple DNA foci

Figure 3.25: The Δ*mepB2* Δ*mepB3* mutant forms chains of cells

Figure 3.26: MepB2 and MepB3 are required for cleavage of septal PG to allow cell division

Figure 3.27: *In vivo* localization of DivIVA-GFP and FtsZ-GFP in the Δ*mepB2* Δ*mepB3* mutant

Figure 3.28: Time-lapse microscopic analysis of the Δ*mepB2* Δ*mepB3* strain

Figure 3.29: Time-lapse microscopic analysis the Δ*mepB2* Δ*mepB3* DivIVA-GFP strain

Figure 3.30: The Δ*mepB2* Δ*mepB3* mutant is hypersensitive to lysozyme

Figure 3.31: Schematic diagram illustrating the activation of cell separation amidases by the FtsEX complex in *E. coli*

Figure 3.32: Construction and restriction profiling of pUAB400+0247

Figure 3.33: Construction and restriction profiling of pUAB400+1192

Figure 3.34: Construction and restriction profiling of pUAB300+FtsX

Figure 3.35: Schematic diagram illustrating the M-PFC assay for FtsX-MepB2/B3 interactions

Figure 3.36: FtsX interacts with MepB2

Figure 3.37: FtsX interacts with MepB3

Figure 3.38: Schematic diagram illustrating the role of mycobacterial MepB proteins in mycobacterial cell division

Figure 4.1: MepB2 and MepB3 are identified as new components of the mycobacterial divisome

List of tables:

Table 1: Databases used to obtain genomic DNA and protein sequences

Table 2: Plasmids created and/or used in this study

Table 2.1: Bacterial strains created and/or used in this study

Table 3: Parameters used for designing primers through Primer3

Table 4: Primers used for screening for the Δ*mepB2*::*aadA* strain

Table 5: Primers used for PCR synthesis of the Δ*mepB3* allele

Table 6: Primers used for screening for the Δ*mepB3* strain

Table 7: Primers used for PCR synthesis of the *mepB2* and *mepB3* alleles for gene complementation studies

Table 8: Primers used for PCR synthesis of the *mepB2*, *mepB3* and *ftsX* alleles for protein interaction studies

Nomenclature:

AMIK:	Amikacin
Amp:	Ampicillin
ATP:	Adenosine triphosphate
BCG:	Bacille Calmette Guerin
BLAST:	Basic Local Alignment Search Tool
CAP:	Capreomycin
CTAB:	Cetyltrimethylammonium bromide
D-ala:	D-alanine
D-gln:	D-glutamine
DMSO:	Dimethyl sulfoxide
DNA:	Deoxyribonucleotide
DOT:	Directly Observed Therapy
EMB:	Ethambutol
ETH:	Ethionamide
FATCAT:	Flexible structure AlignmenT by Chaining Aligned fragment pairs allowing Twists
GFP:	Green Fluorescent Protein
Glc*N*Ac:	*N*-acteyl glucosamine
HIV:	Human Immunodeficiency Virus
Hyg:	Hygromycin
I-TASSER:	Iterative Threading ASSEmbly Refinement
INH:	Isoniazid
iTOL:	interactive Tree Of Life
Kan:	Kanamycin
L-ala:	L-alanine
LA:	Luria-Bertani Agar
LB:	Lysogeny Broth
LTBI:	Latent TB Infection
mDHFR:	murine dehydrofolate reductase
MDR-TB:	Multi Drug Resistant TB
meso-DAP:	*meso*-Diaminopimelate
MIC:	Minimum Inhibitory Concentration

M-PFC:	Mycobacterial Protein Fragment Complementation
Mtb:	*Mycobacterium tuberculosis*
Mur*N*Ac:	*N*-acetyl muramic acid
NCBI:	National Center for Biotechnology Information
NEB:	New England Biolabs
NTHI:	Nontypeable *Haemophilus influenzae*
OD:	Optical Density
PCR:	Polymerase Chain Reaction
PDB:	Protein Data Bank
PPD:	Purified Protein Derivative
PG:	Peptidoglycan
PZA:	Pyrazinamide
RIF:	Rifampicin
SCO:	Single Cross Over
SEM:	Scanning Electron Microscope
Str:	Streptomycin
TB:	Tuberculosis
Trim:	Trimethoprim
UDP:	Uridine diphosphate
WHO:	World Health Organization
XDR-TB:	Extensively Drug Resistant TB

1. Introduction

1.1. Tuberculosis

In 1882, Robert Koch discovered that *Mycobacterium tuberculosis* (*Mtb*) is the causative agent of tuberculosis (TB), a communicable disease that remains a major public health burden worldwide and the leading cause of death from an infectious disease (WHO, 2015). The World Health Organization (WHO) estimates that nearly 2 billion people carry latent TB infection (LTBI) (defined as subclinical TB infection characterized by a delayed-type hypersensitivity reaction as a result of subcutaneous challenge with purified protein derivative [PPD]) (WHO, 2015, Boshoff and Barry, 2005). In 2014 alone nearly 10 million new TB infections were reported, with 1.5 million people dying from TB (WHO, 2015). Geographically, the sub-Saharan African countries have the highest TB incidence rates (Figure 1.1) (WHO, 2015). When ranked by the WHO estimated burden of multidrug-resistant TB (MDR-TB), South Africa is amongst the 10 highest drug-resistant TB–burdened countries in the world, placed fourth behind China, India and Russia (WHO, 2015). Although TB is a curable disease, the administration of the Directly Observed Therapy (DOT) programme is severely compromised, particularly in the high burden countries plagued by co-infection with TB-HIV, the emergence of MDR TB, poor socio-economic conditions, poor patient-compliance to treatment and a high proportion of undiagnosed infection (Pai et al., 2016). Moreover, the only approved vaccine; Bacillus Calmette-Guérin (BCG), does not protect against adult pulmonary TB infection (Sulis et al., 2014, Raviglione, 2008, McShane, 2011). In 2014, 1.2 million new TB cases in HIV-infected people were reported, with 390 000 people dying from HIV-TB comorbidities and nearly half a million new cases of MDR-TB reported, with approximately 190 000 deaths attributed to MDR-TB (WHO, 2015). These facts underscore an urgent need for a global effort to reinforce TB prevention and control measures and accelerate the development of a universally protective anti-TB vaccine. Moreover, the identification and validation of novel drug targets for the development of cost-effective anti-TB drugs remains a pivotal incentive (Lienhardt et al., 2012, Raviglione et al., 2012). The repurposing of existing antibiotics, which retain potency against MDR *Mtb* strains, are active against LTBI and allow for a shortened treatment course to reduce the transmission of the disease is also one of the major objectives of TB research (Zumla et al., 2013a, Hoagland et al., 2016, Maitra et al., 2016).

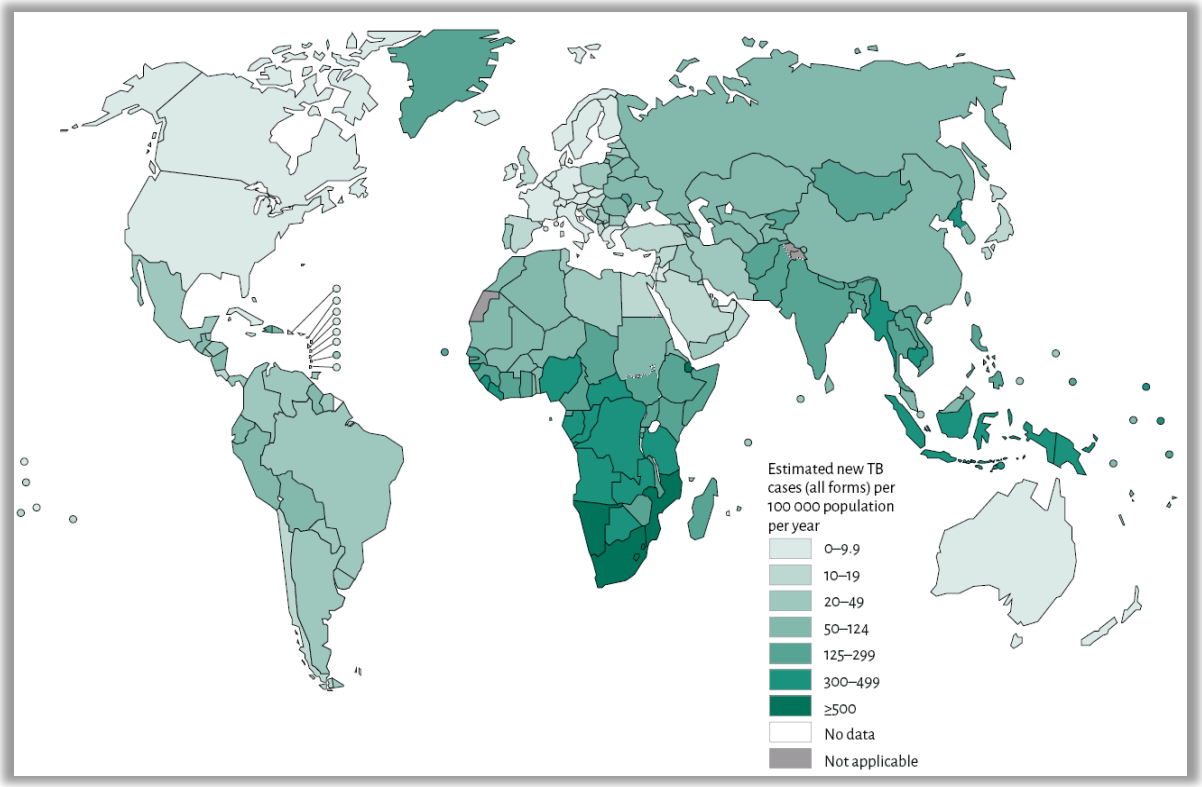


Figure 1.1: **Estimated new TB incidence rates, 2014**: the sub-Saharan African region has the most severe TB burden relative to population (WHO, 2015).

1.2. TB infection, transmission and treatment

TB is an airborne disease and ambulatory individuals with active pulmonary infection serve as the most common source of transmission (Zumla et al., 2013c). Exposed humans contract TB by inhalation of aerosol droplets carrying *Mtb* bacilli expectorated from an individual carrying active disease. The first host-pathogen encounter is mediated by alveolar macrophages through interaction of *Mtb* with specific phagocytic receptors located on the surface of the macrophages (Fortune and Rubin, 2007). These alveolar macrophages engulf the bacilli and produce proinflammatory cytokines and chemokines that recruit more immune cells to the site of infection inducing the formation of a granuloma. The granulomas consist of a compact aggregate of immune cells with a centre consisting of *Mtb* infected macrophages, surrounded by epithelioid cells, multinucleated giant cells and a ring of lymphocytes at the periphery. The granuloma represents a critical immunological feature that is required for control of disease (Ramakrishnan, 2012, Marakalala et al., 2016). LTBI is induced if the granuloma fails to eliminate the infection but rather contains it and prevents tissue damage. Failure of the granuloma to contain disease leads to progression to active pulmonary TB disease. This clinical state presents as a continuous spectrum of events extending from sterilizing immunity, persisting infection, to fulminant active disease,

characterized by the following symptoms: a persistent cough, haemoptysis (coughing up of blood), weight loss, fatigue and fever (Barry et al., 2009). Individuals with active pulmonary TB disease, who are not taking TB treatment, can transmit the disease to others (Dartois, 2014).

Drug sensitive, active TB disease is treated by a daily dose of combination chemotherapy including the first-line drugs: Rifampicin (RIF), Isoniazid (INH), Pyrazinamide (PZA) and Ethambutol (EMB). Briefly, this regimen encompasses treatment with all four drugs for two months (the intensive treatment phase) followed by four months of treatment with RIF and INH (the continuation treatment phase) (Pai et al., 2016). Globally, 3.3% of new TB cases and 20% of previously treated cases have MDR-TB (defined as resistance to RIF and INH). A further 9.7% of these MDR-TB cases have been reported as extensively drug-resistant TB (XDR-TB, defined as resistance to INH, RIF and additional resistance to a fluoroquinolone antibiotic and one of the three injectable second line drugs: Amikacin [AMIK], Kanamycin [KAN] or Capreomycin [CAP]). Treatment of drug resistant TB is expensive and requires prolonged treatment with less effective, toxic drugs (Koul et al., 2011). This highlights an urgent need for the development of shorter treatment regimens. For drug susceptible TB, the long course of treatment is due to the emergence of persister/drug tolerant cells that are less susceptible to antibiotics during treatment (Wakamoto et al., 2013, Aldridge et al., 2014). Therefore, in addition to genetically-based mechanisms of drug resistance, persistence or the induction of epigenetic drug resistance mechanisms causing transient tolerance of antibiotics represents a major complicating factor to TB treatment (Sacchettini et al., 2008). In addition, the mycobacterial cell wall is inherently impermeable to a number of compounds, a characteristic that also partially accounts for the prolonged TB chemotherapy (Hett et al., 2008).

1.3. **The mycobacterial cell wall**

Mycobacteria assemble a complex cell wall that is highly protective against hostile environmental states such as acidic, oxidative and hypoxic conditions (Hett and Rubin, 2008). The mycobacterial cell wall consists of a cytoplasmic membrane, peptidoglycan (PG), arabinogalactan, mycolic acids and an outer capsule-like layer (Figure 1.2) (Hett and Rubin, 2008). Inhibition of the process of cell wall assembly has remained a pivotal component of TB chemotherapy (Favrot and Ronning, 2012). In this context, INH inhibits mycolic acid synthesis and EMB inhibits arabinogalactan and lipoarabinomannan synthesis.

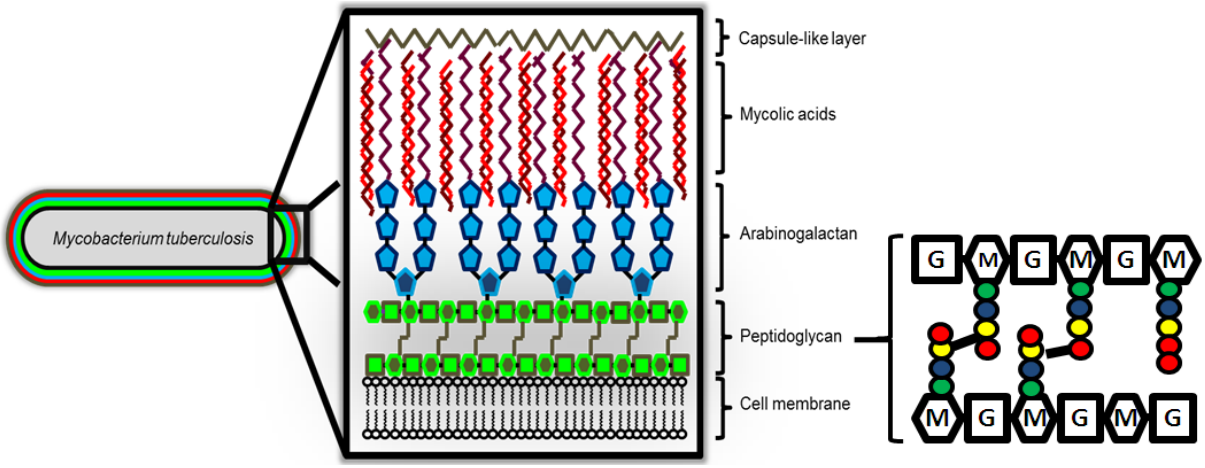


Figure 1.2: **Schematic representation of the basic components of the mycobacterial cell wall**. Shown are the different layers of the cell wall. The innermost layer is the phospholipid bilayer or cell membrane which is fortified by the PG (green), AG (blue), MA (Red) complex. The outer most layer is the mycobacterial capsule (grey) made of glucose polymers as the main constituent. The constituents of the PG layer are indicated. G: *N*-acteyl glucosamine, M: *N*-acetyl muramic acid. Green circle: L-alanine, blue circle: D-glutamine, yellow circle: *meso*-Diaminopimalate and red circle: D-alanine.

Cell wall targeting antibiotics also play an important role in treatment of drug resistant *Mtb* strains and for the elimination of subpopulations of *Mtb* that are tolerant to anti-TB chemotherapy (Sacchettini et al., 2008). During the continuation phase of drug susceptible TB treatment, INH therapy eliminates persistent bacilli in a process recognized as the "sterilization" phase of treatment (Zhang et al., 1992). Ethionamide (ETH), a structural thioamide analogue of INH, which also targets the synthesis of mycolic acids and D-cycloserine, which targets PG biosynthesis, have both proven to be effective for the treatment of drug resistant TB (Wivagg et al., 2014). Consequently, understanding the biosynthesis of cell wall core-components represents an important area of interest for TB research.

1.4. Drug resistance, dormancy and drug tolerance

1.4.1. Genetic drug resistance

The emergence of drug resistant strains of *Mtb* is largely due to genetically encoded alterations in the drug target or changes in the drug activation pathway resulting in a significant reduction in the activity of the drug. Inadequate TB therapy, or inconsistency with compliance to treatment, is considered to be the major factor fuelling the development of chromosomally-encoded drug resistance (Koul et al., 2011). Resistance to INH is associated with mutations in the *katG* and *inhA* genes encoding catalase peroxidase (a bifunctional hemoprotein that has been shown to activate INH) and NADH-dependent enoyl-ACP

reductase InhA (an enzyme that provides precursors of mycolic acids), respectively (Zumla et al., 2013b). As INH and ETH both target InhA, cross-resistance to these antibiotics due to mutations in the *inhA* gene is usually observed (Brossier et al., 2011). ETH is activated by the NADPH-specific FAD-containing mono-oxygenase, EthA, encoded by the *ethA* gene (Brossier et al., 2011). Consequently, mutations in the genes *ethA* or *ethR* (encoding the EthA regulator) cause resistance to ETH (Brossier et al., 2011). PZA resistance is determined by mutations in the *pncA* gene encoding nicotinamidase or pyrazinamidase (an enzyme required for activation of PZA to its active form, pyrazinoic acid). Resistance to EMB is associated with mutations in the *embB* gene, encoding an arabinosyl transferase (an enzyme required for arabinogalactan synthesis) (Wade and Zhang, 2004). RIF resistance is determined by mutations in the beta-subunit of the RNA polymerase (Zumla et al., 2013b). Drug resistance has continually represented a growing threat to the global efforts for TB control and for the development of novel anti-TB drugs. As a result, combination TB regimens, rather than treatment with a single drug, are recommended to prevent further emergence of drug-resistant *Mtb* strains (Pai et al., 2016).

1.4.2. **Dormancy**

During TB infection the mycobacterial cell wall provides a substantial degree of resistance to antimicrobial stresses posed by the immune system. *Mtb* is also equipped to adapt to environmental changes such as hypoxia, nitrogen and nutrient limitation by transitioning to a state of dormancy (defined as a reversible state of metabolic shiftdown in which bacteria persist without cell division) (Kana and Mizrahi, 2010). As mycobacteria do not form spores, transition to this state of dormancy is achieved by a transcriptional response that enables the bacteria to remain viable but not culturable (Kana and Mizrahi, 2010). Dormant bacteria require an exogenous supply of resuscitation promoting factors (Rpfs) to resume growth (Kana et al., 2008). Although the link between resuscitation of dormant bacteria and progression to active disease in individuals that habour LTBI has not been demonstrated, dormant bacteria may represent a subpopulation of bacteria that resist immunological stresses and anti-TB drugs.

1.4.3. **Drug tolerance**

Population-level measures of drug susceptibility have indicated that within a population of genetically identical bacteria, there are subpopulations of cells that vary significantly in their drug susceptibility (Aldridge et al., 2014). These subpopulations can tolerate lethal drug

concentrations (Wakamoto et al., 2013). Mechanisms governing phenotypic drug tolerance range from growth arrest (discussed above as dormancy), induction of drug efflux pumps and biofilm formation. Single-cell studies in mycobacteria identified the presence of population heterogeneity, reflected by differential drug tolerance during mycobacterial growth in the presence of antibiotics (Uhia et al., 2015). Mycobacteria also remodel their cell wall in response to changes in the environment and this was correlated with the ability of *Mtb* to tolerate anti-TB drugs (Larrouy-Maumus et al., 2016). Alongside reversible adaptations in growth rate and drug resistance through chromosomal mutations, cell wall remodelling is another aspect through which mycobacteria dynamically adapt to alterations in environmental conditions.

1.5. **Mycobacterial PG biosynthesis**

The PG serves as a scaffold for attachment of the outer layers of the mycobacterial cell wall and thus it fortifies the cell, enabling it to endure osmotic pressure and environmental stresses (Hett and Rubin, 2008). Hence, the PG is identified as a key structural component for viability in virtually all bacteria and consequently, the enzymes required for PG biosynthesis are highly conserved among mycobacterial species (Kieser and Rubin, 2014). The PG is a polymer constructed from glycan strands connected by cross-links between attached peptide chains, ultimately forming a meshwork surrounding the cell. The glycan strands consist of alternating *N*-acetylglucosamine (Glc*N*Ac) and *N*-acetylmuramic acid (Mur*N*Ac) residues, linked by β(1→4) glycosidic bonds (Jankute et al., 2015). In nascent PG, the peptide chain is most often in the following conformation: L-ala-D-gln-*meso*-DAP-D-ala-D-ala. PG synthesis begins with a cytoplasmic series of steps, including the nonribosomal biosynthesis of the PG precursor molecule lipid II, followed by translocation of lipid II to the periplasm and incorporation of this molecule into the existing PG structure (Jankute et al., 2015). These processes are discussed below in further detail.

1.6. **Cytoplasmic biosynthesis and translocation of lipid II**

The first committed step for lipid II biosynthesis is the formation of UDP-Mur*N*Ac from UDP-Glc*N*Ac, catalyzed by the ATP-dependent enzymes MurA and MurB (Figure 1.3) (Jankute et al., 2015). UDP-Glc*N*Ac is a product of the enzymes GlmM and GlmU (Jankute et al., 2015). Thereafter, the Mur family of amino acid ligases are required for the sequential addition of amino acids to UDP-Mur*N*Ac to form lipid I. The addition of the first amino acid.

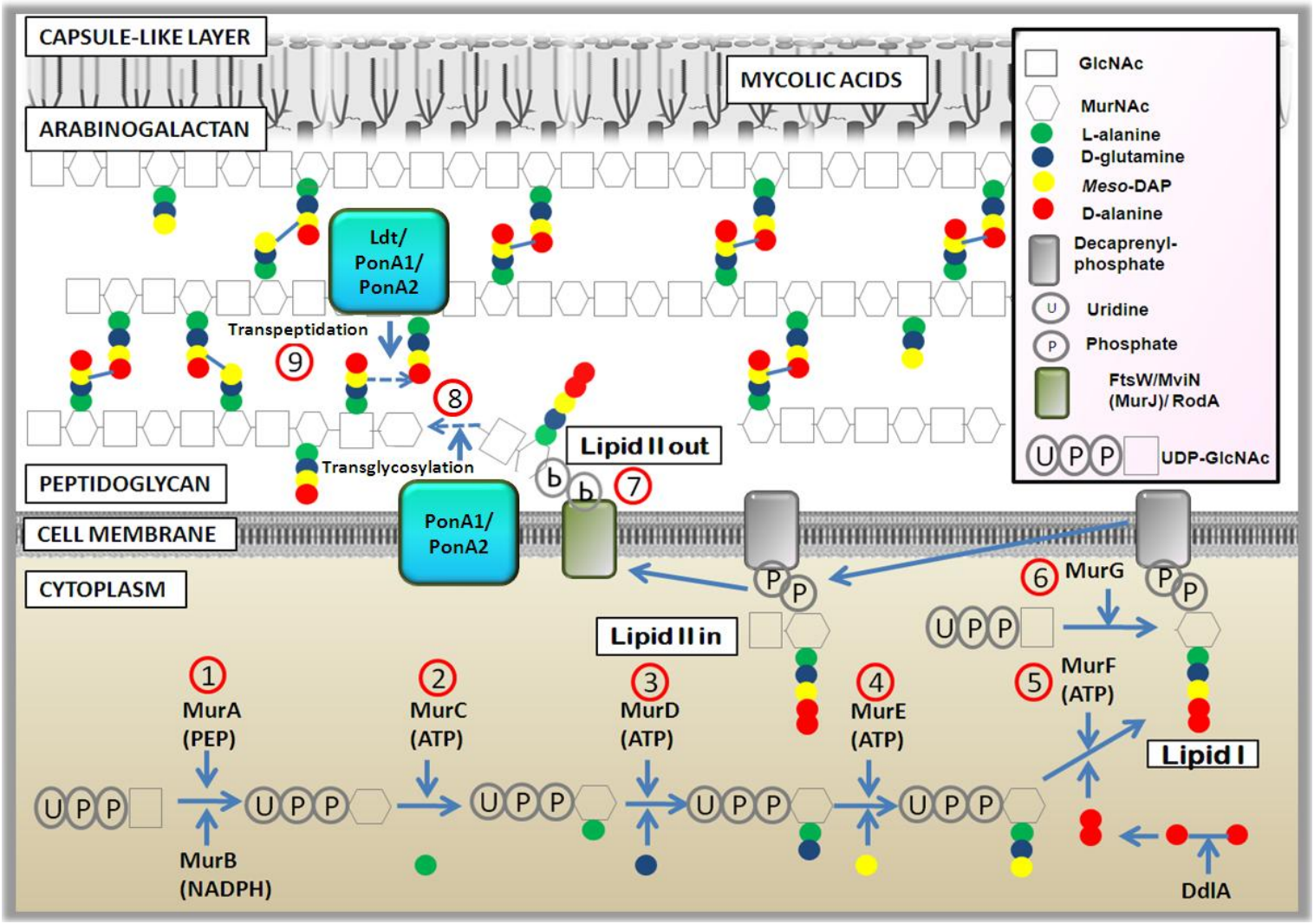


Figure 1.3: **Schematic representation of the peptidoglycan biosynthesis pathway**. (1) Synthesis of UDP-Mur*N*Ac by MurA and MurB. (2) Addition of D-alanine to UDP-Mur*N*Ac by MurC to form UDP-Mur*N*Ac-L-ala. (3) Addition of D-glutamine to UDP-Mur*N*Ac-L-ala by MurD to form UDP-Mur*N*Ac-L-ala-D-glu. (4) Addition of *meso*-Diaminopimelate to UDP-Mur*N*Ac-L-ala-D-glu by MurE to form UDP-Mur*N*Ac-L-ala-D-glu-*meso*-DAP. (5) Addition of a D-ala dipeptide to UDP-Mur*N*Ac-L-ala-D-glu-*meso*-DAP by MurF to form UDP-Mur*N*Ac-L-ala-D-gln-*meso*-DAP-D-ala-D-ala (i.e. Lipid I). Lipid I is then transferred to Dec-P. (6) Addition of Glc*N*Ac to Lipid I by MurG to form Lipid II. (7) MurJ translocates Lipid II to the periplasm. (8 & 9) Incorporation of Lipid II into the cross-linked PG is facilitated by PonA1 and PonA2 through transglycosylase and transpeptidase activities, while L,D-transpeptidases form the 3,3 cross-link. Diagram adapted from (Jankute et al., 2015).

(D-ala) to UDP-Mur*N*Ac is catalyzed by MurC. MurD catalyzes the addition of the second amino acid (D-glu). MurE catalyzes the addition of *meso*-diaminopimelate (*meso*-DAP) and MurF catalyzes the addition of a D-ala dipeptide, which is formed by the D-alanine-D-alanine ligase (DdlA). A phospho-*N*-acetylmuramyl pentapeptide translocase, MraY, also known as MurX, transfers lipid I to a lipid carrier decaprenyl-phosphate (Dec-P). MurG then catalyzes the addition of Glc*N*Ac from UDP-Glc*N*Ac to lipid I via a β(1→4) glycosidic bond, to form lipid II. A lipid II flippase (either MviN [also known as MurJ], FtsW or RodA) finally translocates lipid II into the periplasm (Jankute et al., 2015).

1.6.1. **Periplasmic incorporation of lipid II into the cross-linked PG**

Cell growth in mycobacteria is distinguished by the fact that mycobacterial cells grow by incorporation of new cell wall material at subpolar sites of the cell (Meniche et al., 2014). The tropomyosin-like protein, DivIVA is recognized as the coordinator of polar growth and septal PG synthesis during cell division. DivIVA localizes to the cell poles where it recruits the cell wall biosynthetic machinery (Meniche et al., 2014). Polymerization of lipid II into the existing PG is facilitated by a number of enzymes that form the periplasmic PG biosynthetic machinery (Jankute et al., 2015). Bi-functional penicillin binding proteins, PonA1 and PonA2, facilitate the polymerization of the glycan strands (transglycosylation) and stem peptide cross-linking (transpeptidation) (Figure 1.3). The cross-linking of the stem peptides can occur in two forms, 4,3 cross-links (linkages that occur between the D-alanine at position 4 of one stem peptide and *meso*-DAP at position 3 of the adjacent stem peptide) and 3,3 cross-links (linkages between two *meso*-DAP residues of adjacent stem peptides) (Figure 1.4). The 3,3 cross-links are generated by a family of transpeptidases known as L,D-transpeptidases (Ldt) (Jankute et al., 2015).

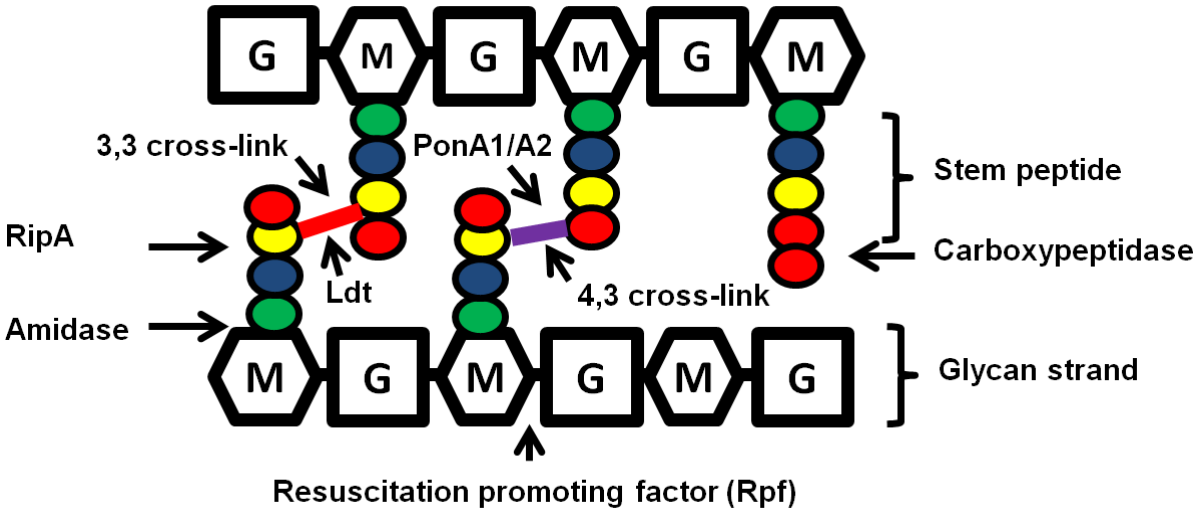


Figure 1.4: **Schematic representation of the cleavage sites of peptidoglycan hydrolases and the different PG cross-linkages**. 4,3 cross-links (purple line) and 3,3 cross-links (red line). The constituents of the PG layer are indicated. G: Glc*N*Ac, M: Mur*N*Ac.green circle: L-alanine, Blue circle: D-glutamine, yellow circle: *meso*-Diaminopimalate and red circle: D-alanine.

1.7. **Mycobacterial cell division**

Cell division is considered to be an important therapeutic target for antibacterial drugs as this process is crucial for bacterial proliferation and pathogenesis (Lock and Harry, 2008). Consistent with this, cell division inhibitors have been developed for mycobacteria (Lin et al., 2014). Following cell growth, a complex of enzymes (termed the divisome), essential for cell division, localizes approximately at mid cell and coordinates septal PG synthesis (Figure 1.5). This allows for cytokinesis of the mother cell into two attached daughter cells. Amidases cleave the bond between the stem peptide and the glycan strand (Figure 1.4). The divisome consists of the cytoskeletal tubilin-like protein FtsZ (which forms the Z-ring, a scaffold for the divisome components), structural elements (SepF, CrgA, FtsQ, FtsW, FhaB, CwsA), PG synthesis enzymes (PonA1, PonA2) and PG hydrolases (important for septal PG breakdown during the final stages of cell separation) (Figure 1.5) (Kieser and Rubin, 2014). Following daughter cell compartmentalization, the septal PG is degraded to allow for cell separation. Septal PG degradation in model organisms, such as *E. coli*, is facilitated by cell separation amidases AmiA, AmiB and AmiC, through activation by LytM domain containing proteins, EnvC and NlpD (further detailed below). EnvC specifically activates *E. coli* cell separation amidases AmiA and AmiB, and NlpD activates AmiC. EnvC is regulated by an ABC transporter-like complex, FtsEX (Yang et al., 2011). Although mycobacteria, do not encode an EnvC ortholog, they encode a similar FtsEX complex but its role in cell division remains unclear (Figure 1.5) (Mavrici et al., 2014). In mycobacteria, the final stages of cell separation is facilitated by a cell separation amidase termed Ami1 (similar to *E. coli* AmiA) and endopeptidases of the class NlpC/p60 (RipA and RipB) (Martinelli and Pavelka, 2016, Hett et al., 2008, Senzani et al., unpublished).

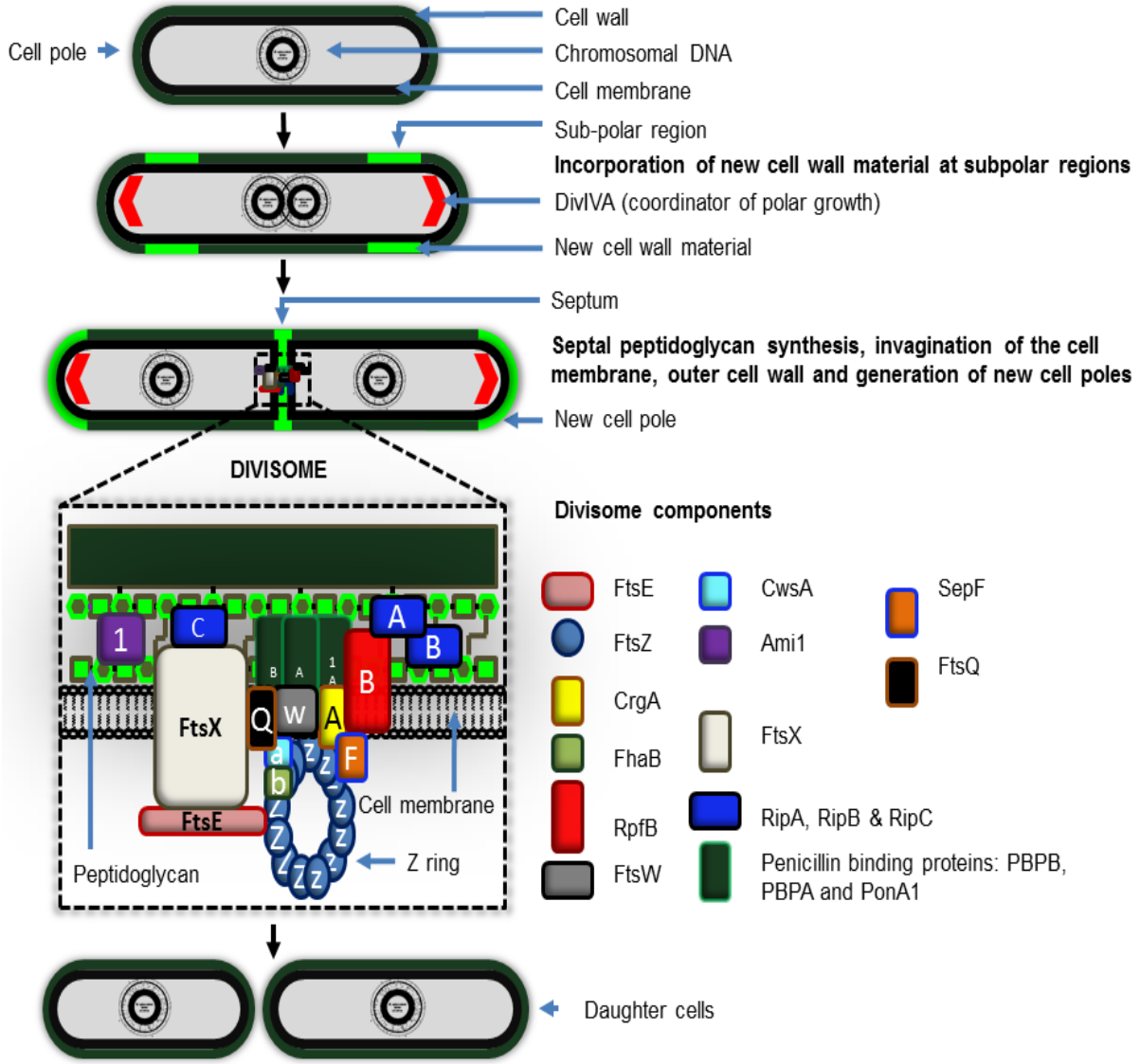


Figure 1.5: **Schematic representation of mycobacterial polar growth and cell division**. Mycobacteria grow by incorporation of new cell wall material at subpolar regions. Chromosomal DNA is duplicated and segregated to the daughter cells. The divisome assembles a PG wall between the daughter cells and the Z-ring constricts causing invagination of the cell membrane and outer cell wall layer. PG hydrolases (Ami1, RipA, RipB and perhaps other PG hydrolases) in the periplasmic space degrade the PG wall between the daughter cells to allow for cell seperation. Divisome proteins that have been experimentally shown to interact are drawn next to each other. FtsZ interacts with FtsE, CrgA, FhaB, CwsA and SepF. RipA interacts with RpfB and PonA1. RipC interacts with FtsX and FtsX interacts with FtsE. Diagram adapted from (Kieser and Rubin, 2014).

1.8. **Targeting mycobacterial PG biosynthesis**

The essentiality of the PG for bacterial viability, and the absence of this polymer in eukaryotic cells identify its biosynthesis as a vulnerable target for anti-TB drug development (Favrot and Ronning, 2012). Indeed, PG targeting efforts for drug development have undergone a recent resurgence of interest (Angala et al., 2014). As evidence of this, a novel oxazolidine derivative that inhibits GlmU, a *N*-Acetyl-glucosamine-1-phosphate uridyltransferase required for the synthesis of UDP-Glc*N*Ac, was developed and shown to significantly reduce the bacillary load in *Mtb* infected mice (Soni et al., 2015). MurA is a target of the antibiotic fosfomycin (Bensen et al., 2012). D-cycloserine inhibits alanine racemase (Alr) and DdlA, both required for PG stem peptide synthesis (Angala et al., 2014). Synthetic *N*-methyl-2-alkenyl-4-quinolones have been developed against MurE (Angala et al., 2014). Thiadiazolidinone inhibitors of Alr have also been developed (Angala et al., 2014). MraY inhibitors have been shown to be effective against drug susceptible and drug resistant *Mtb* isolates (Angala et al., 2014). Lipophilic derivatives of fosmidomycin inhibit IspC, an enzyme required for synthesis of the lipid carrier Dec-P (Angala et al., 2014). Aminopyrimidine-sulfonamides that inhibit DivIVA were also discovered (Singh et al., 2016). Beta-lactam antibiotics which specifically target PG polymerization have not traditionally been used against *Mtb* due to the presence of a highly active beta-lactamase BlaC, which hydrolyzes a wide range of beta-lactam antibiotics (Wivagg et al., 2014). However, the use of beta-lactamase inhibitors, (e.g. clavulanate) in conjunction with meropenem (a beta-lactam), yielded substantial efficacy against TB infection (Hugonnet et al., 2009). This has resulted in renewed interest in the development of novel PG biosynthesis-targeting antibiotics active against both antibiotic tolerant and resistant bacteria (Gold et al., 2016, Baranowski and Rubin, 2016).

1.9. **Mycobacterial PG remodelling**

The PG is continually remodelled to allow bacterial cell division and growth. During cell division, the PG connecting two dividing cells is degraded through the concerted activity of PG hydrolases to allow for cell separation. For cell growth, the existing PG is remodelled to allow insertion of new PG units in the form of the precursor molecule lipid II (Kieser and Rubin, 2014). The PG hydrolases have been classified according to whether they cleave within the glycan strands (classified as glycosidases) or whether the enzyme cleaves the peptide moiety (classified as peptidases) (Figure 1.4 & 1.6) (Vollmer et al., 2008). These are discussed further below.

1.10. **Glycosidases**

Mycobacterial glycosidases (a subclass of which are termed Rpfs) cleave the β(1→4) glycosidic bond between Mur*N*Ac and Glc*N*Ac residues (Figure 1.4) (Kana and Mizrahi, 2010). The Rpfs (RpfA, RpfB, RpfC, RpfD and RpfE) differentially play an important role in reactivation of dormant bacteria during an *in vitro* model of non-culturability (Uhia et al., 2015). Triple, quadruple, or quintuple mutants defective for various combinations of Rpfs are growth attenuated *in vivo* (Downing et al., 2005, Kana et al., 2008) and have been considered as vaccine candidates (Uhia et al., 2015). Vaccination with the Δ*rpfABCD* or the Δ*rpfACDE* mutants was protective against *Mtb* infection in a mouse model of infection (Kondratieva et al., 2011). A quintuple Rpf-defective mutant of *Mtb* is highly susceptible to the beta-lactam class of antibiotics (inhibitors of late steps in PG biosynthesis) and this was found to be due to defects in the maintenance of cell wall integrity (Wivagg and Hung, 2012). Rpfs are identified by a conserved 70 amino acid domain termed the Rpf domain (Uhia et al., 2015). The Rpf domain is similar to C-type lysozyme and the catalytic site of RpfB has been shown to be a target of the lysozyme inhibitor NAG3 (Squeglia et al., 2013). This highlights the Rpfs as targets for anti-TB drug development because their inactivation should block the resuscitation of dormant bacteria. Accordingly, a novel class of Rpf inhibiting compounds (2-nitrophenylthiocyanates) has been discovered (Uhia et al., 2015).

1.11. **Peptidases**

The peptidases include *N*-acetylmuramyl-L-alanine amidases which cleave the bond between the glycan chain and the stem peptide, endopeptidases and carboxypeptidases cleaving L,D-, D,L- and D,D-bonds in the stem peptides, respectively (Vollmer et al., 2008). Carboxypeptidases regulate the amount of PG cross-linking by removing the terminal D-alanine residue of the PG stem peptide (Figure 1.4) (Machowski et al., 2014). As indicated above, the cell separation amidase Ami1 and endopeptidases of the class NlpC/p60 (RipA and RipB) are required for cell division (Hett et al., 2008). In contrast, a distinct cytoplasmic homologue of PG amidases (CwlM) has evolved to regulate PG synthesis through stimulation of MurA (Boutte et al., 2016). The loss of the activity of RipA and RipB has been shown to compromise cell wall integrity, evidenced by the sensitivity of the mutant strain to lysozyme (a PG targeting antimicrobial agent) (Martinelli and Pavelka, 2016). The loss of RipC hypersensitizes mycobacteria to RIF and attenuates *Mtb* growth both *in vitro* and during an *in vivo* mouse model of TB infection (Mavrici et al., 2014, Parthasarathy et al., 2012). RpfB and RipA have been shown to interact and this interaction is suggested to generate a variant of

RipA with enhanced PG hydrolytic activity (Figure 1.5) (Hett et al., 2007). Endopeptidases that have not been studied before in mycobacteria are the M23 class of endopeptidases also known as LytM domain containing peptidases (Figure 1.6). To understand the biological role of M23 peptidases in PG remodelling, the function of these enzymes in model organisms is reviewed below.

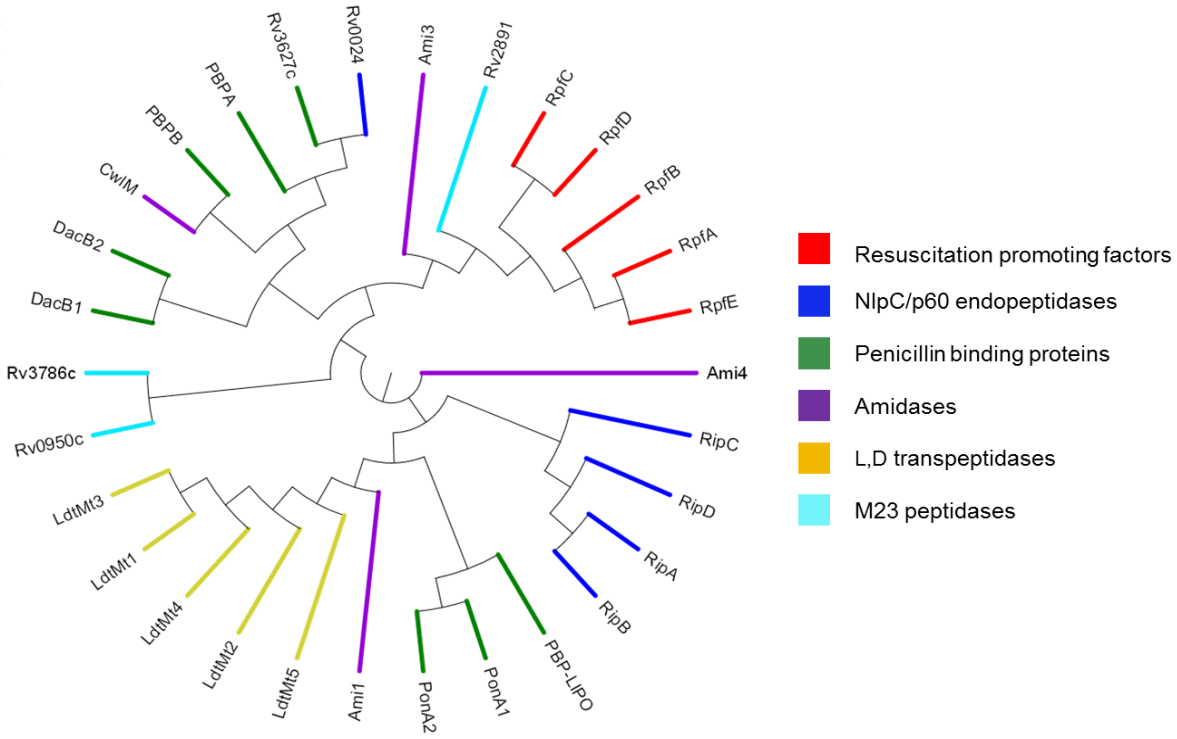


Figure 1.6: **Phylogenetic tree of mycobacterial peptidoglycan remodelling enzymes**. The M23 peptidases have not been studied before in mycobacteria. Full length protein sequences were aligned using Clustal Omega and the phylogenetic tree was generated using iTOL.

1.12. LytM domain containing peptidases (M23 peptidases)

The MEROPS peptidase database identifies members of this family as zinc metallopeptidases with a range of functions (Rawlings et al., 2008). M23 metallopeptidases are divided into two subfamilies: M23A and M23B. An increasing number of these peptidases are undergoing biochemical and functional characterization, and the diversity of the published crystal structures suggests species-specific adaptability of these proteins.

1.13. Structure, substrate specificity and catalytic activity of M23 metallopeptidases

M23 family members are characterized by a conserved M23 domain containing an HXH motif (metal binding site 2, where X is any amino acid) and most members bind a zinc divalent ion (Zn^{2+}) at this site for catalytic activity (Rawlings et al., 2008). A discernible

characteristic of the M23 domain (pfam01551) is a shallow groove containing the Zn^{2+} coordinating residues (Figure 1.7 A). The Zn^{2+} necessary for catalytic activity is usually tetrahedrally coordinated by two histidines, an aspartic acid residue and a water molecule, which occur in two short sequence motifs HXXXD (metal-binding motif 1), and the metal binding site 2 (Figure 1.8 B). The Zn^{2+} cation usually coordinates to the N_{δ} or N_{ε} atom of the histidine residues and to the $O_{\varepsilon 1}$ or $O_{\varepsilon 2}$ atom of aspartic acid (Zastrow and Pecoraro, 2014).

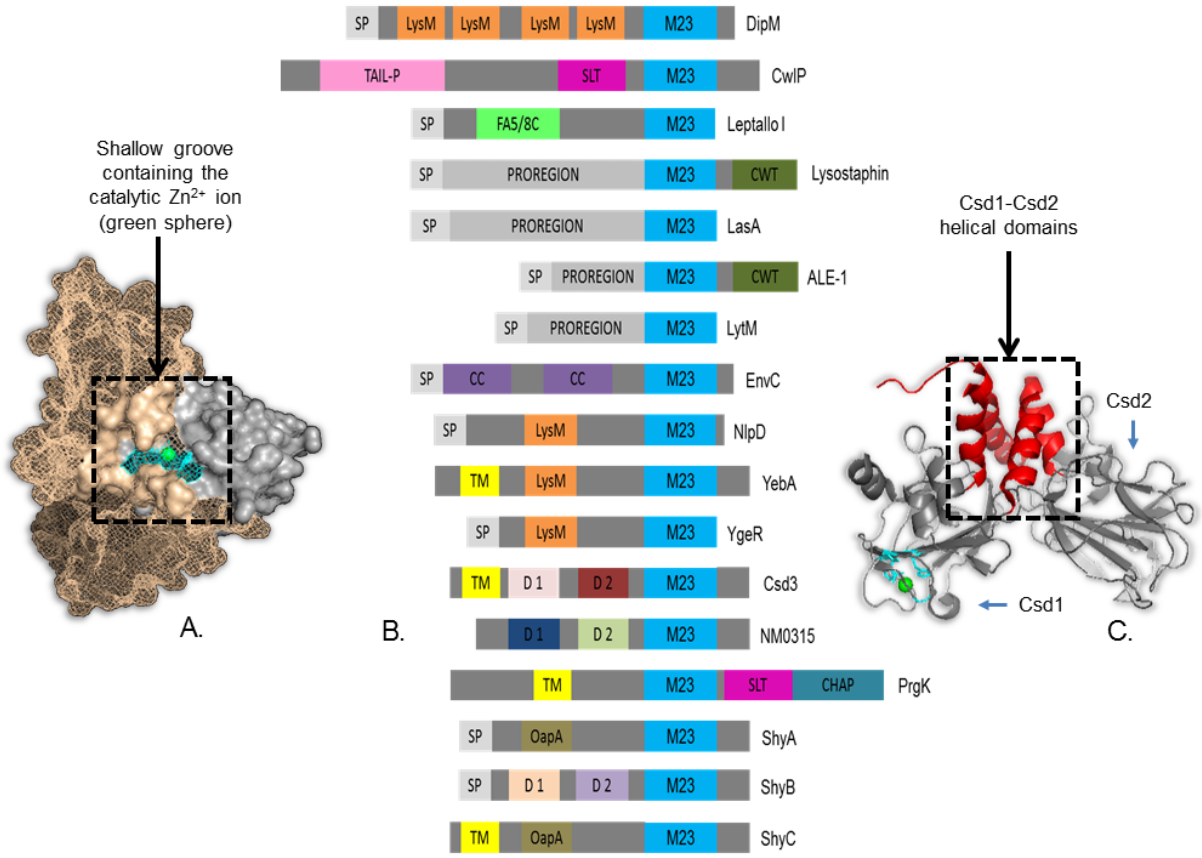


Figure 1.7: **M23 peptidase structure**. (A) Crystal structure of $Csd3_{\Delta 41}$ (PDB ID: 4RNZ), the typical M23 domain shallow groove is indicated by the black box. The M23 domain is indicated in grey. (B) Variation in domain organization of some functionally characterized M23 peptidases: Darker grey indicates regions of unknown function. M23 domain (Light blue), LysM domain (orange), cell wall targeting domain (dark green), soluble transglycosylase domain (SLT) (hot pink), phage related minor tail protein (pink), coiled-coil (CC) domain (purple), transmembrane domain (TM) (Yellow), OapA domain (Tan), Cysteine-, Histidine-dependent amidohydrolase/peptidase (CHAP) domain (Aqua), domains of unknown function are labelled D1 and D2 for respective hydrolases. Signal sequences are labelled SP and proregions are indicated. (C) Csd1Csd2 heterodimer (PDB ID: 5J1L), unique helical domains (red) are indicated by the black box. The pymol graphics package was used to view the indicated protein structures.

A non-Zn^{2+} coordinating, but conserved, histidine in the active site is proposed to mediate deprotonation of a water molecule that coordinates the Zn^{2+} ion (Figure 1.9). This results in the generation of a hydroxide nucleophile which attacks the scissile bond carbonyl carbon of the PG cross-link, resulting in the formation of a bidentate complex and a tetrahedral intermediate. Proton removal from the non-Zn^{2+} coordinating histidine by the lone pair of electrons of the nitrogen of the scissile bond results in hydrolysis of the peptide bond (Figure 1.9) (Zastrow and Pecoraro, 2014, Cohen et al., 2009).

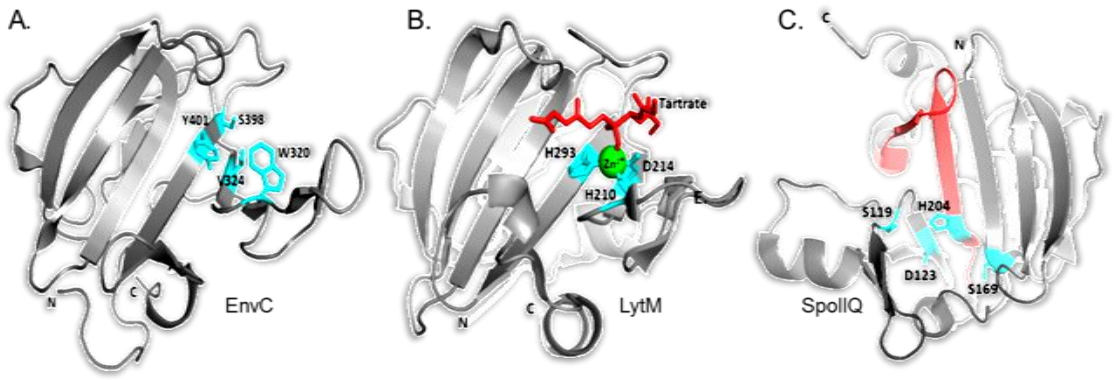


Figure 1.8: **Comparison of the different M23 domain active sites**. Ribbons representation of the degenerate M23 domain of *E. coli* EnvC (PDB ID: 4BH5) (A), tetra-coordinated Zn^{2+} containing active M23 domain of *S. aureus* LytM in complex with tartrate (PDB ID: 2B13) (B), and the degenerate M23 domain of *B. subtilis* SpoIIQ with the highly conserved C-terminus residues indicated in red (PDB ID: 3TUF) (C). Metal ligands are denoted in cyan and the Zn^{2+} cation is indicated as a green sphere. The PDB files for the indicated proteins were obtained from the protein data bank (PDB) through the use of the indicated PDB ID numbers. The pymol graphics package was used to view the indicated protein structures.

The core of the M23 domain consists of antiparallel β-sheets that anchor the catalytic residues important for coordination of the Zn^{2+} cation and the difference in the conformation of the β-sheets may confer substrate specificity (Bochtler et al., 2004, Bateman et al., 2002). Cohen et al. proposed a PG-crosslink hydrolysis reaction by the cell wall depolymerizing bacteriophage phi-29 gene product 13 (gp13) which sheds light on the M23 peptidase mediated PG hydrolysis by tetra-coordinated Zn^{2+} found in M23 peptidases (Figure 1.9) (Cohen et al., 2009). In this model, the metal binding motifs allow Zn^{2+} to polarize the carbonyl carbon of the substrate for susceptibility to nucleophilic attack and subsequent hydrolysis of the 4,3 PG cross-link (Cohen et al., 2009).

In vitro, most well-characterized members of the M23 peptidase family are shown to cleave glycyl-glycine bonds (Spencer et al., 2009). Interestingly, M23 peptidases are also present in

bacteria that do not possess glycyl-glycine peptide linkages in their PG, including mycobacteria (Ragumani et al., 2008). This suggests that these enzymes retain alternative specificities.

1.13.1. **Structural diversity in M23 peptidases**

M23 peptidases show architectural diversity (Figure 1.7). For example, extracellularly secreted M23 peptidases, that target other bacteria in the environment, tend to have a N-terminal (after proteolytic removal of the N-terminal proregion, see Figure 1.7) or centrally located catalytic M23 domain. In contrast, a C-terminally located M23 domain is usually observed in M23 peptidases that process the PG of the host bacterium producing the enzyme.

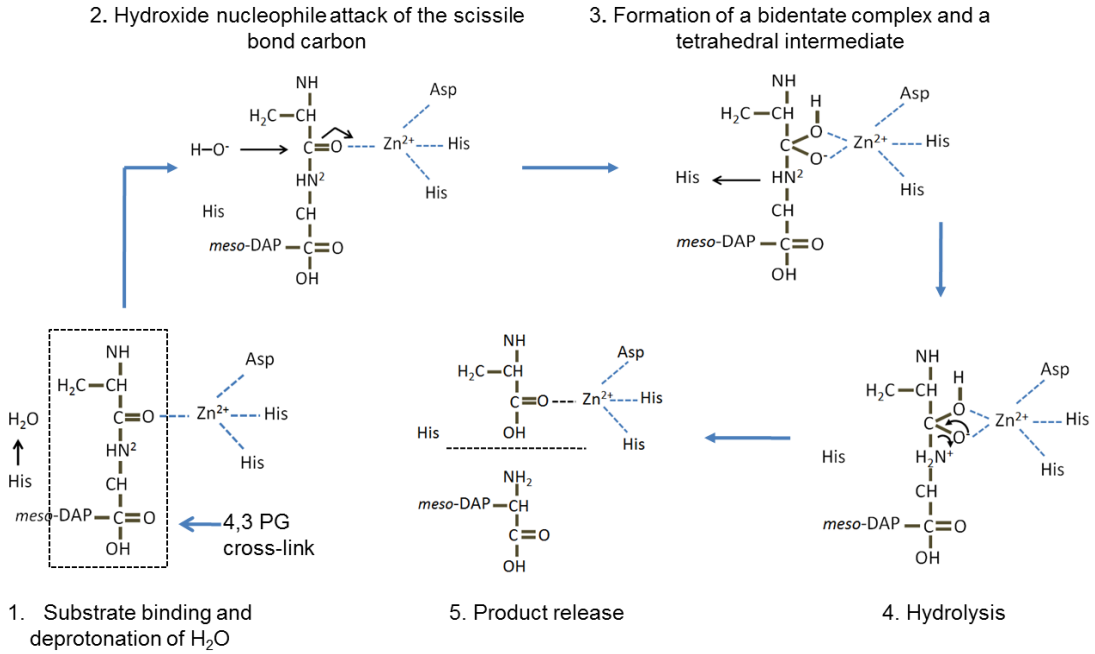


Figure 1.9: **Proposed hydrolysis reaction of the 4,3 peptidoglycan cross-link by catalytically active M23 proteins**. 1. Binding of the substrate, polarization of the scissile bond carbonyl carbon and deprotonation of water. 2. Hydroxide nucleophilic attack of the scissile bond carbon and proton removal from a non-Zn^{2+} co-ordinating histidine by the lone pair on the nitrogen of the scissile bond. 3. Formation of a bidentate complex and a tetrahedral intermediate. 4. Hydrolysis. 5. Product release. Diagram adapted from (Cohen et al., 2009).

A single bacterial species may encode multiple copies of these proteins with highly distinctive roles and in some cases, these enzymes can display redundant roles (Firczuk and Bochtler, 2007). Several studies suggest that different expression patterns may govern the activity of the multiple copies of M23 peptidases, and thus result in different physiological roles for these enzymes (Firczuk and Bochtler, 2007). For example, *V. cholerae* encodes 2

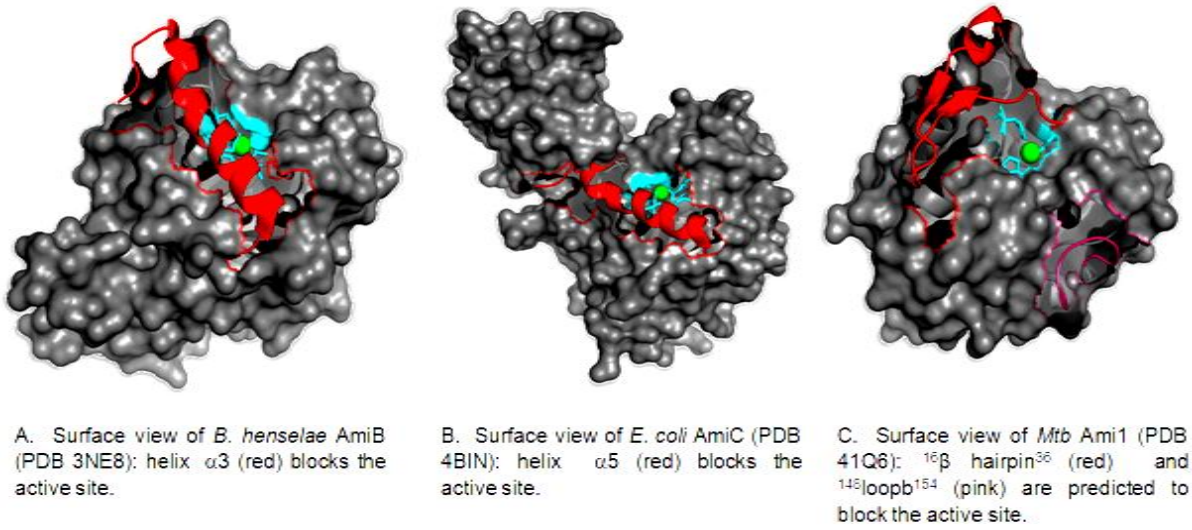
cell division M23 proteins: EnvC and NlpD, required for activation of a cell separation amidase during cell division and 3 cell elongation M23 proteins: ShyA, ShyB and ShyC.

1.14. **Functional diversity of M23 peptidases**

1.14.1. **The role of M23 peptidases in cell division as regulatory factors**

Binary fission is the ultimate step of the prokaryotic cell cycle (Adams and Errington, 2009). This process is usually divided into three steps: (I) the invagination of the cytoplasmic membrane, PG and the outer membrane, (II) daughter cell separation and (III) generation of new poles (Figure 1.5) (Adams and Errington, 2009). In model organisms such as *E. coli*, the latter process requires the regulated action of the cell division amidases, together with their M23 activators, to cleave the septal PG (Uehara et al., 2009, Ercoli et al., 2015, Moll et al., 2014, Tidhar et al., 2009). EnvC, NlpD and sporulation enzyme SpoIIQ do not display PG hydrolytic activity as these enzymes lack important Zn^{2+} coordinating residues necessary for PG hydrolytic activity (Figure 1.8 A and 1.8 C, respectively) (Meisner et al., 2012, Peters et al., 2013). The M23 domain that does not have the Zn^{2+} coordinating residues is referred to as a degenerate M23 domain. Despite this catalytic deficiency, EnvC and NlpD play critical roles in activation of amidases, through protein interaction. Recent studies reveal that these proteins evolved for tight regulation of PG hydrolases during growth and cell division (Dominguez-Gil et al., 2016). Consistent with this, mechanisms responsible for the activation of nascent autolysins include allosteric activation of these proteins as they translocate to the periplasm to sites of PG biosynthesis, in order to regulate their potential bacterial lytic activity (Uehara et al., 2009, Peters et al., 2011, Uehara et al., 2010). X-ray crystallography, or 3D protein modelling has unveiled the presence of autoinhibitory domains within the active site of most cell separation amidases, among other PG hydrolases, indicating that amidase activity is blocked prior to cell division (Yang et al., 2012). This was demonstrated with the *Bartonella henselae* (*B. henselae*) AmiB, *E. coli* AmiC and Ami1 of *Mtb* (Figure 1.10) (Yang et al., 2012, Rocaboy et al., 2013, Kumar et al., 2013). These observations correlate with the fail-safe mechanism demonstrated by Peters et al. where the PG hydrolases interact with their activators at a spatial and temporal level to ensure that PG synthesis is followed by PG hydrolysis at the expansion or division site to prevent osmotic fragility (Peters et al., 2011). The active site of *Mtb* Ami1 is shown to be only partially occluded (Figure 1.10 C); pointing to a divergent mechanism for amidase regulation in mycobacteria.

E. coli mutants defective for both EnvC and NlpD fail to cleave the connecting (septal) PG and form long chains of cells with distinct cytoplasmic compartments connected by shared layers of PG and a partially constricted outer membrane (Uehara et al., 2010, Uehara et al., 2009). This phenotype is similar to that of an *E. coli* mutant lacking all cell separation amidases (Heidrich et al., 2002, Heidrich et al., 2001, Priyadarshini et al., 2007). Biochemical and genetic studies suggest that the *E. coli* amidases require activation through direct contact with EnvC and NlpD (Uehara et al., 2009). Additional studies suggest that EnvC and NlpD activate their associated amidases by inducing conformational changes that remove autoinhibitory domains from the amidase active sites (Figure 1.10) (Yang et al., 2012). The ability of EnvC to activate amidases is abrogated when point mutations are introduced into its



A. Surface view of *B. henselae* AmiB (PDB 3NE8): helix α3 (red) blocks the active site.

B. Surface view of *E. coli* AmiC (PDB 4BIN): helix α5 (red) blocks the active site.

C. Surface view of *Mtb* Ami1 (PDB 41Q6): ^{16}β hairpin^{36} (red) and ^{145}loopb^{154} (pink) are predicted to block the active site.

Figure 1.10 **Surface view of autoinhibited cell separation amidases**. (A) Inactive AmiB ([PDB ID: 3NE8], helix a3 [red] blocks the active site) (B) Inactive AmiC ([PDB ID: 4BIN]: helix α5 [red] blocks the active site). and (C) Inactive Ami1 (Ami1 [PDB ID: 41Q6]: ^{16}β hairpin ^{36}[red] and ^{148}loopb^{154} [pink] are predicted to block the active site). Catalytic active site residues (cyan) and the catalytic Zn^{2+} cation (green) are shown as ball-and-stick models. The pymol graphics package was used to view the indicated protein structures.

degenerate M23 domain (Peters et al., 2013). Peters et al. suggest that some of the PG hydrolases are likely to have developed alternative functions such as serving as activators of other proteins in addition to, or at the cost of, their own catalytic activity (Peters et al., 2013). Although a model for AmiC activation remains to be described, it is believed that the degenerate M23 domain of NlpD similarly mediates the activation of AmiC through allosteric regulation (Rocaboy et al., 2013). Through microscale thermophoresis assays (Jerabek-Willemsen et al., 2011), Rocaboy et al. demonstrated that AmiC directly interacts with NlpD and this interaction is suggested to generate an AmiC variant that is catalytically active

(Rocaboy et al., 2013). *E. coli* encodes two additional M23 peptidases; namely, YebA, which was shown to be a D,D-endopeptidase and the uncharacterized YgeR (Singh et al., 2012). Analysis of the genome of non-typeable *Haemophilus influenzae* (NTHI) identified three M23 peptidases (Ercoli et al., 2015). The NTHI M23 peptidases were named YebA, EnvC and NlpD on the basis of their homology to the *E. coli* M23 peptidases (Ercoli et al., 2015). Interestingly, an *envC* NTHI mutant showed a drastic reduction of periplasmic proteins, suggesting that NTHI EnvC plays a role in maintenance of the surface protein content by facilitating the passage of these surface proteins through crosslinked PG. This highlights the species-specific adaptability of the M23 proteins (Ercoli et al., 2015). Inactivation of NTHI *yebA* resulted in an aberrant division phenotype, characterized by altered cell architecture and extensive membrane blebbing suggesting that in other bacteria, catalytically active M23 peptidases similar to YebA could be directly involved in cell division (Ercoli et al., 2015). Indeed, the analysis of the *Caulabacter crescentus* genome revealed a M23 peptidase involved in cell division called DipM, among seven genes that encode putative M23 peptidases (Moll et al., 2010). Since then, DipM orthologs have been identified in other bacterial species including the cyanobacterium *Synechococcus elongatus* (*S. elongatus*) and even in photosynthetic eukaryotes such as the glaucophyte *Cynophora paradoxa* and the moss *Physcomitrella patens* (Moll et al., 2010, Goley et al., 2010, Miyagishima et al., 2014). Comparable to *C. crescentus* DipM, *S. elongatus* DipM also localizes at mid-cell where it is involved in cell division (Miyagishima et al., 2014). These observations suggest that M23 peptidases with active catalytic sites represent a new class of bacterial PG endopeptidases directly involved in cell division, in addition to amidases and NlpC/P60-type endopeptidases such as RipA and RipB.

1.14.2. **M23 peptidases in cell growth**

Among the most frequently discussed topics in molecular biology are the molecular determinants of bacterial cell growth, elongation and cell division (Turner et al., 2012, Cabeen and Jacobs-Wagner, 2005, Uehara et al., 2010). The concerted activity of PG-synthesizing and PG-hydrolyzing enzymes contributes to the remodeling of the PG and, consequently, the generation of a particular cell shape (Cabeen and Jacobs-Wagner, 2005). In bacterial species that expand through incorporation of new PG material along their lateral axis, it is believed that cleavage of the PG network is necessary for its expansion. In particular, parallel glycan strands which are presumed to lie perpendicular along the length of rod-shaped cells must be disconnected, via cleavage of the connecting crosslinks, to allow for

cell elongation (Holtje, 1998). In *V. cholerae*, the cell elongation-specific M23 peptidases are encoded by *vca0079*, *vca0503* and *vca0630*, renamed *sidewall hydrolase* (*shy*) *A*, *B* and *C*, respectively. These peptidases have been shown to be individually dispensable for growth and cell division but are essential for cell elongation. Time-lapse microscopy of a ShyA ShyC deletion-mutant, with an inducible copy of *shyA*, revealed a 50% decrease in cell elongation rate after *shyA* expression was repressed (Dorr et al., 2013). Also, ShyA is essential for growth in a *shyC* mutant. In addition to *E. coli* YebA, *V. cholerae* ShyA, B and C represent the first set of biochemically characterized M23 peptidases involved in cell elongation; a process previously assumed to be facilitated by members of the NlpC/P60 family of endopeptidases such as *E. coli* Spr and YdhO peptidases and penicillin-binding proteins (Singh et al., 2012). An *E. coli* s*pr*, *ydhO* and *yebA* triple mutant is unable to incorporate new PG material and undergoes rapid lysis upon shift to restrictive conditions (Singh et al., 2012). These findings suggest that cross-link specific peptidases are collectively essential for bacterial growth and that PG crosslink cleavage is essential for enlargement of the PG sacculus. The polar growth of mycobacteria could similarly require constant remodelling of polar PG by PG endopeptidases to allow insertion of new cell wall material.

1.14.3. **M23 peptidases in bacterial virulence and pathogenesis**

The virulence of many pathogenic bacteria has long been attributed to their ability to maintain cell wall integrity and to express cell wall related virulence factors (Boneca, 2005, Silhavy et al., 2010). NTHI EnvC is involved in the expression of cell wall related virulence factors. An *envC* defective NTHI strain is impaired in adherence to epithelial cells, in biofilm formation and also shows a reduced resistance to normal human serum (Ercoli et al., 2015). A *T. pallidum* M23 peptidase encoded by the gene *tp0155*, and five M23 peptidase homologues of *T. denticola* encoded by the genes *tde1136, tde1738, tde2189, tde2318* and *tde2753*, are identified as novel fibronectin-binding proteins, implicated in bacterial colonization of damaged host tissues during infection (Cameron et al., 2004, Bamford et al., 2010). The inactivation of *csd3* in *H. pylori* leads to a stocky and branched phenotype, which affects the ability of the bacterium to colonize mice, despite a normal motility phenotype *in vitro* (Bonis et al., 2010). Other cell shape determining M23 peptidases of *H. pylori* have also been shown to be necessary for efficient stomach colonization in a mouse stomach colonization assay (Sycuro et al., 2010). NlpD is demonstrated to be a novel *Yersinia pestis* virulence factor, essential for the development of plague (Tidhar et al., 2009). Similarly, for *V. cholerae*, NlpD is essential for intestinal colonization in the infant mouse model of cholera (Moll et al., 2014,

Tidhar et al., 2009). Other examples highlighting the association of M23 peptidases with bacterial pathogenesis are demonstrated with the M23 peptidase NG1686 of *Neisseria. gonorrhoeae* and NMB0315 of *N. meningitidis.* NG1686 mediates hydrogen peroxide resistance and survival of killing by polymorphonuclear leukocytes during infection (Stohl et al., 2012). We hypothesize that mycobacterial M23 peptidases could also play an analogous role in bacterial pathogenesis.

1.14.4. **M23 peptidases in cell shape determination**

PG peptide moiety cross-linking is necessary in most bacteria to preserve cell wall integrity and the degree of cross-linking can be regulated to create morphological diversity among bacteria. Biophysical modelling suggests that the regulation of PG cross-linking is important for generating cell shape (Huang et al., 2008). The involvement of M23 peptidases in shape determination has been demonstrated with *H. pylori*, which normally assumes a helical cell shape (Bonis et al., 2010, Sycuro et al., 2010). Sycuro et al. identified three M23 peptidases that are important for generating the helical shape of *H. pylori* through alterations of PG cross-linking. M23 peptidases Csd (cell shape determinant) 1, 2 and 3 uniquely contribute to the generation of the helical shape as deletion thereof yields cells unable to develop the helical shape, consequently affecting bacterial pathogenesis. Csd2 habors a degenerate M23 domain and this suggests that this enzyme may not be directly involved in PG remodelling. Biochemical studies indicate that Csd1 and Csd2 form a 1:1 heterodimer through the use of unique helical domains only observed in these M23 proteins (Figure 1.7 C). The monomers of Csd1 in two heterodimer models display non-canonical modes of Zn^{2+} coordination indicating the ability of M23 peptidases to use otherwise non-canonical motifs for Zn^{2+} coordination (An et al., 2016). The interaction between Csd1 and Csd2 is suggested to induce substrate specificity for Csd1 (the catalytically active subunit of the Csd1 Csd2 heterodimer) (An et al., 2016). Inactivation of *csd2* and *csd3* yields a variety of highly aberrant cell morphologies. However, based on the heterogeneity of shapes observed during a heterologous cross-species complementation analysis using *C. jejuni* and *V. cholerae* homologues, Sycuro et al. suggested that it is difficult to predict whether Csd homologues contribute to maintenance of cell morphology in other bacteria. Analysis of the PG peptide side chain content of the Csd mutants relative to wild type *H. pylori* revealed an increase in PG stem peptide cross-linked dimers (Sycuro et al., 2010). This suggested that Csd peptidases are PG cross-link specific endopeptidases that are necessary for regulating the degree of

cross-linking in the PG sacculus to induce the helical shape of *H. pylori* without affecting cell wall integrity or septation (Sycuro et al., 2010).

While *H. pylori* in log phase display a helical morphology, the cells undergo a shape transition to a non-culturable coccoid form during prolonged culture in stationary phase (Costa et al., 1999). All Csd mutants were capable of transitioning to the non-culturable coccoid form during stationary phase with the *H. pylori csd3* mutant being slightly delayed in the process. Indeed, when subjected to hostile environmental conditions, bacteria can survive by entering a viable but non-culturable state characterized by substantial changes in morphology (Cellini, 2014). Consistent with this, *Mtb* suspensions isolated from murine peritoneal macrophages lysates after phagocytosis were found to contain a range of morphological types including rods, ovoid forms and coccoid forms. These findings are indicative of changes in PG structure that might be facilitated by PG hydrolases or the alterations in the activity of PG cross-linking transpeptidases. (Meisner and Moran, 2011, Blaylock et al., 2004). *V. cholerae* has also been shown to tolerate antibiotics targeting PG synthesis including penicillin by transitioning to a more resilient coccoid form. The latter requires the activity of ShyA, which prevents lysis and enables formation of viable non-dividing coccoids after exposure to a cell wall targeting antibiotic (Dorr et al., 2015). Consequently, ShyA represents a class of M23 peptidases crucial for the endopeptidase-mediated tolerance of PG targeting antibiotics.

1.14.5. **M23 peptidases in sporulation**

When nutrients become limiting, spore-forming species such as *Bacillus* and *Clostridium* species undergo a differentiation process that leads to the production of highly resistant endospores (Higgins and Dworkin, 2012, Paredes-Sabja et al., 2014, Crawshaw et al., 2014, Galperin et al., 2012). Studies from the 1950s suggested the ability of mycobacteria to form spores; however, these studies were recently refuted (Uhia et al., 2015). Endospores have a pair of PG layers of different structure: an inner elementary cell wall, which will become the basis of the new vegetative cell wall after germination and an outer spore-specific cortex. The spore cortex PG is very loosely cross-linked; a characteristic intimately linked to heat resistance. *B. subtilis* YunA, renamed LytH, is a M23 peptidase identified as a novel sporulation-specific component with a role in cortex structure determination (Horsburgh et al., 2003). Spores of a *B. subtilis lytH* mutant have slightly reduced heat resistance, suggesting a difference in cortex structure. Analysis of the spore cortex PG muropeptide

content of a *B. subtilis lytH* mutant revealed the loss of muropeptides containing single L-alanine side chains (Horsburgh et al., 2003). This suggested that LytH is the first characterized L,D-M23 peptidase involved in the production of the single L-alanine side chains by cleaving nascent tetrapeptides in the spore cortex.

The degenerate M23 protein SpoIIQ is a forespore membrane protein important for dictating the localization of a number of spore maturation specific proteins to the mother cell-forespore interface during bacterial endospore formation (Meisner and Moran, 2011). Meisner et al. demonstrated that SpoIIQ interacts with the mother cell membrane protein SpoIIIAH through its degenerate M23 domain. This enables the recruitment of several mother cell proteins to the mother cell-forespore channel, which is essential for forespore nurturing (Meisner et al., 2012, Crawshaw et al., 2014). This is evidenced by observations that the disruption of SpoIIQ results in a strain defective for sporulation (Meisner and Moran, 2011). SpoIIQ has a highly conserved group of residues at the C-terminus (Figure 1.8 C) (Camp and Losick, 2008). This region contains two of the degenerate M23 domain active site histidine residues (His202 and His204) and is shown to be important for SpoIIQ-SpoIIIAH interactions (Camp and Losick, 2008, Rodrigues et al., 2013). Moreover, Rodrigues et al. demonstrated that introduction of point mutations in the M23 domain of SpoIIQ impairs the localization of this enzyme to the forespore septal membrane by preventing interaction of SpoIIQ with SpoIID and SpoIIP, which participate in anchoring SpoIIQ in the septal membrane (Rodrigues et al., 2013). These studies suggest that M23 proteins in sporulating bacteria are evolved for protein-protein interactions that govern the localization of sporulation specific enzymes, as these are highly conserved among other spore formers especially in members of the *Bacillus* genus. However, *Clostridium difficile* (*C. difficile*) SpoIIQ retains a M23 domain coordinating the Zn^{2+} cation. This suggests that *C. difficile* SpoIIQ could contribute directly to PG remodelling as a *C. difficile* SpoIIQ mutant is impaired in spore engulfment (Serrano et al., 2015). Moreover, Serrano et al. demonstrated that the *C. difficile* SpoIIQ with a catalytically active M23 domain also interacts with *C. difficile* SpoIIIAH. However, in contrast to the degenerate *B. subtilis* SpoIIQ, the loss of the Zn^{2+} in *C. difficile* SpoIIQ impairs SpoIIQ-SpoIIIAH interactions. Furthermore, to study the role of the *C. difficile* SpoIIQ M23 domain, the Zn^{2+} coordinating histidine residue of metal-binding motif 1 in the *C. difficile* SpoIIQ M23 domain was substituted with a serine found at a similar position in the degenerate *B. subtilis* SpoIIQ ortholog. This modification impaired *C. difficile* SpoIIQ-SpoIIIAH interactions and consequent SpoIIIAH localization resulting in a subtle spore engulfment defect. Thus, intact

M23 domains able to bind Zn^{2+} may not be essential for spore engulfment in *C. difficile*. However, the specialized secretion system formed by the *spoIIIAH*-encoded proteins and SpoIIQ maintains the stability of the forespore membranes and the potential for macromolecular synthesis in the forespore during late stages of morphogenesis (Serrano et al., 2015). These studies further show the species-specific evolution of M23 proteins.

As MDR-TB is on the rise, efforts for anti-TB drug development continually highlight mycobacterial cell wall biosynthesis as an area rich with potential targets; particularly, PG biosynthesis which has been targeted to develop novel anti-TB drugs able to cure MDR-TB infection (Angala et al., 2014, Diacon et al., 2016). The role of mycobacterial M23 peptidases in PG biosynthesis has not been explored before. Considering this, the aims and objectives of this project are listed below.

1.15. **Hypothesis**

We hypothesize that mycobacterial M23 peptidases form a novel group of PG hydrolases that play an important role during PG remodelling to allow efficient cell growth, cell division and maintenance of cell wall integrity. To test this hypothesis, mutants of *M. smegmatis* that are defective in the M23 peptidases were generated and phenotypically characterized.

1.16. **Aims and objectives of this study**

1.16.1. **Aims**

I. Considering the importance of M23 peptidases of various model organisms in diverse processes essential for bacterial viability and pathogenesis, the main aim of this study is to investigate the function of mycobacterial M23 peptidases through gene knockout.

II. To identify interacting partners for mycobacterial M23 peptidases to enhance our understanding of cell wall remodelling in mycobacteria.

1.16.2. **Specific objectives**

I. To conduct bio-informatics analyses to identify mycobacterial LytM domain-containing proteins.

II. To create mutant strains lacking selected LytM domain-containing proteins individually and in combination.

III. To perform phenotypic characterization to analyze cell wall related defects in the mutant strains.

IV. To define the role of M23 peptidases in mycobacterial cell wall remodelling through protein interaction studies.

2. Materials and methods

2.1. Bio-informatics and software used

2.1.1. Databases used to obtain genomic DNA and protein sequences of interest

Table 1: Databases used to obtain genomic DNA and protein sequences

Name	Website address	Use
Smegmalist	http://mycobrowser.epfl.ch/smegmalist.html	Smegmalist was used to interrogate *M. smegmatis* DNA and protein sequences of interest.
Tuberculist	http://tuberculist.epfl.ch	Tuberculist was used to interrogate *Mtb* DNA and protein sequences of interest.
Leproma	http://genolist.pasteur.fr/Leproma/	Leproma was used to interrogate *M. leprae* DNA and protein sequences of interest.
EcoCyc	http://www.ecocyc.org/ECOLI/organism-summary	EcoCyc was used to interrogate *E. coli* DNA and protein sequences of interest.
KEGG	http://www.genome.jp/kegg/kegg2.html	KEGG was used to interrogate DNA and protein sequences of interest for the following bacterial species: *Enterococcus faecalis V583*, *Bacillus megaterium* DSM, *Listeria monocytogenes* EGD-e, NTHI strain 176, *V. cholerae* O1 biovar E1 Tor strain N16961, *C. crescentus* CB15N, *Streptococcus equi. subspecies zooepidemicus* 4881, *S. elongatus* PCC 7942, *Corynebacterium glutamicum* ATCC 13032, *Rhodococcus equi* 103S, *T. denticola* ATCC 35405, *B. anthracis* AMES, *B. cereus* ATCC 14579, *Thiomicrospira crunogena* XCL-2, *H. pylori* G27, *P. aeruginosa* PA01, *B. subtilis*, *Deep-sea Pseudoalteromona sp.* CF6-2, *C. jejuni* NCTC 11168, *Nautilia profundicola* Am-H,

	Myxococcus xanthus DK1622, *Brucella arbortus* 2308, *Candidatus Ruthia magnifica* Cm, *Leptospira interrogans* serovar Copenhageni, *T. pallidum* subsp. pallidum str. Nichols, *Nitratiruptor* sp. SB155-2, *N. gonorrhoeae*, *N. meningitis* serogroup B, *Thiomicrospira crunogena* XCL-2, *S. aureus, Streptococcus equi subsp. Equi* NCTC 8325, *S. simulans, C. difficile* 630, *Persephonella marina* EX-H1, *C. paradoxa, Candidatus Ruthia magnifica* Cm, *Polaromonas sp.* JS666, *Shigella flexineri 2a* strain 301.

The various bio-informatics tools and software packages used in this study for analysis of the genes and proteins of interest are indicated below.

2.1.2. **NCBI BLAST** (http://blast.ncbi.nlm.nih.gov/Blast.cgi)

The Basic Local Alignment Search Tool (BLAST) is an online tool that allows for the comparison of DNA and protein sequences to identify regions of similarity between sequences of interest. This tool was used to identify genes that encode for M23 peptidases in the genome of *M. smegmatis* mc^2155, *Mtb* H37Rv and *M. leprae* TN.

2.1.3. **pFam database** (http://pfam.xfam.org/about)

The protein families database (pFam) is an online tool that allows for the identification and location of functional domains in a protein sequence. This tool was used to identify the presence of the M23 peptidase domain in the mycobacterial M23 proteins identified by NCBI BLAST.

2.1.4. **SignalP 4.1 Server** (http://www.cbs.dtu.dk/services/SignalP/)

The SignalP 4.1 server allows for identification and location of signal peptides within protein sequences and predicts the cleavage sites of the identified signal peptide. This tool was used to identify signal peptides within the protein sequences of interest.

2.1.5. **Clustal Omega** (http://www.ebi.ac.uk/Tools/msa/clustalo/)

The Clustal Omega server is an online multiple-sequence alignment tool that aligns nucleotide or amino acid sequences to identify regions of similarity. This tool was to align various protein sequences of M23 peptidases and for the generation of a phylogenetic tree of M23 peptidases analyzed.

2.1.6. **iTOL version 3** (http://itol.embl.de/)

The interactive Tree Of Life (iTOL) server is an online tool for the display, annotation and management of phylogenetic trees. This tool was used for the annotation and management of the M23 peptidase phylogenetic tree generated using Clustal Omega.

2.1.7. **I-TASSER** (http://zhanglab.ccmb.med.umich.edu/I-TASSER/)

The Iterative Threading ASSEmbly Refinement (I-TASSER) server is a protein threading and protein function prediction tool. This tool was used for the threading and functional prediction of the identified mycobacterial M23 peptidases.

2.1.8. **PyMOL** (https://www.pymol.org/)

The PyMOL software is a molecular visualization system. This software was used for the visualization and analysis of the predicted protein structures of the identified mycobacterial M23 peptidases.

2.1.9. **Fiji** (http://imagej.net/Fiji)

Fiji software is an open source image processing package. This software was used for analysis of microscope images taken using the Zeiss Observer Z1 inverted fluorescence microscope.

2.1.10. **STRING** (http://string-db.org/)

The STRING database is an online database of known and predicted protein-protein interactions. This tool was used for the prediction of protein interacting partners for the identified mycobacterial M23 peptidases.

2.1.11. **GraphPad prism 6** (http://www.graphpad.com/scientificsoftware/prism/)

GraphPad prism 6 is a data management and analysis software. This software was used to construct graphs and figures for data analysed from this study. Additionally, it was used for statistical analysis to compare statistically significant differences between data groups.

2.1.12. **FATCAT** (http://fatcat.sanfordburnham.org/fatcat/)

The FATCAT (Flexible structure AlignmenT by Chaining Aligned fragment pairs allowing Twists) server is a protein structure comparison tool. This tool was used for the comparison of the tertiary structures of the identified mycobacterial M23 peptidases.

2.2. Bacterial strains and plasmids created and/or used

The plasmids and bacterial strains created and/or used in this study are indicated in Table 2 and Table 2.1, respectively.

Table 2: **Plasmids created and/or used in this study**.

Plasmids	Description	Source/ Reference
p2NIL	*E. coli* cloning vector. Kan^R	(Parish and Stoker, 2000)
pGOAL17	Plasmid carrying *lacZ*, *bla* and *sacB* genes as a *Pac*I cassette. Amp^R	(Parish and Stoker, 2000)
pMV306H	Genetic complementation vector, which integrates at the *attB* site in the mycobacterial genome. Hyg^R	H. Boshoff
pTweety	Complementation vector carrying an integrase gene. Kan^R	(Pham et al., 2007)
pGEM3Z(+)f	*E. coli* cloning vector. Amp^R	Promega
pGEM+5526 ::*hyg*	Derivative of pGEM3Z(+)f carrying the Δ*mepB1* (MSMEG_5526) deletion allele.	This study
p0247KO	Derivative of p2NIL carrying the Δ*mepB2* (MSMEG_0247) deletion allele and the *lacZ* and *sacB* genes. Kan^R	This study
pUC57+0247	Gene deletion plasmid carrying the Δ*mepB2* allele and a crelox sequence. Amp^R	GeneScript
p0247KO+*aadA*	*mepB2* gene deletion plasmid carrying the streptomycin resistance gene *aadA*. Str^R	This study
pNIT	Mycobacterial replication plasmid that allows the inducible expression of the phage Che9c RecET recombination system, and constitutive expression of the *sacB* gene. Kan^R	(Murphy et al., 2015)
p1192KO	Derivative of p2NIL carrying the *mepB3* (MSMEG_1192) deletion allele and the *lacZ* and *sacB* genes. Kan^R	This study
pMV306H+0247	Derivative of pMV306H carrying a wild type *mepB2* allele with its native promoter. Hyg^R	This study
pTweety+1192	Derivative of pTweety carrying a wild type *mepB3* allele with its native promoter; Kan^R	This study

pMV306H+GFP	Derivative of pMV306H carrying a green fluorescence protein (GFP). Hyg^R	CBTBR
pMV306H+0247GFP	Derivative of pMV306H+GFP carrying a wild type *mepB2* allele with its native promoter. This plasmid expresses a MepB2+GFP fusion protein. Hyg^R	This study
pMV306H+1192GFP	Derivative of pMV306H+GFP carrying a wild type *mepB3* allele with its native promoter. This plasmid expresses a MepB3+GFP fusion protein. Hyg^R	This study
pTweety+DivIVGFP	Derivative of pTweety carrying a wild type DivIVA allele tagged with GFP. This plasmid expresses a DivIVA+GFP fusion protein . Kan^R	CBTBR M. Maphatsoe
pTweety+FtsZGFP	Derivative of pTweety carrying a wild type FtsZ allele tagged with GFP. This plasmid expresses a FtsZ+GFP fusion protein. Kan^R	CBTBR M. Maphatsoe
pUAB300	*E. coli* - Mycobacterial shuttle plasmid carrying the mDHFR fragment 1 and 2, together with a glycine linker. Hyg^R	(Singh et al., 2006)
pUAB400	*E. coli* - Mycobacterial shuttle plasmid carrying mDHFR fragment 3. Kan^R	(Singh et al., 2006)
pUAB300+FtsX	Derivative of pUAB300 carrying the wild type allele of FtsX (MSMEG_2090). Hyg^R	This study
pUAB400+0247	Derivative of pUAB400 carrying the wild type allele of *mepB2*. Kan^R	This study
pUAB400+1192	Derivative of pUAB400 carrying the wild type allele of *mepB3*. Kan^R	This study
pUAB300+RipA	Derivative of pUAB300 carrying the wild type allele of *ripA*. Hyg^R	CBTBR
pUAB400+RpfB	Derivative of pUAB400 carrying the wild type allele of *rpfB*. Kan^R	CBTBR
pFLAGEM	*E. coli*-Mycobacterial episomal shuttle vector carrying the 3X FLAG epitope sequence and the Tet-operator. Hyg^R	CBTBR
pFLAGEM+0247	Derivative of pFLAGEM carrying the wild type *mepB2*	This study

	allele; Hyg^R	
pFLAGEM+1192	Derivative of pFLAGEM carrying the wild type *mepB3* allele. Hyg^R	This study

Table 2.1: **Bacterial strains created and/or used in this study.**

Strain	Description	Source/ Reference
E. coli DH5α	*SupE44 ΔlacU169 hsdR17 recA1 endA1 gyrA96 thi-1 relA1*	Promega, Madison, WI
mc^2155	High frequency transformation mutant of *M. smegmatis* ATCC 607	
Δ*mepB1*	Derivative of mc^2155 with a marked deletion in *mepB1* (MSMEG_5526). Constructed by electroporation of plasmid pGEM+5526+*hyg* into the strain mc^2155. Hyg^R	This study
Δ*mepB2*	Derivative of mc^2155 with a marked deletion in *mepB2* (MSMEG_0247). Constructed by electroporation of plasmid p0247KO+*aadA* into the strain mc^2155. Str^R	This study
Δ*mepB2*::*mepB2*	Genetically complemented derivative of Δ*mepB2* with a full length copy of *mepB2* at the *attB* site. Constructed by electroporation of plasmid pMV306H+0247 into the strain Δ*mepB2*. Hyg^R	This study
Δ*mepB3*	Derivative of mc^2155 with an unmarked deletion in *mepB3* (MSMEG_1192). Constructed by electroporation of plasmid p1192KO into the strain mc^2155.	This study
Δ*mepB3*::*mepB3*	Genetically complemented derivative of Δ*mepB3* with a full length copy of *mepB3* at the *tRNA* glycine site. Constructed by electroporation of plasmid pTweety+1192 into the strain Δ*mepB3*. Kan^R	This study
Δ*mepB2* Δ*mepB3*	Derivative of Δ*mepB3* with a marked deletion of *mepB2*. Constructed by electroporation of plasmid p0247KO+*aadA* into the strain Δ*mepB3*. Str^R	This study
Δ*mepB2*Δ*mepB3*:	Genetically complemented derivative of Δ*mepB2*	This study

:*mepB2 mepB3*	Δ*mepB3* with a full length copy of *mepB2* and *mepB3* at the *attB* site and *tRNA* glycine site respectively. Constructed by electroporation of plasmids pMV306H+0247 and pTweety+1192 into Δ*mepB2* Δ*mepB3*. Kan^R Hyg^R	
0247GFP	Derivative of Δ*mepB2* expressing a GFP tagged wild type allele of *mepB2* at the *attB* site. Constructed by electroporation of plasmid pMV306H+0247GFP into strain Δ*mepB1*. Hyg^R	This study
1192GFP	Derivative of Δ*mepB3* expressing a GFP tagged wild type allele of *mepB3* at the *attB* site. Constructed by electroporation of plasmid pMV306H+1192GFP into Δ*mepB3*. Hyg^R	This study
$mc^2$155::DivIVA GFP	Derivative of $mc^2$155 expressing a GFP tagged wild type allele of DivIVA at the at the *tRNA* glycine site. Constructed by electroporation of plasmid pTweety+DivIVA-GFP into $mc^2$155. Kan^R	This study
$mc^2$155::FtsZGFP	Derivative of $mc^2$155 expressing a GFP tagged wild type allele of FtsZ at the *tRNA* glycine site. Constructed by electroporation of plasmid pTweety+FtsZ-GFP into $mc^2$155. Kan^R	This study
Δ*mepB2* Δ*mepB3* ::DivIVAGFP	Derivative of Δ*mepB2* Δ*mepB3* expressing a GFP tagged wild type allele of DivIVA at the *tRNA* glycine site. Constructed by electroporation of plasmid pTweety+DivIVA-GFP into Δ*mepB2* Δ*mepB3*. Kan^R	This study
Δ*mepB2* Δ*mepB3* ::FtsZGFP	Derivative of Δ*mepB2* Δ*mepB3* expressing a GFP tagged wild type allele of FtsZ at the at the *tRNA* glycine site. Constructed by electroporation of plasmid pTweety+FtsZ-GFP into Δ*mepB2* Δ*mepB3*. Kan^R	This study
0247FLAG	Derivative of $mc^2$155 with a FLAG tagged wild type allele of *mepB2* at the *attB* site. Constructed by electroporation of plasmid pFLAGEM+0247 into $mc^2$155. Hyg^R	This study

1192FLAG	Derivative of mc^{2}155 with a FLAG tagged *mepB3* allele at the *attB* site. Constructed by electroporation of plasmid pFLAGEM+1192 into strain mc^{2}155. Hyg^R	This study
mc^{2}155::FtsX	Derivative of mc^{2}155 carrying plasmid pUAB300+FtsX. Hyg^R	This study
mc^{2}155::MepB2	Derivative of mc^{2}155 carrying plasmid pUAB400+0247. Kan^R	This study
mc^{2}155::MepB3	Derivative of mc^{2}155 carrying plasmid pUAB400+1192. Kan^R	This study
mc^{2}155::FtsX MepB2	Derivative of mc^{2}155 carrying plasmids pUAB300+FtsX and pUAB400+0247. Kan^R Hyg^R Trim^R	This study
mc^{2}155::FtsX MepB3	Derivative of mc^{2}155 carrying plasmids pUAB300+FtsX and pUAB400+1192. Kan^R Hyg^R Trim^R	This study
mc^{2}155::RipA RpfB	Derivative of mc^{2}155 carrying plasmids pUAB300+RipA and pUAB400+RpfB. Kan^R Hyg^R Trim^R	CBTBR
mc^{2}155::pUAB400+pUAB300	Derivative of mc^{2}155 carrying plasmids pUAB300 and pUAB400. Kan^R Hyg^R	CBTBR

Amp^R: Ampicillin resistance, Hyg^R: Hygromycin resistance, Kan^R: Kanamycin resistance, Str^R: Streptomycin resistance, Trim^R: Trimethoprim resistance.

2.3. Bacterial growth conditions

2.3.1. Growth conditions for *E. coli* DH5α and derivative strains

E. coli DH5α and derivative strains were grown in Lysogeny broth (LB) or on Luria-Bertani agar (LA) at 37 °C with supplementation of the media with appropriate antibiotics. The antibiotic concentrations used were as follows: Kanamycin (Kan): 50 μg/ml, Hygromycin (Hyg): 200 μg/ml, Streptomycin (Str): 50 μg/ml or Ampicillin (Amp): 100 μg/ml. Liquid cultures were grown at 37 °C with shaking at a 100 rpm.

2.3.2. Growth conditions for *M. smegmatis* mc^{2}155 and derivative strains

M. smegmatis mc^{2}155 and derivative strains were grown at 37 °C in Middlebrook 7H9 broth supplemented with 0.2% glucose, 0.2% glycerol, 0.085% NaCl, 0.05% Tween 80 and appropriate antibiotics (hereafter referred to as Middlebrook 7H9 broth) or on Middlebrook 7H10 agar supplemented with 0.5% glycerol, 0.2% glucose, 0.085% NaCl and appropriate

antibiotics (hereafter referred to as Middlebrook 7H10 agar). The antibiotics used for supplementation of the media were at the following concentrations: Kan: 25 μg/ml, Hyg: 50 μg/ml or Str: 100 μg/ml. Middlebrook 7H9 broth cultures were grown at 37 °C with shaking at 100 rpm.

2.4. DNA extractions

2.4.1. *M. smegmatis* mc^{2}155 chromosomal DNA extractions

2.4.1.1. Small scale chromosomal DNA extraction

The colony boil method was used for small scale chromosomal DNA extraction. Briefly, a single colony of *M. smegmatis* mc^{2}155 or derivative strains was scraped from an agar plate and resuspended in 50 μl of distilled water (dH_2O). Subsequently, 50 μl of chloroform was added and mixed with the cells by vortexing. The mixture was then incubated at 65 °C for 10 minutes. Thereafter, the sample was centrifuged at 12470 *X g* for 5 minutes and the supernatant was transferred into a clean tube. For PCR, 5 μl of this sample was used as DNA template.

2.4.1.2. Large scale chromosomal DNA extraction

The Cetyltrimethylammonium bromide (CTAB) DNA extraction method was used for large scale chromosomal DNA extraction. *M. smegmatis* mc^{2}155 and derivative strains were grown at 37 °C on Middlebrook 7H10 agar for 2 days. The cells were harvested by scraping from the agar plates and this was followed by resuspension of cells in 500 μl of TE buffer. The cells were incubated at 95 °C for 20 minutes. Following the incubation, the cells were put on ice for 10 minutes. Thereafter, 50 μl of lysozyme (10 mg/ml) was added and the mixture was incubated at 37 °C for an hour. Subsequently, 6 μl of proteinase K (10 mg/ml) and 70 μl of 10% SDS were added and the mixture was incubated at 65 °C for an hour. Following this, 100 μl of NaCl (5M) and 80 μl of pre-warmed CTAB/NaCl (10% N-cetyl-N,N,N-trimethyl ammonium bromide, 4.1% NaCl dissolved in dH_2O) were added. The mixture was incubated at 65 °C for 10 minutes. Thereafter, 750 μl of chloroform: Isoamyl alcohol solution (24:1 ratio) was added to the cells, which was mixed by inverting the tubes, followed by centrifugation at 12470 *X g* for 10 minutes. The top aqueous layer was transferred into a clean tube into which 450 μl of isopropanol was added. The DNA was precipitated by centrifugation at 12470 *X g* for 30 minutes. Thereafter, the supernatant was discarded and the pellet was washed with 1 ml of 70% ethanol by centrifugation at 12470 *X g* for 5 minutes and

dried using an Epperndorf Concentrator 5301. The DNA pellet was resuspended in 50 µl of nuclease free water and quantified using the NanoDrop ND-1000 Spectrophotometer (NanoDrop technologies). The DNA was stored at 4 °C until further use.

2.4.2. **Plasmid DNA extraction from *E. coli* DH5α**

2.4.2.1. **Small scale plasmid DNA extraction from *E. coli* DH5α**

The alkaline lysis mini-preparation method was used for small scale plasmid DNA extraction. *E. coli* DH5α derivative strains carrying plasmids of interest were grown overnight at 37 °C in 2 ml of LB media supplemented with appropriate antibiotics. Thereafter, the cells were harvested by centrifugation at 12470 *X g* for 5 minutes and resuspended in 80 µl of solution 1 (50 mM glucose, 25 mM Tris-HCl [pH 8] and 10 mM EDTA). Following this, 160 µl of solution 2 (1% SDS and 0.2 M NaOH) was added, mixed with the cells by inversion and incubated at ambient temperature for 5 minutes. Subsequently, 120 µl of solution 3 (3 M potassium acetate, 11.5% acetic acid) was added and mixed vigourously and incubated on ice for 5 minutes. The sample was then centrifuged at 12470 *X g* for 10 minutes and the supernatant was transferred into a clean tube. Following this, 3 µl of RNAse A (10 mg/ml) was added to the supernatant and this mixture incubated at 42 °C for 15 minutes. Plasmid DNA was precipitated by addition of 600 µl of isopropanol and centrifugation at 12470 *X g* for 30 minutes. The supernatant was discarded and the pellet was washed with 1 ml of 70% ethanol and dried using an Epperndorf concentrator 5301. The plasmid DNA pellet was resuspended in 50 µl of nuclease free water and quantified using the NanoDrop ND-1000 Spectrophotometer (NanoDrop technologies). The DNA was stored at 4 °C until further use.

2.4.2.2. **Large scale plasmid DNA extraction from *E. coli* DH5α**

The Nucleobond DNA extraction kit (Macherey-Nagel) was used for large scale plasmid DNA extraction following manufacturer's instructions. Briefly, *E. coli* DH5α strains carrying plasmids of interest were grown overnight at 37 °C in 50 ml of LB media supplemented with appropriate antibiotics. The cells were harvested by centrifugation at 1180 *X g* for 15 minutes. The supernatant was discarded and the pellet of cells was resuspended in 4 ml of Buffer S1 (50 mM Tris-HCl, 10 mM EDTA, 100 µg/ml Rnase, pH 8.0) with subsequent addition 4 ml of Buffer S2 (200 mM NaOH, 1% SDS). The sample was mixed by inversion and incubated at ambient temperature for 3 minutes. Thereafter, 4 ml of Buffer S3 (2.8 M KAc, pH 5.1) was added to the sample, mixed by inversion and incubated on ice for 5

minutes. The mixture was then centrifuged at 1180 *X g* for 30 minutes. A nucleobond Ax100 column was equilibrated with 2.5 ml of Buffer N2 (100 mM Tris, 15% ethanol, 900 mM KCl, 0.15% Triton X-100, adjusted to pH 6.3 with H_3PO_4). This was followed by addition of the clarified supernatant through the column. Thereafter, 10 ml of Buffer N3 (100 mM Tris, 15% ethanol, 1.15 M KCl, adjusted to pH 6.3 with H_3PO_4) was used to wash the column. 5 ml of Buffer N5 (100 mM Tris, 15% ethanol, 1 M KCl, adjusted to pH 8.5 with H_3PO_4) was then used for elution of plasmid DNA from the column into a clean tube. The plasmid DNA was precipitated by addition of 3.5 ml of isopropanol to the sample and centrifugation of the mixture at 12470 *X g* for 30 minutes. The pellet was washed with 1 ml 70% ethanol. Thereafter, the supernatant was discarded and the pellet was dried using an Eppendorf Concentrator 5301.

As an alternative method for large scale plasmid purification, the small scale plasmid DNA extraction protocol described above (section 2.4.2.1) was up-scaled. Briefly, *E. coli* DH5α derivative strains carrying plasmids of interest were grown overnight at 37 °C in 50 ml of LB media supplemented with appropriate antibiotics. The cells were harvested by centrifugation at 1180 *X g* for 15 minutes. The supernatant was discarded and the pellet was resuspended in 0.8 ml of solution 1. Thereafter, 1.6 ml of solution 2 was added, mixed by inversion and incubated at ambient temperature for 10 minutes. Afterwards, 1.2 ml of solution 3 was added, mixed with the cells and incubated on ice for 10 minutes. The sample was centrifuged at 1180 *X g* for 30 minutes and 900 µl of the resultant supernatant was transferred into clean tubes. Following this, 3 µl of RNAse A (10 mg/ml) was added to the samples and the samples were incubated at 42 °C for 15 minutes. Plasmid DNA was precipitated by addition of 600 µl of isopropanol and centrifugation of the sample at 12470 *X g* for 30 minutes. The supernatant was discarded and the pellet was washed with 1 ml of 70% ethanol and dried using an Epperndorf concentrator 5301. The plasmid DNA pellet was resuspended in 50 µl of nuclease free water and quantified using the NanoDrop ND-1000 Spectrophotometer (NanoDrop technologies). The DNA was stored at 4 °C until further use.

2.5. DNA manipulations

2.5.1. DNA amplification

2.5.1.1. Designing PCR primers

The online software Primer3 (http://bioinfo.ut.ee/primer3/) was used to design PCR primers using the parameters indicated in Table 3.

Table 3: **Parameters used for designing primers through Primer3.**

	Size (bp)	Tm (°C)	% GC
Minimum	18	55	30
Optimum	21	60	50
Maximum	24	65	70

2.5.1.2. Polymerase Chain Reaction (PCR)

2.5.1.2.1. Phusion High-Fidelity DNA polymerase reaction

The Phusion High-Fidelity DNA polymerase (Thermo Scientific) was used according to the manufacturer's instructions for PCR synthesis of DNA fragments used for cloning. Briefly, PCR reactions were conducted in a final volume of 50 µl by the addition of 5 µl 5 X HF buffer, 8 µl of dNTPs (0.2 mM each), 100 ng of DNA template, 2.5 µl of primers (1 mM each), 1 U of Phusion DNA polymerase, 3% of dimethyl sulfoxide (DMSO) and nuclease free dH_2O to make up the final volume. A thermo-cycler (Bio-Rad Laboratories) was used to incubate the samples using the following parameters: 3 minutes of initial denaturation at 98 °C, 35 cycles of 30 seconds of secondary denaturation at 98 °C, 30 seconds of annealing at 65 °C, 1 minute of extension at 72 °C and 10 minutes of final extension at 72 °C. PCR DNA products were visualized on a 1% agarose gel as indicated in section 2.5.4.

2.5.1.2.2. Roche FastStart Taq DNA polymerase reaction

The Roche FastStart Taq DNA polymerase (Roche Applied Science) was used according to the manufacturer's instructions for PCR confirmation of clones or *M. smegmatis* gene deletion mutants. Briefly, PCR reactions were conducted in a final volume of 50 µl by the addition of 5 µl of 10 X Roche FastStart Taq DNA polymerase buffer, 10 µl of GC buffer, 2.5 µl of primers, 100 ng of DNA template, 1 U of Roche FastStart Taq DNA polymerase, 8 µl of dNTPs (0.2 mM each) and nuclease free dH_2O to make up the final volume. A thermo-cycler (Bio-Rad Laboratories) was used to incubate the samples using the following parameters: 3 minutes of initial denaturation at 95 °C, 35 cycles of 30 seconds of secondary denaturation at 95 °C, 30 seconds of annealing at 65 °C, 1 minute of extension at 72 °C and 10 minutes of final extension at 72 °C. PCR DNA products were visualized on a 1% agarose gel as indicated in section 2.5.4.

2.5.2. **DNA purification by sodium acetate precipitation**

The sodium-acetate DNA precipitation protocol was used to remove contaminating proteins, salt and other impurities from extracted chromosomal DNA, plasmid DNA or PCR DNA products. Briefly, the volume of the DNA was adjusted to 100 µl with dH_2O and 10 µl of sodium acetate (3 M, pH 5.2) was added and the sample was mixed. Thereafter, 390 µl of ice-cold 100% ethanol was added, the sample was mixed and centrifuged at 12470 $X\ g$ for 15 minutes. The supernatant was discarded and the pellet was dried using an Eppendorf concentrator 5301 and resuspended in 50 µl of nuclease free water. The DNA was stored at 4 °C.

2.5.3. **Restriction digestions**

Restriction digestions of plasmids used in this study were performed through the use of restriction enzymes purchased from Fermentas (Fermantas), New England Biolabs (NEB) or Roche Applied Science (Roche). Restriction digests of plasmids and PCR products were performed following manufacturer's instructions. Briefly, restriction digestions were conducted in a final volume of 20 µl per reaction with the addition of 1 µg of plasmid or PCR DNA, 2 µl of a restriction enzyme specific buffer, 1 U of restriction enzyme, 2 µl of 100 X BSA (Bovine serum albumin) when necessary, dH_2O was added to make up the final volume. The sample was incubated at 37 °C for an hour, unless stated otherwise by the manufacturer's instructions. Afterwards, the restriction digestion reaction was terminated by heat inactivation at 65 °C for 10 minutes unless stated otherwise by the manufacturer.

2.5.4. **Agarose gel electrophoresis**

Agarose gel electrophoresis was used for visualization of extracted chromosomal DNA, plasmid DNA or PCR DNA products. The DNA was separated on 1% agarose gels prepared with 1 X TAE buffer (1 mM EDTA and 40 mM Tris-acetate) and the addition of ethidium bromide to a final concentration of 0.5 µg/ml. Electrophoresis was performed in agarose gel electrophoresis tanks (Bio-Rad Laboratories) containing 1 X TAE buffer at 90 V for 45 minutes. DNA molecular weight markers were also loaded on the agarose gel for estimation of the molecular weight of the DNA sample analyzed. The DNA on the agarose gel was visualized using a SYNGENE G-Box system.

2.5.5. **DNA fragment purification**

The NucleoSpin PCR clean-up and gel extraction kit (Macherey-Nagel) was used according to the manufacturer's instructions for purification of PCR DNA products or DNA fragments excised from an agarose gel. Briefly, the agarose gel slice containing the excised DNA fragment was solubilized by incubation at 50 °C for 5 minutes and for both the solubilized gel slice on PCR DNA product clean-up, 1 volume of sample was mixed with 2 volumes of buffer NTI. Thereafter, the sample was loaded into a NucleoSpin PCR clean-up column, which was inserted into a collection tube. For DNA binding, the sample was centrifuged for 30 seconds at 11 000 rpm. The flow-through in the collection tube was discarded and 700 µl of buffer NT3 was added into the column, followed by centrifugation at 11 000 rpm for 30 seconds. The flow-through in the collection tube was discarded and the column was dried by centrifugation at 11 000 rpm for 1 minute. The DNA was eluted into a clean microcentrifuge tube by the addition of 20 µl of buffer NE into the column and centrifugation of the sample at 11 000 rpm for 1 minute. The DNA was stored at 4 °C until further use.

2.5.6. **Dephosphorylation and phosphorylation of DNA**

Antarctic Alkaline Phosphatase (NEB) was used to remove phosphate groups at the 5′ end of linearized plasmid DNA to prevent self-ligation according to the manufacturer's instructions. Dephosphorylation reactions were conducted in a final volume of 20 µl per reaction by the addition of 1 µg of linearized plasmid DNA, 1 U of Antarctic Alkaline Phosphatase, 2 µl of Antarctic Alkaline Phosphatase buffer (NEB) and dH_2O to make up the final volume. The sample was incubated at 37 °C for an hour and the reaction was terminated by heat inactivation at 65 °C for 20 minutes.

2.5.7. **DNA ligation**

T4 DNA ligase (NEB or Thermo Scientific) was used for ligation of PCR DNA fragments into plasmid DNA according to the manufacturer's instructions. Briefly, the ligation reaction was performed in a final volume of 20 µl per reaction by the addition of 50 ng of plasmid DNA, 2 µl of T4 DNA ligase buffer, 5 U of T4 DNA ligase, "X" amount (ng) of DNA insert (X - calculated using the formula indicated below) and dH_2O was added to make up the final volume. To optimize the ligation efficiency, 1:1, 2:1 and 1:2 molar ratios of vector to insert were used for ligations. The samples were incubated at ambient temperature for 20 minutes

and the ligation reaction was terminated by heat inactivation at 65 °C for 10 minutes. The DNA ligation products were used to transform chemically competent *E. coli* DH5α cells as indicated in section 2.6.2. The amount of insert for each ligation (using 50 ng of vector as a starting concentration standard) was calculated as follows:

$$\text{Amount of insert (ng)} = \frac{\text{Amount of vector (50 ng) x Size of insert (bp)}}{\text{Size of vector (bp)}}$$

2.5.8. **DNA sequencing**

DNA sequencing was performed at the DNA sequencing Facility of Stellenbosch University. The BigDye Terminator v3.1 Cycle sequencing kit (Applied Biosystems) was used for DNA sequencing and the DNASTAR Software (DNASTAR) was used for analysis of the DNA sequencing data.

2.5.9. **Southern blotting**

Southern blotting was used for confirmation of gene deletions in *M. smegmatis*. The different steps of this method are discussed below.

2.5.9.1. **Synthesis of the DNA probe**

The PCR DIG Probe Synthesis kit (Roche Applied Science) was used for synthesis of the Alkali-labile digoxigenin (DIG)-dUTP probe according to the manufacturer's instructions. Briefly, the PCR reaction was conducted in a final volume of 50 µl per reaction by the addition of 5 µl of 10 X Roche FastStart Taq DNA polymerase buffer, 10 µl of GC buffer, 2.5 µl of primers (1 mM each), 100 ng of DNA template, 1 U of Roche FastStart Taq DNA polymerase, 4 µl of dNTPs (0.2 mM each), 2.5 µl of PCR DIG labeling mix and nuclease free dH_2O to make up the final volume. A negative control, unlabelled PCR product was synthesized as indicated in section 2.5.1.2.2 without the addition of the DIG labeling mix. A thermo-cycler (Bio-Rad Laboratories) was used to incubate the samples using the following parameters: 3 minutes of initial denaturation at 95 °C, 35 cycles of 30 seconds secondary denaturation at 95 °C, 30 seconds of annealing at 65 °C, 1 minute of extension at 72 °C and 10 minutes of final extension at 72 °C. Thereafter, the DIG-labelled sample and the negative, un-labelled control PCR product were separated on a 1% agarose gel as indicated in section 2.5.4. Incorporation of the DIG label into the synthesized DNA fragment results in a higher molecular weight product. The probe was stored at -20 °C until further use.

2.5.9.2. **Electro-blotting**

Chromosomal DNA was extracted from the wild type *M. smegmatis*, derivative single cross over strains (SCOs) and double cross over (DCO) mutant strains according to the protocol indicated in section 2.4.1.2. Appropriate restriction enzymes for restriction digestion of the chromosomal DNA were selected using the Clone manager v6 software (Sci Ed Central). Thereafter, 2 μg of chromosomal DNA was digested in a final reaction volume of 20 μl by the addition of 5 U of the selected restriction enzyme, 2 μl of the restriction enzyme specific buffer and nuclease free water to make up the final volume. The sample was incubated at 37 °C overnight. The digested DNA was then separated on a 0.8% agarose gel with a molecular weight marker IV (Fermentas) at 80 V for 2 hours. The agarose gel was visualized using a SYNGENE G-Box system. Depurination of the DNA in the agarose gel was conducted by incubation in 0.2 M HCl (depurination solution) for 15 minutes with shaking. The depurination solution was discarded and the agarose gel was subsequently washed with 1 X TBE (89 mM Tris-Borate and 2 mM EDTA) buffer (pH 8.3). The 1 X TBE buffer was discarded and the DNA was denaturated by incubation in denaturation solution (0.5 M NaOH and 1.5 M NaCl) with shaking at ambient temperature for 30 minutes, followed by washing with 1X TBE. Then, a Hybond^{TM}-neutral nitrocellulose membrane (Amersham Biosciences) was placed on top of the agarose gel and this was sandwiched between 2 Whatman filter papers and 2 porous sponge layers. The sandwiched agarose gel was placed in an agarose gel cassette (Bio-Rad Laboratories) and this was then placed in a SB10 gel tank (Bio-Rad Laboratories) containing 1 X TBE buffer. The DNA on the agarose gel was transferred to the Hybond^{TM}-neutral nitrocellulose membrane at 600 mA for 2 hours. Thereafter, the DNA was cross-linked to the nitrocellulose membrane by ultra-violet light irradiation using the following parameters: energy: 2500 mJ/cm^3, time: 2 minutes, in a UVC 500 Crosslinker (Amersham Biosciences).

2.5.9.3. **Hybridization**

The nitrocellulose membrane with the DNA was placed in a roller bottle (Thermo Scientific) and 10 ml of DIG Easy Hyb solution (Roche Applied Science) was added into the roller bottle and incubated at 54 °C for 30 minutes. Thereafter, the DIG Easy hyb solution was discarded and the DIG labelled probe, synthesized as described in section 2.5.9.1, was denatured by incubation at 95 °C for 5 minutes, followed by cooling on ice for 5 minutes. The denatured probe was added into the roller bottle containing the nitrocellulose membrane.

The roller bottle was incubated overnight at 54 °C in a Hybaid Micro-4 hybridization oven (Thermo Scientific). The nitrocellulose membrane was then washed with solution 1 (2 X SSC and 0.1% SDS) at ambient temperature for 5 minutes with shaking. Solution 1 was discarded and solution 2 (0.5 X SSC and 0.1% SDS) was used to wash the nitrocellulose membrane twice for 15 minutes at 68 °C in the hybridization oven.

2.5.9.4. **Immunological detection**

The nitrocellulose membrane was washed at ambient temperature for 5 minutes in wash buffer (0.1 M maleic acid buffer and 0.3% Tween 20) and incubated in 50 ml of 1 X blocking solution (10 ml of 10 X blocking solution [Roche Applied Science], diluted in 90 ml of 0.1 M maleic acid buffer) for 30 minutes with shaking. The blocking solution was discarded and the nitrocellulose membrane was incubated for 30 minutes in 30 ml of antibody solution (30 ml of 1 X blocking solution mixed with 3 µl of Anti-Digoxygenin antibody [Roche Applied Science]). The nitrocellulose membrane was then washed twice with wash buffer for 15 minutes and, thereafter, incubated in detection buffer (0.1 M Tris-HCl, 0.1 M NaCl in dH_2O [pH 9.5]) for 5 minutes. The membrane was placed in a hybridization bag (Roche Applied Science) with the DNA side facing up followed by the addition of 1 ml of chloro-5-substituted adamantyl-1,2-dioxetane phosphate (CSPD) substrate. The CSPD was spread to cover the whole nitrocellulose membrane which was incubated at ambient temperature for 10 minutes. Excess CSPD was removed and the hybridization bag was sealed and incubated at 37 °C for 30 minutes. The nitrocellulose membrane was then exposed to X-ray film (Thermo Scientific) for 30 minutes. The X-ray films were developed manually by incubation in developing solution for 30 seconds, followed by rinsing in dH_20 for 30 seconds and incubation in fixing solution for 30 seconds, followed by rinsing in dH_20 for 30 seconds. The film was hung to dry.

2.6. **Bacterial transformations**

2.6.1. **Preparation of chemically competent *E. coli* DH5α cells**

Chemically competent *E. coli* DH5α were prepared using the calcium chloride protocol. A single colony of *E. coli* DH5α was inoculated into 50 ml of LB and incubated overnight at 37 °C with shaking at 100 rpm. Thereafter, 1 ml of the pre-culture was inoculated into 100 ml of LB and incubated at 37 °C with shaking at a 100 rpm for 2 hours. The cells were harvested by centrifugation at 1180 *X g* for 5 minutes at 4 °C. The supernatant was discarded and the cells

were resuspended in 10 ml of cold $CaCl_2$ (0.1 M) and immediately placed on ice for 20 minutes. The cells were centrifuged as before, resuspended in 5 ml of cold $CaCl_2$ (0.1 M) and used immediately for transformations with plasmids.

2.6.2. **Transformation of chemically competent *E. coli* DH5α cells**

A 100 µl aliquot of chemically competent *E. coli* DH5α cells was mixed with plasmid DNA. The cells were incubated on ice for 15 minutes and transformed by heat shock at 42 °C for 90 seconds. Subsequently, 200 µl of pre-warmed LB media was added and the cells were incubated at 37 °C for an hour, with shaking at a 100 rpm. Thereafter, the cells were inoculated on LA plates supplemented with the appropriate antibiotic. The LA plates were incubated overnight at 37 °C. Single colonies were picked and screening for positive clones, performed as described in sections 2.4.2.1, 2.5.3 and 2.5.4.

2.6.3. **Preparation of electro-competent mc^2155 or derivative strains**

M. smegmatis cells were inoculated into 50 ml of Middlebrook 7H9 broth and grown to an optical density $(OD)_{600}$ of 0.5-0.8. The cells were harvested by centrifugation at 1180 *X g* for 10 minutes at 4 °C. The supernatant was discarded and the cells were resuspended and washed in 10 ml of ice cold 10% glycerol and harvested as before. The washing step was repeated twice and the cells were resuspended in 2 ml of ice cold 10% glycerol and used immediately for transformation with plasmids as described below.

2.6.4. **Electroporation of plasmids into *M. smegmatis***

Approximately 1 µg of plasmid DNA was used to transform electro-competent *M. smegmatis* cells or derivative strains by mixing 300 µl of cells with the plasmid DNA and transferring the mixture into a pre-chilled 0.2 cm electroporation cuvette (Bio-Rad Laboratories). The cells were incubated on ice for 15 minutes and the Bio-Rad Gene Pulser XCell™ (Bio-Rad Laboratories) system was used to perform plasmid DNA electroporations with the following parameters: voltage: 2500 V, unit of capacitance: 25 µF, resistance: 1000 Ω and distance: 0.2 cm. After electroporation, 800 µl of LB media was added to the electroporation cuvette and the cells were transferred into a clean tube and incubated at 37 °C overnight. Thereafter, the cells were pelleted by centrifugation at 12470 *X g* and the supernatant was discarded followed by the resuspension of the cells in 500 µl of Middlebrook 7H9 broth. The cells were

inoculated onto Middlebrook 7H10 agar containing appropriate antibiotics and incubated at 37 °C for 3-5 days.

2.6.5. **Generation of *M. smegmatis* mutant strains**

2.6.5.1. **Two-step allelic exchange homologous recombination method for generation of *M. smegmatis* mutant strains**

The two-step allelic exchange homologous recombination method, described by Gordhan and Parish (Gordhan and Parish, 2001), was used for deletion of genes of interest from *M. smegmatis* mc^2155 or derivative mutant strains. The underlying premise of the approach is shown in Figure 2.1. Briefly, a mutated copy of the gene of interest is synthesized by ligation of upstream and downstream regions of the gene. This mutated gene is incorporated into a suicide plasmid according to the protocol outlined in section 2.5.7. The selectable marker gene *lacZ,* encoding beta-galactosidase, and the counter-selectable marker gene *sacB,* encoding levansucrase, were excised from the plasmid pGOAL17 as a single linear DNA fragment according to the protocol outlined in section 2.5.3. The DNA fragment carrying the selectable markers was cloned into the suicide plasmid carrying the mutated gene according to the protocol outlined in section 2.5.7. The resultant plasmid construct was sequenced according to the protocol described in section 2.5.8 prior to electroporation of this plasmid into *M. smegmatis* or derivative strains. Electroporation of this plasmid DNA into wild type *M. smegmatis* or derivative mutant strains, performed according to the protocol outlined in section 2.6.4, results in the integration of the suicide plasmid into the chromosome through either upstream or downstream regions of homology. The resultant strain (a single cross-over [SCO] strain) is identified as a blue colony that is kanamycin (kan) resistant when grown on Middlebrook 7H10 agar supplemented with Kan (25 μg/ml), and 2% X-gal. These phenotypes of the transformant strain are due to the presence of the selectable markers *aph:* for kanamycin resistance and *lacZ*: a gene encoding for beta-galactosidase, as indicated above, which uses X-gal as a substrate and produces a blue pigment. Subsequently, the SCO strain was grown until stationary phase in 5 ml of Middlebrook 7H9 broth supplemented with Kan (25 μg/ml). Thereafter, a 100 μl aliquot of this pre-culture was inoculated in 5 ml of Middlebrook 7H9 broth without antibiotic and grown until stationary phase.

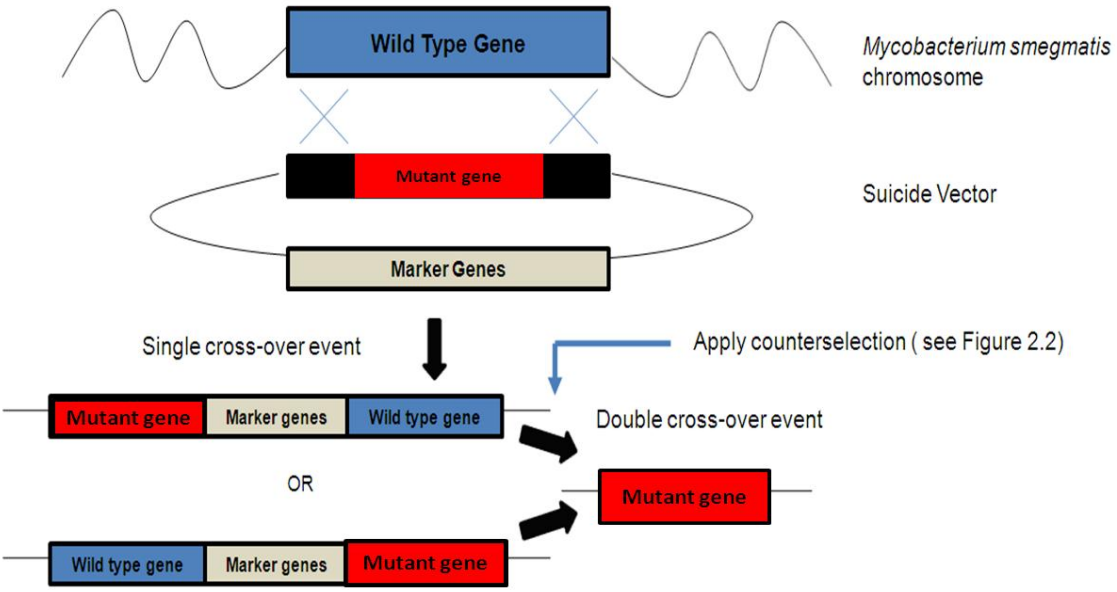


Figure 2.1: **Schematic representation of the two step, allelic exchange homologous recombination**. A non-replicating plasmid carrying a mutated version of the gene is introduced into *M. smegmatis*. Homologous recombination leads to generation of a single cross-over strain, Single cross-overs carry both wild type and mutated alleles of the gene and any marker genes found on the plasmid, whereas double cross-overs will carry one copy of the mutant allele and no marker genes. Adapted from (Gordhan and Parish, 2001).

This process allows for the second cross-over event to occur whereby cells lose the suicide plasmid and can retain either the wild type gene or the mutant gene. As indicated above, the additional counter-selectable marker levansucrase encoded by the *sacB* gene uses sucrose as a substrate and produces the polymeric levan $(2,6\text{-}\beta\text{-D-fructosyl})_n$, which disturbs cell metabolism and growth, leading to cell death. Therefore, SCO integrants that have not released the suicide plasmid from the chromosome cannot survive when grown on Middlebrook 7H10 agar supplemented with 5% sucrose. This facilitates the second cross-over event.

For counterselection, a 100 µl aliquot of the cells grown in the absence of antibiotic was serially diluted from 10^1 to10^6 and a 100 µl of each dilution was inoculated onto Middlebrook 7H10 agar supplemented with only 2% X-gal and also onto Middlebrook 7H10 agar supplemented with 2% X-gal and 5% sucrose. Cells in which a second cross-over event had occurred formed white colonies that survived on Middlebrook 7H10 agar supplemented with 5% sucrose and 2% X-gal. The white colonies were picked and grown in Middlebrook 7H9 broth and 10 µl of the culture was spotted onto Middlebrook 7H10 agar supplemented with Kan (25 µg/ml). Importantly, the white colonies were stored and those that could not grow on Middlebrook 7H10 agar supplemented with Kan (25 µg/ml) were taken forward for PCR

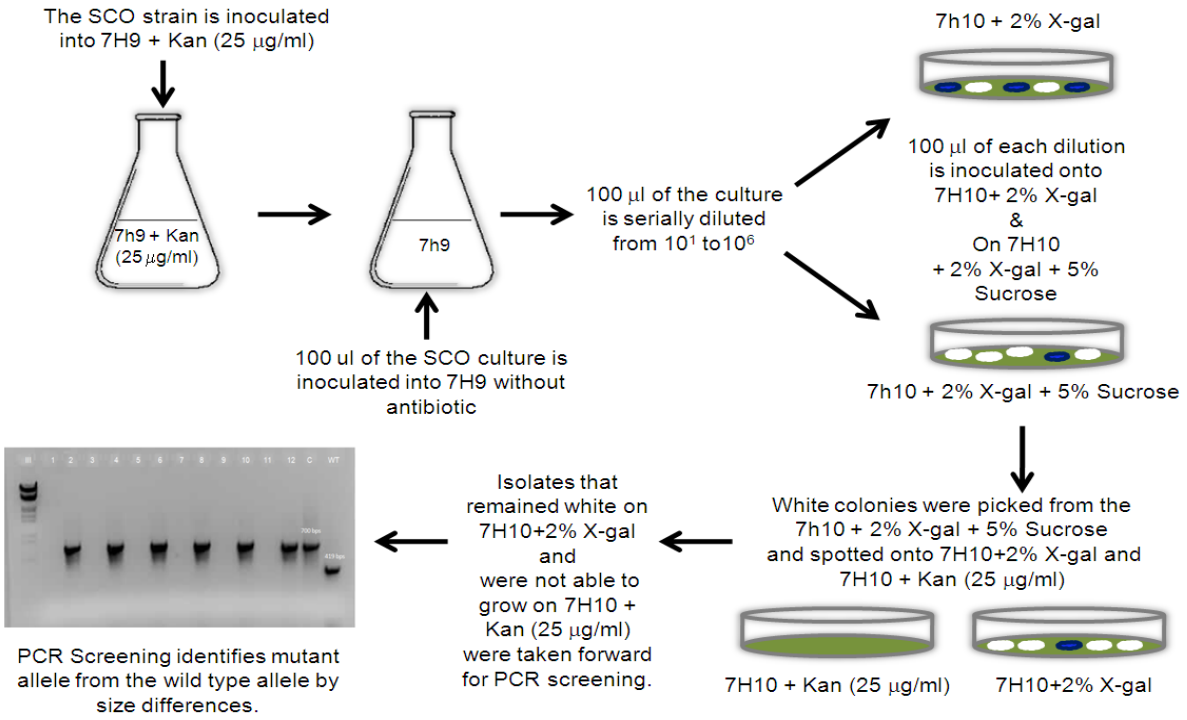


Figure 2.2: **Flow diagram depiction of the process of generating a gene deletion mutant by the two-step allelic exchange homologous recombination method**. See text for details.

screening as cells can either revert back to wild type or become mutants by loosing the wild type gene and retaining the mutated copy (Figure 2.1). Southern blotting was used as indicated in section 2.5.9 to confirm gene deletions.

As the two-step allelic exchange homologous recombination method for gene deletions is time consuming due to multiple steps and requirement of special reagents, we have recently adopted a more effiecient method for gene deletions termed the mycobacterial recombineering method. This method is detailed below.

2.6.5.2. Generation of *M. smegmatis* mc^{2}155 mutant strains by the mycobacterial recombineering method

The mycobacterial recombineering technique for targeted gene deletion was used as previously described (van Kessel and Hatfull, 2007). Briefly, 1 μg of plasmid pNIT encoding recombination enzymes and 1 μg of a linear DNA fragment carrying a streptomycin or hygromycin marked mutated gene of interest were co-electroporated into *M. smegmatis* or derivative strains according to the protocol outlined in section 2.6.4. Immediately after electroporation, the cells were rescued with LB media supplemented with isovaleronitrile to a final concentration of 10%, to induce expression of the recombination enzymes. The cells were rescued overnight at 37 °C with shaking at 100 rpm. Thereafter, the cells were

inoculated onto Middlebrook 7H10 agar supplemented with streptomycin (25 μg/ml) and the plates were incubated at 37 °C for 3-5 days. The colonies that grew were screened for the mutated gene according to the protocol described in sections 2.4.1.1 and 2.5.1.2.2. Primers that were used were designed to detect the presence of the hygromycin or streptomycin resistance genes- *hyg* or *aadA*, respectively, and to detect the chromosomal location of the mutated gene by using a forward primer that binds upstream of the mutated gene and a reverse primer that binds within the hygromycin or streptomycin resistance genes. This approach allowed for confirmation of site-specific integration of the mutant allele. Southern blotting was used as indicated in section 2.5.9 to confirm gene deletions. The resulting mutant was cured of plasmid pNIT by growing the cells to stationary phase in 5 ml of Middlebrook 7H9 broth supplemented with Kan (25 μg/ml) and subsequent inoculation into 5 ml of Middlebrook 7H9 broth without antibiotic. Thereafter, a 100 μl of the culture was serially diluted from 10^1 to 10^6 and a 100 μl aliquot of each dilution was inoculated onto Middlebrook 7H10 agar supplemented with 5% sucrose. As plasmid pNIT carries a *sacB* selection marker which functions as indicated in section 2.6.5.1, mutant cells that were cured of pNIT were able to survive and form colonies on Middlebrook 7H10 agar supplemented with 5% sucrose. The colonies were picked and stored.

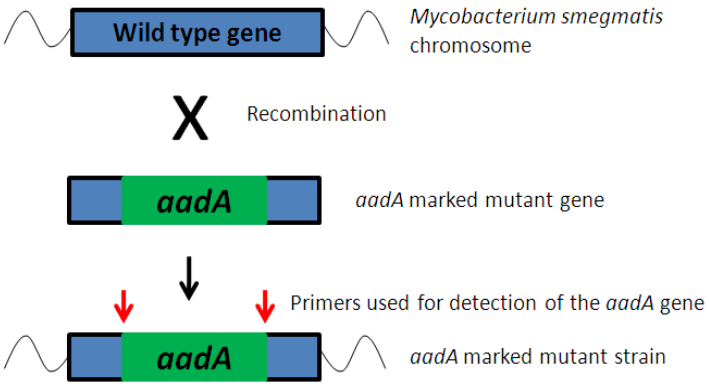


Figure 2.3: **Schematic representation of the the mycobacterial recombineering method.** A linear DNA fragment carrying the mutated gene of interest marked with an antibiotic resistance gene (e.g. streptomycin resistance gene-*aadA*) is introduced into *M. smegmatis* together with plasmid pNIT. Homologous recombination leads to the replacement of the wild type gene with the *aadA* marked mutant gene. Primers (red arrows) specific for the gene- *aadA* are used to detect the *aadA* marked mutant strain.

2.6.6. **Generation of complemented *M. smegmatis* strains**

Genetic complementation of mutated strains was performed to confirm that the phenotypic variation observed from these strains was due to the inactivation of the gene of interest and not due to polar effects. The whole open reading frame (ORF) of the gene of interest with at least 150 bp of the upstream region (to include the promoter region of the gene) was cloned into either plasmid, pTweety or pMV306H, according to the process described in section 2.5.7. The resultant plasmid construct was sequenced prior to electroporation into *M. smegmatis* mutant strains according to the process indicated in section 2.5.8. The plasmid constructs were electroporated into the appropriate mutant strain according to the process described in section 2.6.4. This process allows for the integration of the complementation gene into either the *attB* site or the tRNA glycine site in the genome when complementation was conducted using either the pMV306H or pTWEETY plasmids, respectively. In order to verify genetic complementation of the mutant strains, small scale chromosomal DNA was extracted as indicated in section 2.4.1.1 and used for PCR to detect the presence of the complementing gene as indicated in section 2.5.1.2.2.

2.7. **Localization of proteins of interest**

The localization of proteins of interest was achieved by cloning of the open reading frame (ORF) of the gene of interest without the stop codon into the plasmid pMV306H-GFP to create a protein fusion with the rseGFP. The primers for the synthesis of the relevant ORF were designed to allow C-terminal tagging of the protein of interest with the rseGFP. The DNA ligation process was performed as indicated in section 2.5.7 and resulting plasmid constructs were sequenced as indicated in section 2.5.8. Thereafter, the plasmid constructs were electroporated into either wild type *M. smegmatis* or derivative strains according to the protocol outlined in section 2.6.4. The resultant colonies were picked and grown in 5 ml of Middlebrook 7H9 broth supplemented with the appropriate antibiotic to an OD_{600} of 0.6. The cells were harvested by centrifugation at 12470 *X g*. The supernatant was discarded and the pellet of cells was resuspended in 50 μl of Middlebrook 7H9 broth and 5 μl of the cells was mounted onto a slide with a 2% agarose pad. The slides were visualized with a Zeiss Observer Z1 inverted fluorescence microscope and images were analyzed with the ZEN lite software (Zeiss). Any image manipulation (brightness, contrast etc) was applied to the entire image.

2.8. **Analysis of protein-protein interacting partners**

The STRING database was used for the prediction of possible interacting partners for a protein interest. The mycobacterial protein fragment complementation (M-PFC) system (Figure 2.4) was used as previously described (Singh et al., 2006) to test the interaction of the predicted potential interacting partners for a protein of interest. Briefly, the M-PFC system is based on the functional reconstitution of the two murine dihydrofolate reductase (mDHFR) domains, fused independently to two putative interacting proteins (Figure 2.4). The interaction between the two proteins of interest results in the reassembly of the two mDHFR domains into a functional mDHFR, which confers resistance to Trimethoprim (Trim). The ORFs of the genes of interest were cloned separately into plasmids pUAB400 and pUAB300 as described in section 2.5.7 and the resulting plasmids were sequenced as indicated in section 2.5.8. Thereafter, the plasmids were electroporated into wild type *M. smegmatis* according to the protocol outlined in section 2.6.4. The resultant colonies were picked, resuspended in 50 µl of Middlebrook 7H9 broth, inoculated onto Middlebrook 7H10 agar supplemented with Kan (25 µg/ml), Hyg (50 µg/ml) and Trim (7.5 µg/ml), and grown at 37 °C for 5-7 days. For M-PFC system controls, the *M. smegmatis* mc^2155 derivative strain

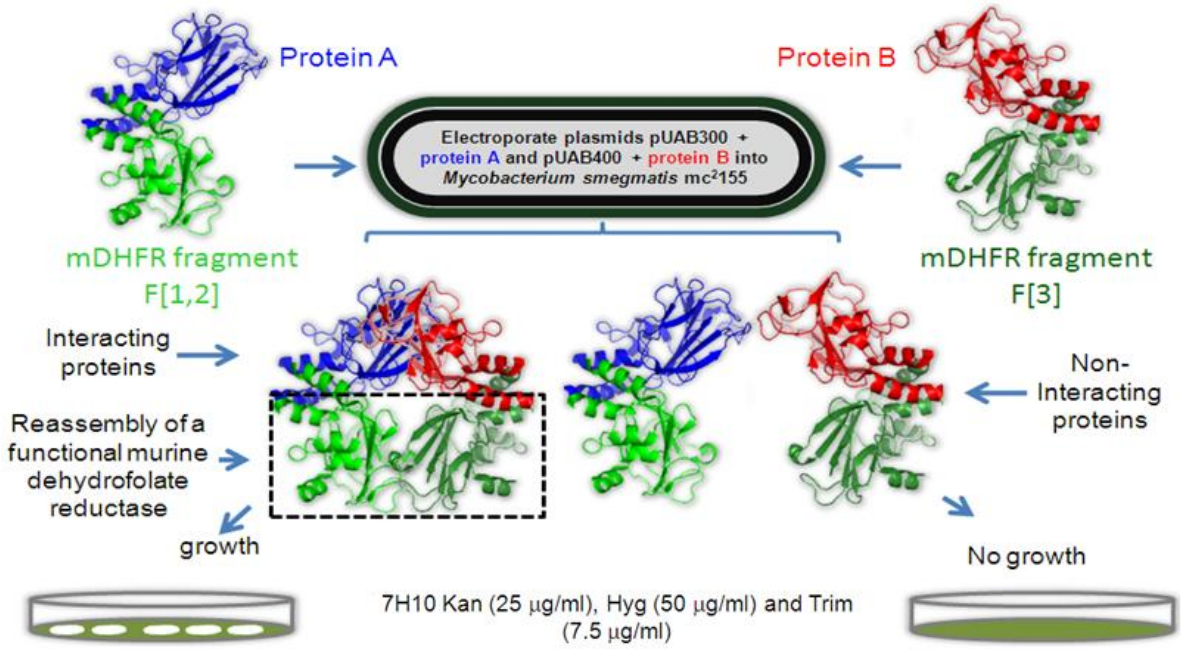


Figure 2.4: **Schematic diagram illustrating the M-PFC assay principle**. Proteins A and B are fused to complementary mDHFR fragments F[1,2] and F[3]. Co-transformation of *M. smegmatis* mc^2155 with plasmids encoding the proteins A and B fused with the complementary mDHFR fragments results in the reconstitution of a functional mDHFR and subsequent growth of the strain on Middlebrook 7H10 broth supplemented with Trim (7.5 µg/ml), Kan (25 µg/ml), Hyg (50 µg/ml) only if proteins A and B are interacting partners. Diagram adapted from (Singh et al., 2006).

mc^2::pUAB5439+pUAB3145 was used as a positive control based on proven interaction between MSMEG_5439 (RpfB) and MSMEG_3145 (RipA) (Hett et al., 2007) and the strain mc^2::pUAB300+pUAB400 (plasmid only control) was used as a negative control.

2.9. Phenotypic analysis of *M. smegmatis* $mc^2$155 mutant strains

2.9.1. Growth rate analysis

The growth rates of the mutant strains in comparison to the wild type and the genetically complemented strains were assessed by conducting three independent growth curve experiments with plating for colony formation unit (CFU/ml) determination. Briefly, the bacterial strains were grown overnight at 37 °C with shaking at a 100 rpm in 5 ml of Middlebrook 7H9 broth, supplemented with appropriate antibiotics when necessary. Thereafter, the pre-culture of each strain was diluted to an OD_{600} of 0.01 in 50 ml of Middlebrook 7H9 broth, supplemented with appropriate antibiotics when necessary. The cultures were incubated at 37 °C with shaking at a 100 rpm and the growth rate was assessed by generating a scatter plot from data obtained by recording the OD_{600} of each culture and plating for CFU/ml on Middlebrook 7H10 agar at three hour intervals. The GraphPad Prism 6 software was used for statistical analysis (Student's *t*-test was conducted to compare the growth rate difference of the mutant strains in relation to the wild type and complemented strains).

2.9.2. Antibiotics and lysozyme MIC determination

The Middlebrook 7H9 broth microdilution MIC assay (Larrouy-Maumus et al., 2016) was used to test the sensitivity of the mutant strains to antibiotics and lysozyme in comparison to the wild type and genetically complemented strains in 96-well plates (Thermo Scientific). Briefly, the bacterial strains were grown to an OD_{600} of 0.3 at 37 °C with shaking at a 100 rpm in 5 ml of Middlebrook 7H9 broth supplemented with appropriate antibiotics when necessary. Thereafter, the cultures were diluted 100 fold in Middlebrook 7H9 broth followed by inoculation into 96 well plates containing Middlebrook 7H9 broth and serially diluted concentrations of antibiotics to be tested or lysozyme. The antibiotics used were the following: Rifampicin (200 μg/ml), Isoniazid (250 μg/ml), Teicoplanin (100 μg/ml), Ethambutol (300 μg/ml), Vancomycin (100 μg/ml) and Imipenem (100 μg/ml). The starting concentration for lysozyme was 2 mg/ml.

2.9.3. **Fluorescence microscopy**

2.9.3.1. **Fluorescent BODIPY Vancomycin staining**

The Fluorescent BODIPY Vancomycin stain (Life Technologies) was used according to the manufacturer's instructions for analysis of peptidoglycan (PG) synthesis in the mutant strains in comparison to the wild type and complemented strains. The fluorescent vancomycin stain binds to the terminal dipeptide D-alanine-D-alanine found on the peptidoglycan stem peptide periplasmic precursor lipid II and consequently indicates the sites of new peptidoglycan synthesis. The bacterial strains were grown to an OD_{600} of 0.6 at 37 °C with shaking at a 100 rpm in 5 ml of Middlebrook 7H9 broth supplemented with appropriate antibiotics when necessary. Subsequently, 2 ml of the cells were havested by centrifugation at 12470 *X g* for 5 minutes and the supernatant was discarded followed by washing of the cells with 500 µl 0.01 M PBS (pH 7.4) and subsequent resuspension in 500 µl of 0.01 M PBS. Thereafter, 1.25 µl of vancomycin (200 µg/ml) and 2.5 µl of fluorescent BODIPY vancomycin (100 µg) was added to the cells followed by incubation at 37 °C with shaking for 1.5 hours. Following this, 500 µl of 0.01 M PBS was used to wash the cells three times and the cells were then resuspended in a 100 µl of 0.01 M PBS. For visualization, 5 µl of the cells was spotted on glass slides with 2% agarose pads. The slides were visualized with the Zeiss Observer Z1 inverted fluorescence microscope and the images taken were analyzed with the ZEN lite software (Zeiss) and Fiji software (ImageJ). Any image manipulation (brightness, contrast etc) was applied to the entire image.

2.9.3.2. **Click Chemistry D-alanine analogue staining**

The Click Chemistry technique was also used for *in vivo* labeling of sites of new PG synthesis (Siegrist et al., 2013). The technique involves the incubation of cells with an alkyne-functionalized D-alanine analogue which is incorporated into the PG during cell wall synthesis. The alkyne-functionalized D-alanine was visualized by reactions with Click Chemistry probes. For this, 1 µl of 1 mM alkyne functionalized D-alanine was added to harvested cells grown to an OD_{600} of 0.6 and resuspended in 2 ml of Middlebrook 7H9 broth. The cells were incubated for 2 hours at 37 °C with shaking at 100 rpm. Subsequently, the cells were washed three times with PBSTB buffer (1 X PBS, 0.05% BSA and 0.01% Tween 20) and fixed for 10 minutes in 1 ml of 2% formaldehyde diluted in 1 X PBS. Thereafter, the cells were centrifuged at 12470 *X g* for 5 minutes and the supernatant was discarded. The Click Chemistry reaction was conducted as follows: 920 µl of PBSTB buffer was used to

resuspend the cells and 20 μl of $CuSO_4$ (50 mM), 20 μl of TBTA (tris-(benzyltriazolylmethyl) amine) (6.4 mM), 20 μl of sodium ascorbate (60 mM) and 20 μl of an Azido probe (1 mM diluted in DMSO) were added in the order stated to the cells and mixed gently. The cells were incubated at ambient temperature for 45 minutes and subsequently washed three times with 1 X PBS. Thereafter, 5 μl of the cells was spotted onto glass slides which were visualized with the Zeiss Observer Z1 inverted fluorescence microscope and the images taken were analyzed with the ZEN lite software (Zeiss) and the Fiji software (ImageJ). Any image manipulation (brightness, contrast etc) was applied to the entire image.

2.9.3.3. **DMN-Trehalose staining**

The DMN-Trehalose stain was also used for *in vivo* labeling of the mycobacterial cell wall. The stain was synthesized by Carolyn R. Bertozzi (Stanford University) and team by attachment of trehalose (a component of the mycobacterial cell wall) to a solvatochromic dye that only produces green fluorescence when incorporated into the bacterial cell wall (Figure 2.5). Briefly, cells were grown at 37 °C with shaking to an OD_{600} of 0.6 and, thereafter, harvested by centrifugation at 12470 *X g* for 5 minutes. The DMN-Trehalose stain (100 μM) was added to cells resuspended in 1 ml of Middlebrook 7H9 broth. The cells were incubated at 37 °C with shaking at 100 rpm for an hour, pelleted by centrifugation at 12470 *X g* for 5 minutes and resuspended in 50 μl of dH_2O. Thereafter, 5 μl of the cells was spotted onto glass slides which were visualized with the Zeiss Observer Z1 inverted fluorescence microscope and the images taken were analyzed with the ZEN lite software (Zeiss) and the Fiji software (ImageJ). Any image manipulation (brightness, contrast etc) was applied to the entire image.

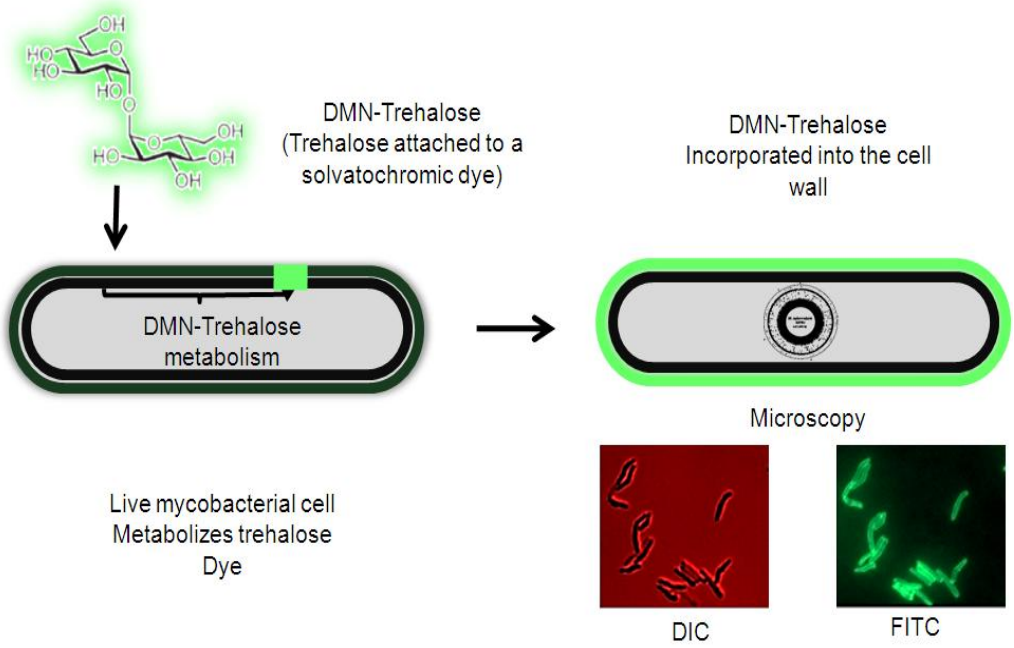


Figure 2.5: **Schematic diagram illustrating the DMN-Trehalose staining process**. Live mc^2155 cells are stained with DMN-trehalose stain and then viewed by fluorescence microscope under the FITC channel.

2.9.3.4. **Membrane and DNA staining with the FM4/64 and the DAPI stains, respectively**

The cell membrane stain FM4/64 (ThermoFisher Scientific) and the DNA stain DAPI (Sigma-Aldrich) were used for staining of the cell membrane and bacterial DNA, respectively, following the manufacturer's instructions. Briefly, the cells were grown in 5 ml of Middlebrook 7H9 broth supplemented with appropriate antibiotics to an OD_{600} of 0.6 and harvested by centrifugation at 12470 *X g*. The cells were then resuspended in 2 ml of Middlebrook 7H9 broth, 2 µl of the DAPI stain and 5 µl of the FM4/64 stain were added to the cells and incubated at 37 °C for 20 minutes. Subsequently, the cells were washed twice with 1 X PBS, harvested by centrifugation at 12470 *X g* and resuspended in 50 µl of 1 X PBS. Thereafter, 5 µl of the cells was spotted onto glass slides which were visualized with the Zeiss Observer Z1 inverted fluorescence microscope and the images taken were analyzed with the ZEN lite software (Zeiss) and the Fiji software (ImageJ). Any image manipulation (brightness, contrast etc) was applied to the entire image.

2.9.4. **Scanning electron microscopy (SEM)**

Scanning electron microscopy was conducted to phenotypically characterize the mutant strains in comparison to the wild type and genetically complemented strains. Briefly, the cells were grown in 50 ml of Middlebrook 7H9 broth supplemented with appropriate antibiotics at

37 °C with shaking to an OD_{600} of 0.6 and thereafter, harvested by centrifugation at 1180 *X g* for 5 minutes. The cells were washed with 1 X PBS and resuspended in 2.5% gluteraldehyde, followed by overnight incubation at 4 °C. Thereafter, the cells were washed twice with 1X PBS, followed by staining with 100 µl of 2% osmium and incubation at ambient temperature for an hour. The cells were then washed with 1 X PBS and dehydrated by 2 minutes of resuspension in a series of ethanol concentrations starting with 30% of ethanol, then in 50% of ethanol, followed by 70% of ethanol and twice in 100% of ethanol. The dehydrated cells were then stored in 100% of ethanol at ambient temperature. Prior to imaging, the cells were spotted on filter and coated twice with carbon and the FEI Nova NanoSEM 230 scanning electron microscope was used for viewing the cells. All preparations for SEM were done in-house but the imageing of cells was outsourced to the Centre of Imaging and Analysis at the University of Cape Town.

2.10. **Morphological analysis of the mutant strains through flow cytometry**

Flow cytometry was used for analysis of the morphology of the mutant strains in comparison to the wild type and genetically complemented strains. Cells were grown in 5 ml of Middlebrook 7H9 broth supplemented with appropriate antibiotics at 37 °C with shaking to an OD_{600} of 0.6. Thereafter, 200 µl of the culture was transferred to a 96-well plate (ThermoFisher Scientific). The CytoFLEX flow cytometer (Beckman Coulter) was used for analysis of the morphology of the mutant strains by analyzing side scatter.

2.11. **Time-lapse microscopy**

The mc^2155 and derivative strains were grown in microfluidic devices and time-lapse microscopic analysis of these strains were conducted as previously described (Dhar and Manina, 2015). Briefly, the bacterial cultures were grown to exponential phase in ink-well bottles at 37 °C. A microfluidic device was used to grow the bacteria and a Delta vision Personal DV imaging system (GE Healthcare Life Sciences) using a 100 X objective (Olympus Plan Semi Apochromat, 1.3 NA) was used for imaging. Images were acquired at 10 minutes intervals using a CoolSnap HQ2 camera. Images were acquired on FITC (GFP fluorescent reporter strains; excitation 490/20 nm; emission 528/38 nm). Middlebrook 7H9 medium (ThermoFisher Scientific) was circulated through the microfluidic device at a flow rate of 25 µl/min ImageJ v 1.47n.

3. Results

3.1. Identification of mycobacterial LytM domain containing proteins (M23 peptidases) and bio-informatic analysis

To identify the mycobacterial genes encoding M23 peptidases, the M23 domain of the well-characterized *E. coli* M23 protein, EnvC, was blasted against the *M. tuberculosis* and *M. smegmatis* genomes through the use of the NCBI protein blast tool. Three genes encoding M23 proteins (Rv0950c, Rv2891 and Rv3786c) were identified in the genome of *M. tuberculosis* (Figure 3.1) and four (MSMEG_0247, MSMEG_1192, MSMEG_2518 and MSMEG_5526) were identified in the genome of *M. smegmatis* (Figure 3.1). *M. smegmatis* mc^2155 was used in this project as a model organism to study *M. tuberculosis*. The bio-informatics analysis identified two *M. smegmatis* M23 proteins (MSMEG_0247 and MSMEG_1192) with recognizable signal peptides and the characteristic M23 domain metal binding motif, HxH, important for catalytic activity and a cytosolic M23 protein (MSMEG_5526) was also identified (Figure 3.2, 3.3 and Appendix A). The phylogenetic analysis indicated that MSMEG_0247 and MSMEG_1192 are related to cell division M23 proteins of model organisms such as *E. coli*, *V. cholerae*, *P. aeruginosa* and *H. influenza,* and MSMEG_5526 showed homology to MepB (CGWP011013932.1) of *C. glutamicum* (Figure 3.1) (Brocker et al., 2010). The I-TASSER protein threading server was used to predict the tertiary structures of these three proteins for analysis of the substrate binding active site. The predicted tertiary structures indicated the presence of a C-terminal Zn^{2+}-containing M23 domain in all three proteins (Figure 3.2). From our analysis, the identified M23 proteins were predicted to be novel mycobacterial PG endopeptidases identical to MepB of *C. glutamicum* (Brocker et al., 2010). Hence, we propose the naming of MSMEG_5526, MSMEG_0247 and MSMEG_1192 as MepB1, MepB2 and MepB3 (Metallopeptidase B1, B2 and B3, respectively). The predicted active site Zn^{2+} coordinating residues for MepB1 are His237, Asp241, His316 and His318. The Zn^{2+} cation of MepB2 is coordinated by Tyr243, Glu247, His332 and His334 and the Zn^{2+} cation of MepB3 is coordinated by Glu225, Pro229, His326 and His328 (Figure 3.3). This suggested that MepB1, MepB2 and MepB3 are PG hydrolases with a potential role in PG remodelling during mycobacterial cell division and growth. None of these enzymes are degenerate suggesting that they retain PG hydrolytic activity rather than serving as activators of other enzymes. To determine the role of MepB1, MepB2 and MepB3 in mycobacterial PG biosynthesis, we targeted the *mepB1*, *mepB2* and *mepB3* genes for deletion from the genome of *M. smegmatis*. The *mepB* mutants are studied in detail below (see Figure 3.4 for the experiments conducted for analysis of the role of the MepB proteins).

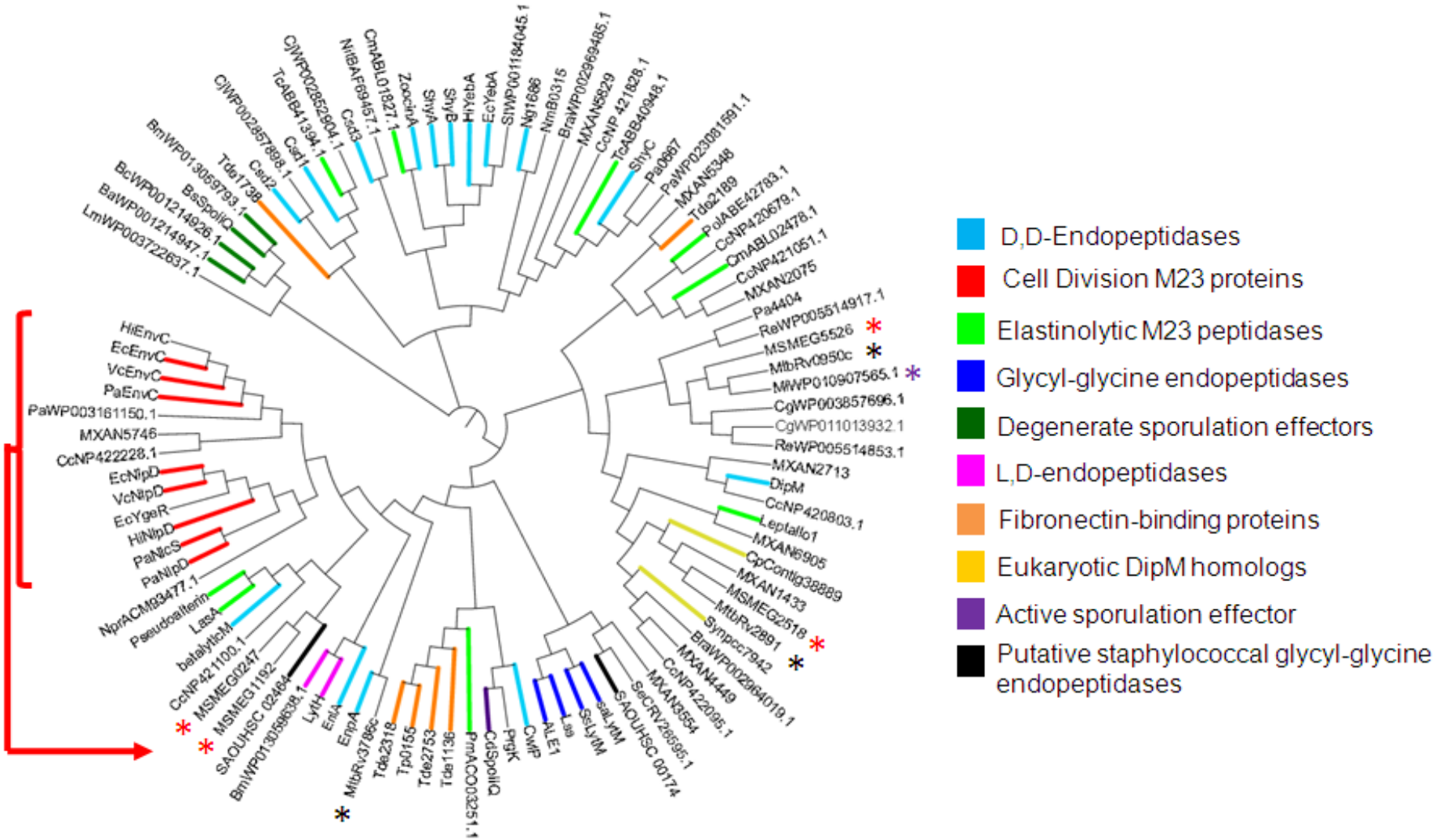


Figure 3.1: **Phylogenetic analysis of M23 peptidases from different bacterial species**. Full length protein sequences were aligned using Clustal Omega and the phylogenetic tree was generated using iTOL (Interactive Tree Of Life). Red asterisks indicate the *M. smegmatis* M23 protein homologs, black asterisks indicate the *M. tuberculosis* M23 protein homologs and the purple asterisks indicate the *M. leprae* M23 protein homolog.

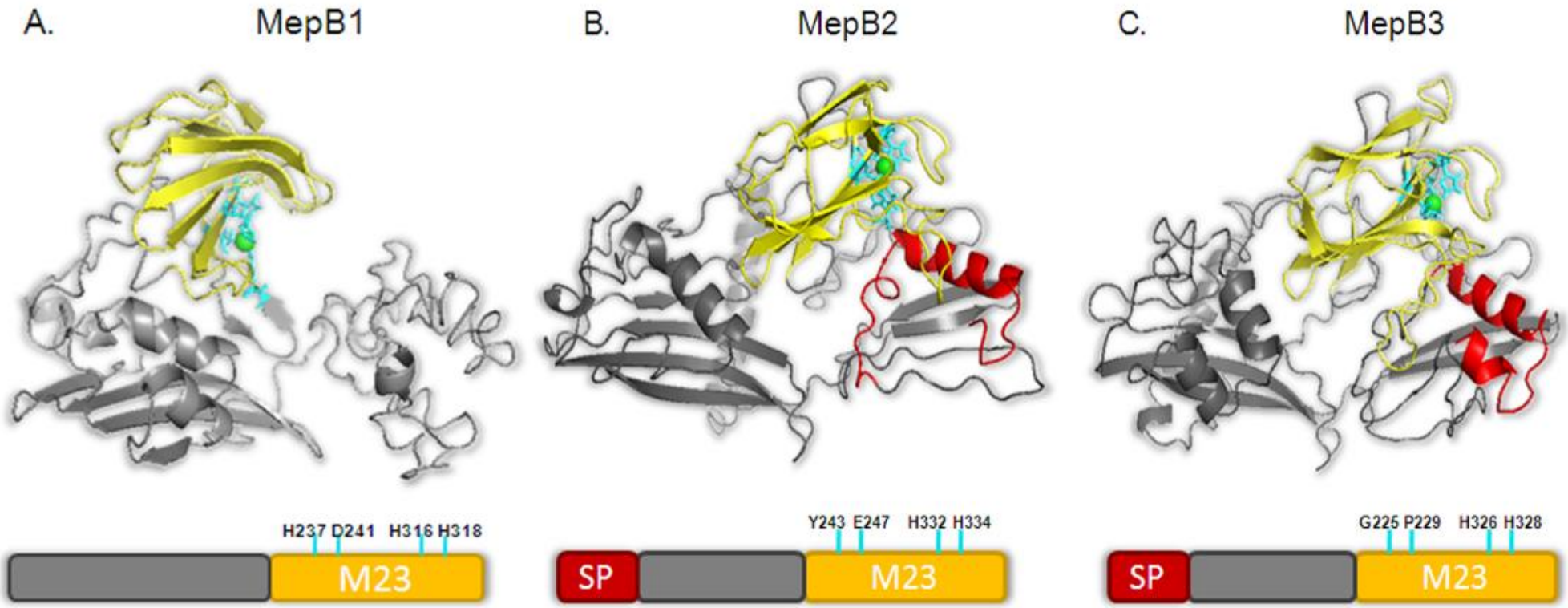


Figure 3.2: **Predicted tertiary structures and schematic representation of the domain organization of the mc^{2}155 M23 proteins**. MepB1 (A) and MepB2 (B) and MepB3 (C). The Zn^{2+} cation (green) and the Zn^{2+} coordinating residues (cyan) are shown as ball-and-stick models. SP: signal peptide (red). H: histidine, D: aspartic acid, Y: tyrosine, G: glutamine and P: proline. The I-TASSER server was used to generate the tertiary structures of the MepB proteins and the pymol graphics package was used to view the generated strutures.

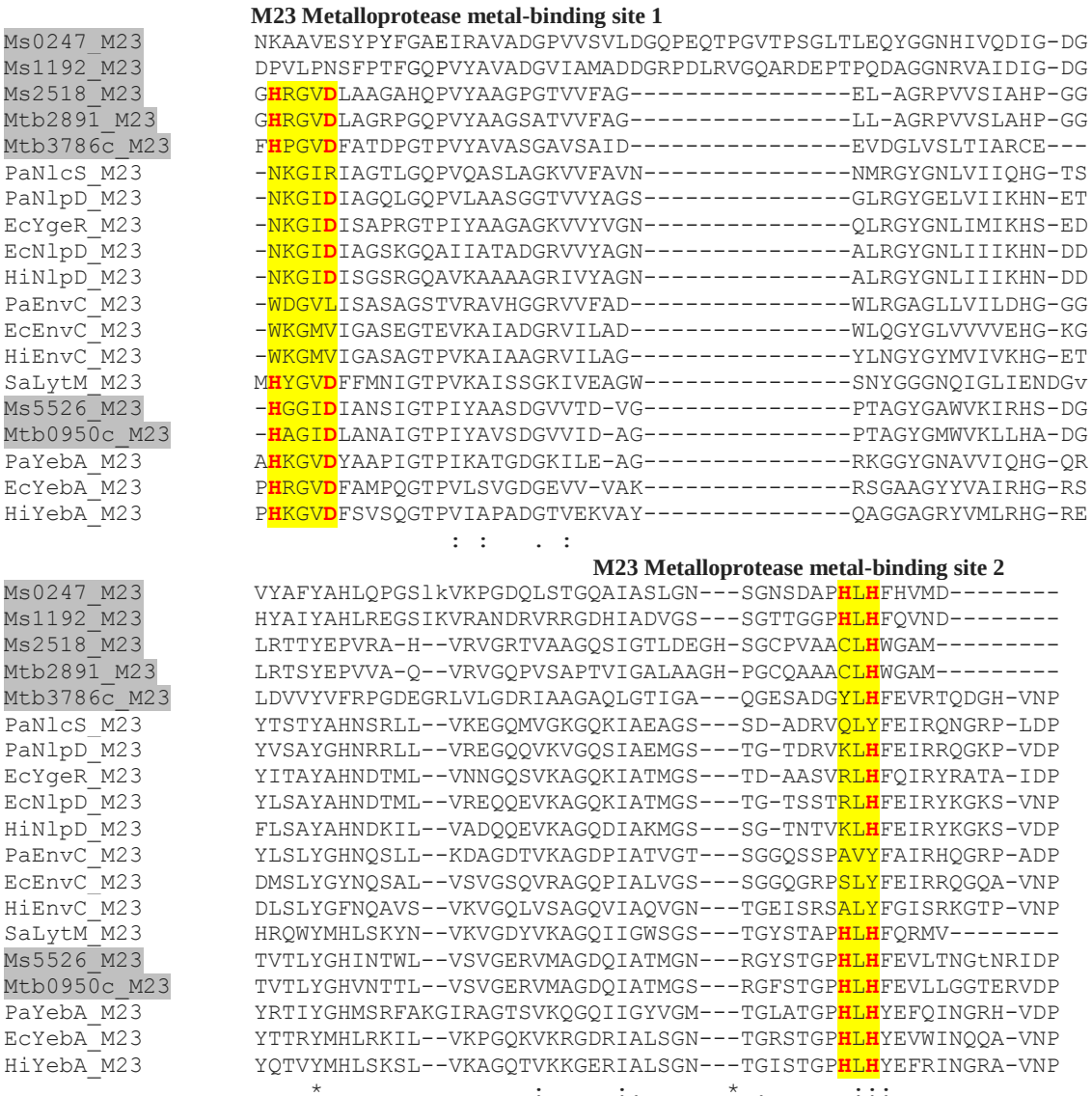


Figure 3.3**: Alignment of the M23 domain from different M23 peptidases**. Motifs highlighted in yellow represent the zinc cation binding motifs. Residues in red font are the zinc binding ligands important for coordination of the zinc cation. The Pfam database was used to identify the LytM domain from full length protein sequences of the M23 proteins indicated and Clustal Omega was used to perform multiple sequence alignments. MepB1 (MSMEG_5526) retains a canonical metal binding site 1 for zinc cation binding and both MepB2 (MSMEG_0247) and MepB3 (MSMEG_1192) have a different metal binding site 1 for zinc cation binding.

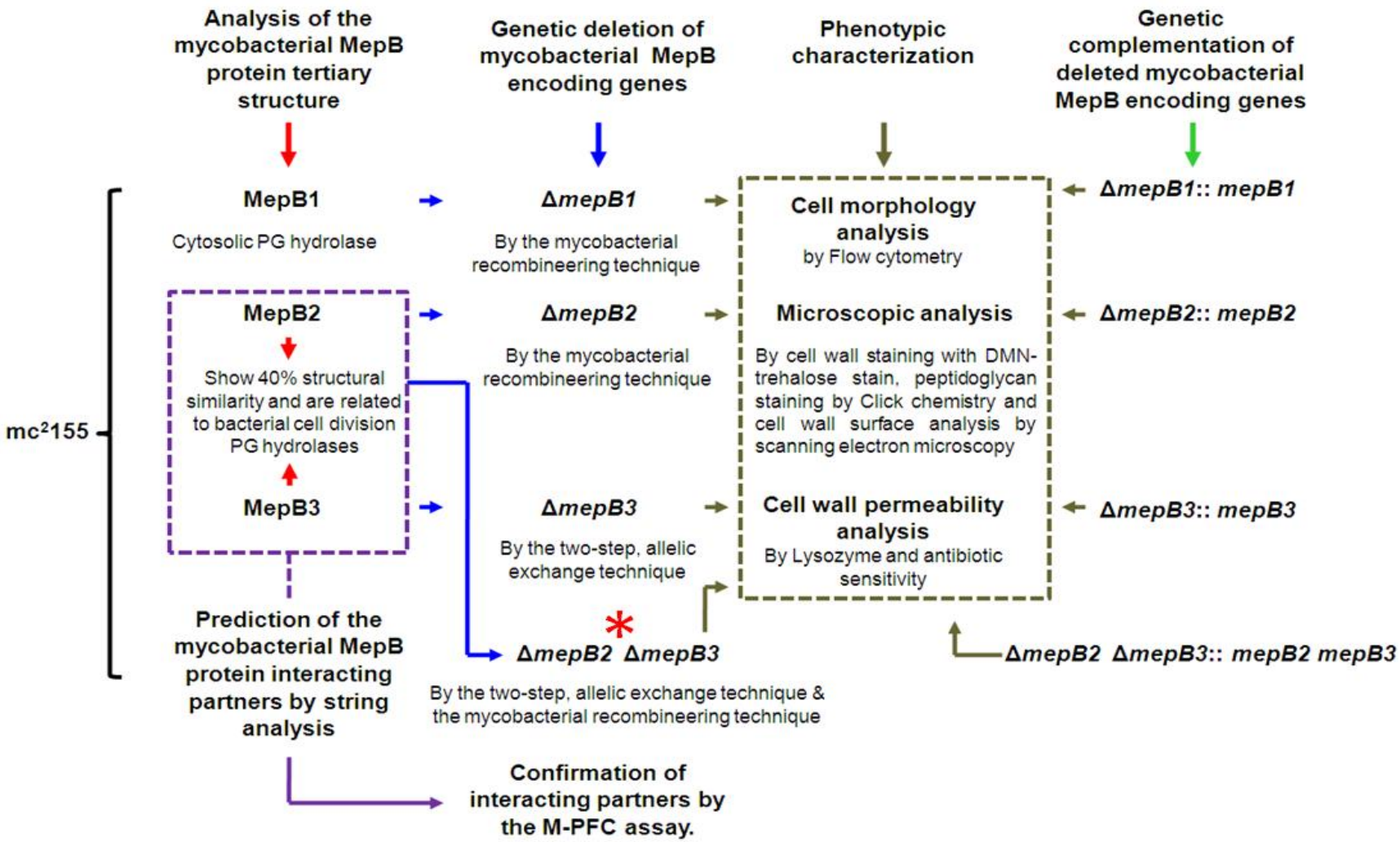


Figure 3.4: **Flow diagram for the study of mycobacterial M23 proteins**. Panel 1 (red arrows) indicates the mycobacterial M23 proteomic complement studied herein. Panel 2 (blue arrows) indicates the genetic deletion of mycobacterial MepB encoding genes and the methods used. Panel 3 (Olive arrows) indicates the methods used for phenotypic charaterization of Δ*mepB* mutants generated. Panel 4 (green arrows) indicates the genetic complementation of the Δ*mepB* mutants. Red asterisks: the Δ*mepB2* Δ*mepB3* mutant was created by deletion of the *mepB2* gene from the Δ*mepB3* single mutant to create a Δ*mepB2* Δ*mepB3* double mutant.

3.2. Generation of *M. smegmatis* mutant strains lacking the genes *mepB1*, *mepB2* and *mepB3*, individually and in combination

The *mepB1*, *mepB2* and *mepB3* genes were deleted from the genome of *M. smegmatis* through the two-step allelic exchange method and the mycobacterial recombineering technique. These methods both involve the substitution of the wild type gene with a mutated/inactivated copy by homologous recombination. Initially, we used the two-step allelic exchange method to delete the *mepB3* gene. However, this system was time consuming as stated above; therefore, for deletion of *mepB1* and *mepB2*, we employed the more efficient mycobacterial recombineering technique (Murphy et al., 2015). Both methods require the construction of suicide plasmids carrying the mutated/inactivated copy of the target gene which serves as the basis for allelic exchange. The process for construction of these suicide plasmids is detailed below for each *mepB* gene.

3.2.1. Construction of plasmids used for deletion of the *mepB1*, *mepB2* and *mepB3* genes

3.2.1.1. Construction of the *mepB1* gene deletion plasmid

As mentioned above, the mycobacterial recombineering technique was adopted for deletion of the *mepB1* gene. A 540 bp region upstream and a 589 bp region downstream of *mepB1* were used to design the mutated *mepB1* allele (Figure 3.5). A hygromycin resistance cassette carrying the gene *hyg* (conferring resistance to the antibiotic-hygromycin) was then inserted between the upstream and downstream regions of the Δ*mepB1* allele, to create a *hyg*-marked *mepB1* deletion allele. This allowed quick selection of Δ*mepB1* mutants on 7H10 media supplemented with 50 μg/ml of hygromycin. The *mepB1* deletion allele was cloned into the plasmid pGEM as indicated in section 2.5.7. A selected clone was verified by restriction profiling (Figure 3.6) and DNA sequencing as indicated in sections 2.5.3 and 2.5.8, respectively. Restriction profiling yielded all the expected banding patterns (Figure 3.6) and sequencing of the plasmid identified no mutations from PCR amplification (data not shown).

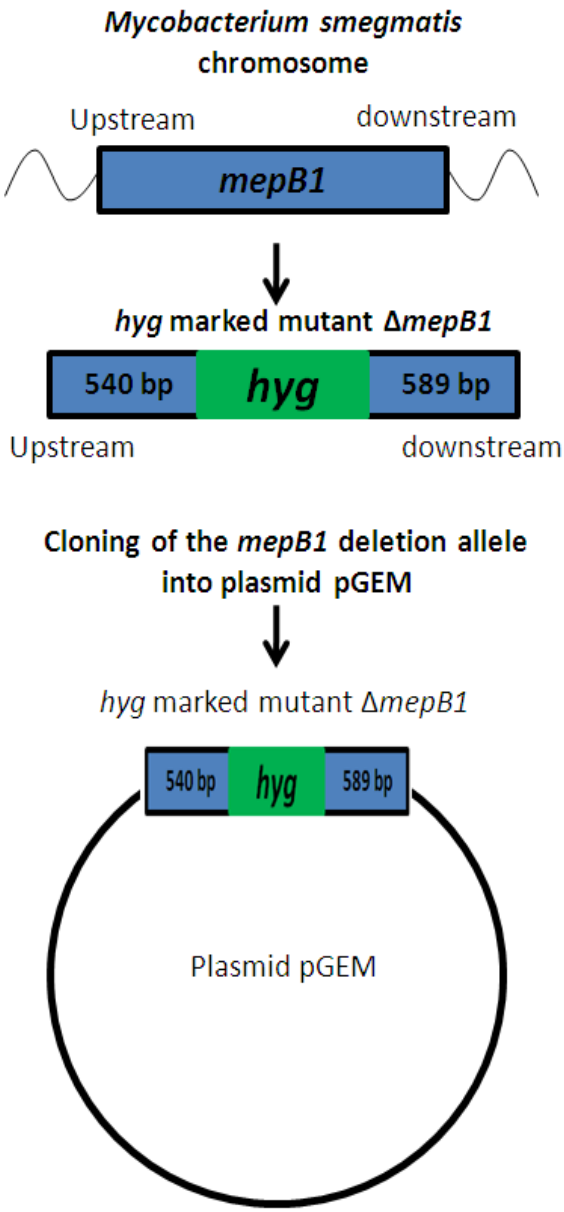


Figure 3.5: **Schematic diagram illustrating the construction of the *mepB1* gene deletion plasmid.** A 540 bp region upstream and a 589 bp region downstream of *mepB1* were used to design the mutated *mepB1* allele. A hygromycin resistance cassette carrying the gene *hyg* was inserted between the upstream and downstream regions of the Δ*mepB1* allele, to create a *hyg*-marked *mepB1* deletion allele. The *hyg*-marked *mepB1* deletion allele was cloned into the plasmid pGEM. See Figure 3.6 for the verification of the *mepB1* deletion plasmid.

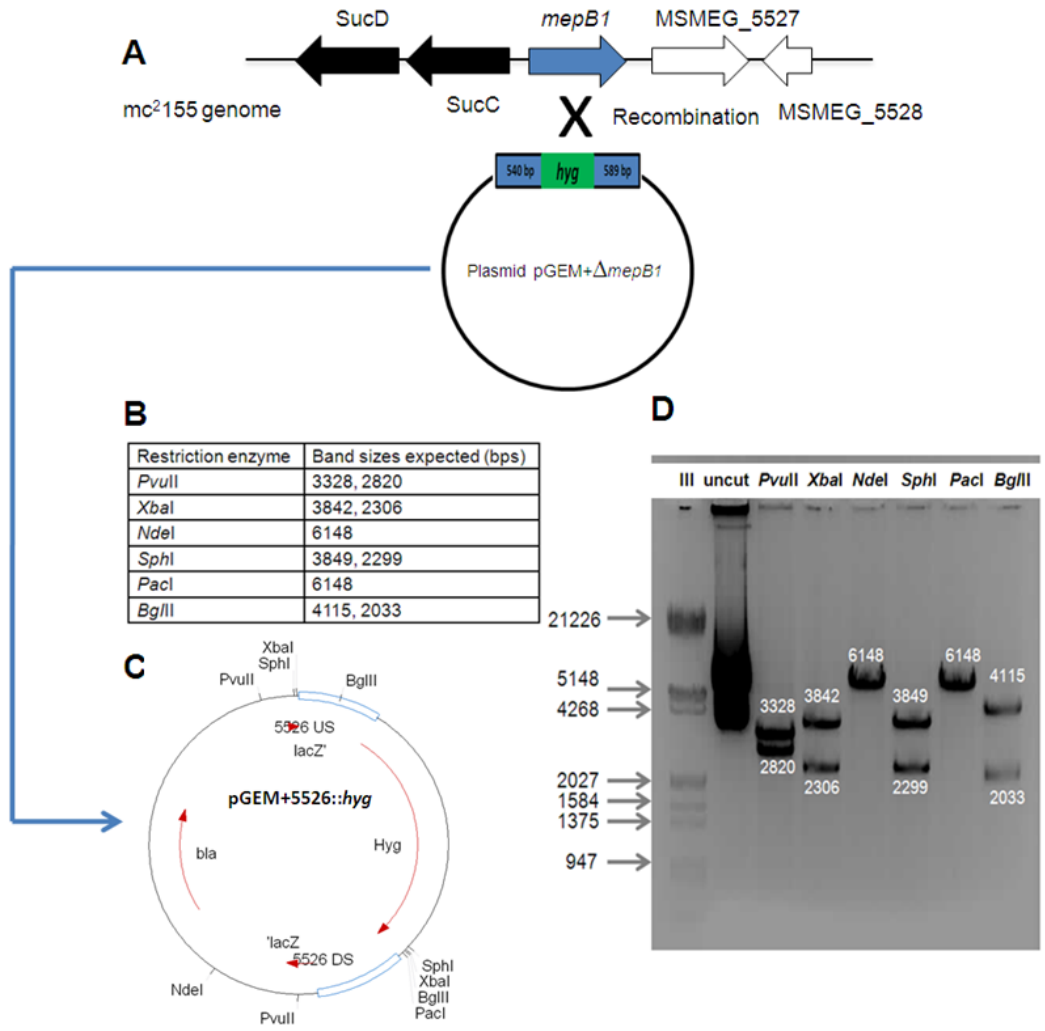


Figure 3.6: **Restriction profile of pGEM+5526::*hyg***. (A) mc^{2}155 genome map indicating the location of the *mepB1* gene and the recombination event required for deletion of the *mepB1* gene. (B) Table indicating the restriction enzymes used for restriction analysis of pGEM+5526::*hyg* and the DNA band sizes expected. (C) Plasmid map of pGEM+5526::*hyg*. (D) Agarose gel (1%) indicating the DNA band sizes expected (labeled in base pairs). All expected band sizes were observed.

3.2.1.2. Construction of the *mepB2* gene deletion plasmid

As mentioned above, the mycobacterial recombineering technique was also adopted for deletion of the *mepB2* gene. Three hundred base pair regions upstream and downstream of *mepB2* were used to design the mutated *mepB2* allele (Figure 3.7). A Cre-Lox recombination sequence was inserted between the 300 bp upstream and downstream sequences of *mepB2* and engineered for insertion of a streptomycin resistance gene (*aadA*) through insertion of a *Hpa*I restriction site within the Cre-Lox recombination sequence (this DNA fragment is hereafter referred to as the *mepB2* deletion fragment). The Cre-Lox recombination sequence allowed for the removal of the inserted *aadA* gene from the generated *aadA*-marked Δ*mepB2* mutant, to unmark the Δ*mepB2* mutant. *Pac*I restriction sites were inserted at the 5′ and 3′

ends of the *mepB2* deletion fragment. This allowed the excision of the *mepB2* deletion fragment from the replication plasmid pUC57sim for the recombination event during construction of the Δ*mepB2* mutant. The *mepB2* deletion fragment was synthesized and incorporated into the replication plasmid pUC57sim by GenScript®. A streptomycin resistance cassette carrying the gene *aadA* (conferring resistance to streptomycin) was then

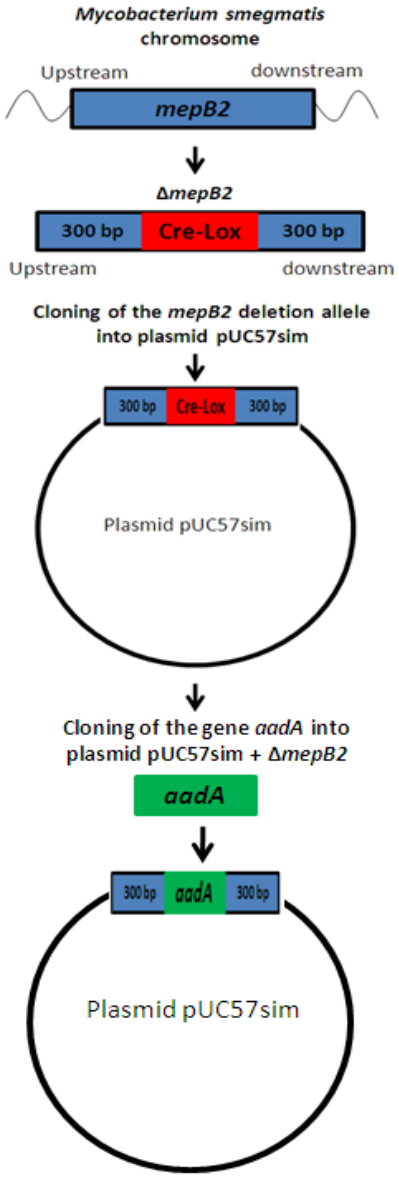


Figure 3.7: **Schematic diagram illustrating the construction of the *mepB2* deletion plasmid.** 300 bp regions upstream and downstream of *mepB2* were used to design the mutated *mepB2* allele. A Cre-Lox recombination sequence (red box) was inserted between the upstream and downstream sequences of *mepB2*. The *mepB2* deletion fragment was synthesized and incorporated into the replication plasmid pUC57sim. A streptomycin resistance cassette (green box) carrying the gene *aadA* was inserted between the upstream and downstream regions of the Δ*mepB2* allele by incorporation into the Cre-Lox recombination sequence, to create an *aadA*-marked *mepB2* deletion allele. See Figure 3.8 for the verification of the *mepB2* deletion plasmid.

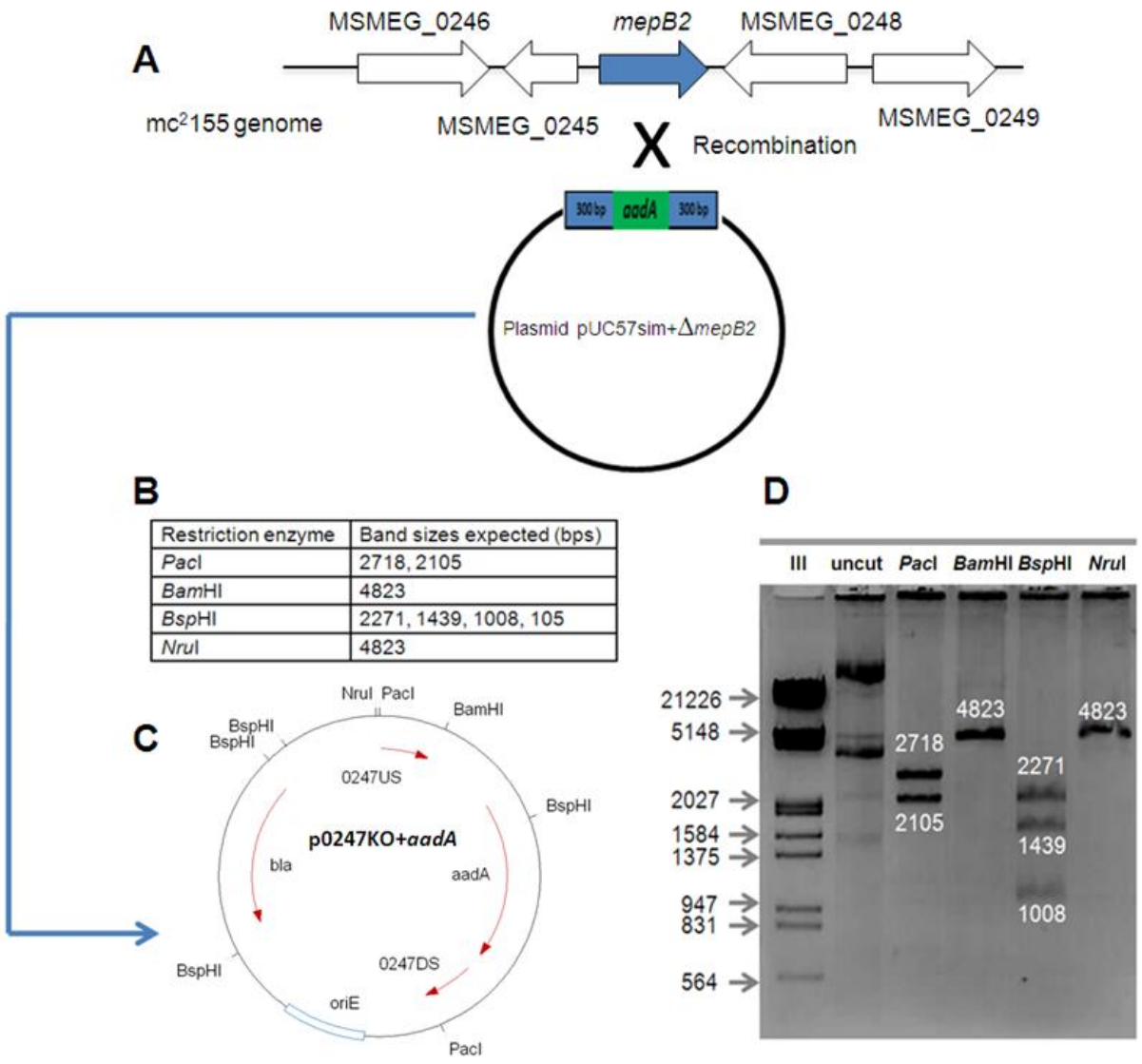


Figure 3.8: **Restriction profile of p0247KO+*aadA***. (A) mc^{2}155 genome map indicating the location of the *mepB2* gene and the recombination event required for deletion of the *mepB2* gene. (B) Table indicating the restriction enzymes used for restriction analysis of p0247KO+*aadA* and the DNA band sizes expected. (C) Plasmid map of p0247KO+*aadA*. (D) Agarose gel (1%) indicating the DNA band sizes expected (labeled in base pairs). All the expected band sizes were observed, with the exception of the 105 bp band produced by the restriction enzyme *Bsp*HI. The 105 bp band was too small to be detected, this was due to the high velocity of small DNA fragments during agarose gel electrophoresis.

cloned into the *Hpa*I restriction site as indicated in section 2.5.7. A selected clone was verified by restriction profiling (Figure 3.8) as indicated in section 2.5.3. Restriction profiling yielded all the expected banding patterns (Figure 3.8), except for the 105 bp band produced by the restriction enzyme *Bsp*HI. This band was too small to be detected. This was due to the high velocity of small DNA fragments during agarose gel electrophoresis; however, the plasmid was valid for use. Sequencing of the plasmid identified no mutations from PCR amplification (data not shown).

3.2.1.3. Construction of the *mepB3* gene deletion plasmid

As mentioned above, the two-step allelic exchange technique was adopted for deletion of the *mepB3* gene (Gordhan and Parish, 2001) as the recombineering approach proved challenging. Two thousand base pair regions upstream and downstream of *mepB3* were used to design the mutated *mepB3* allele (Figure 3.9). The *mepB3* deletion plasmid (p1192KO) was constructed as indicated in section 2.6.5.1. Briefly, the 2000 bp regions upstream and downstream of *mepB3* were PCR amplified as indicated in section 2.5.1.2 (see Table 5 for the PCR primers used and Table 3 for the parameters used). Restriction sites for the restriction enzyme *Acc*65I were engineered at the 5′ and 3′ ends of the upstream and downstream fragments, respectively. Furthermore, an *Xba*I restriction site was engineered at both the 3′ and 5′ ends of the upstream and downstream fragments, respectively. This allowed for construction of the *mepB3* deletion allele when the *mepB3* upstream and downstream PCR fragments (digested with restriction enzymes *Xba*I and *Acc*65I) were cloned into plasmid p2NIL digested with the restriction enzyme *Acc*65I. Thereafter, a *Pac*I cassette carrying the selection markers: *sac*B and *lac*Z was cloned into the plasmid p2NIL+the *mepB3* deletion allele as indicated in section 2.6.5.1. A selected clone was verified by restriction profiling (Figure 3.10) and DNA sequencing as indicated in sections 2.5.3 and 2.5.8, respectively. Restriction profiling yielded all the expected banding patterns (Figure 3.10) and plasmid DNA sequencing identified no mutations from PCR amplification (data not shown).

3.2.2. Generation of the Δ*mepB1,* Δ*mepB*2 and Δ*mepB*3 deletion mutants

3.2.2.1. Generation of the Δ*mepB1* deletion mutant

For deletion of the mepB1 gene, the mepB1 deletion allele carrying a hygromycin resistance marker was excised from plasmid pGEM+5526::hyg using the restriction enzyme PvuII and purified as indicated in section 2.5.5. One microgram of the hyg-marked mepB1 deletion allele was co-electroporated into mc2155, as indicated in section 2.6.4, with plasmid pNIT that allows the inducible expression of the phage Che9c RecET recombination system important for the recombination event. The ΔmepB1 mutant was generated as indicated in section 2.6.5.2. PCR was used as indicated in section 2.6.5.2 to identify ΔmepB1 mutants (Figure 3.11). PCR revealed the deletion of the wild type *mepB1* gene by the *hyg*-marked *mepB1* deletion allele (represented by a 2831 bp band of the *hyg*-marked *mepB1* deletion allele in comparison to a 2002 bp band of the wild type *mepB1* gene [Figure 3.11 C]).

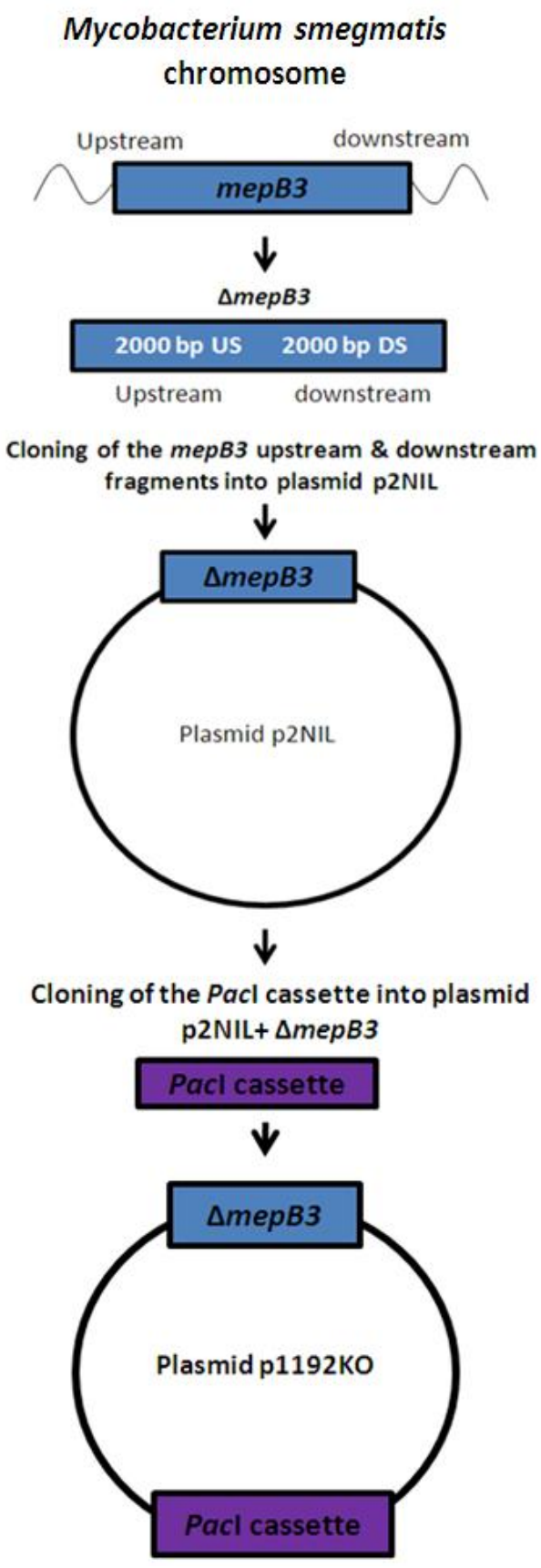


Figure 3.9: **Schematic diagram illustrating the construction of the *mepB3* deletion plasmid.** 2000 bp regions upstream and downstream of *mepB3* were used to design the mutated *mepB3* allele. The *mepB3* upstream and downstream DNA fragments were cloned into plasmid p2NIL. Thereafter, a *Pac*I cassette carrying the selection markers: *sac*B and *lac*Z was cloned into the plasmid p2NIL+ Δ*mepB3*. See Figure 3.10 for the verification of the *mepB3* deletion plasmid.

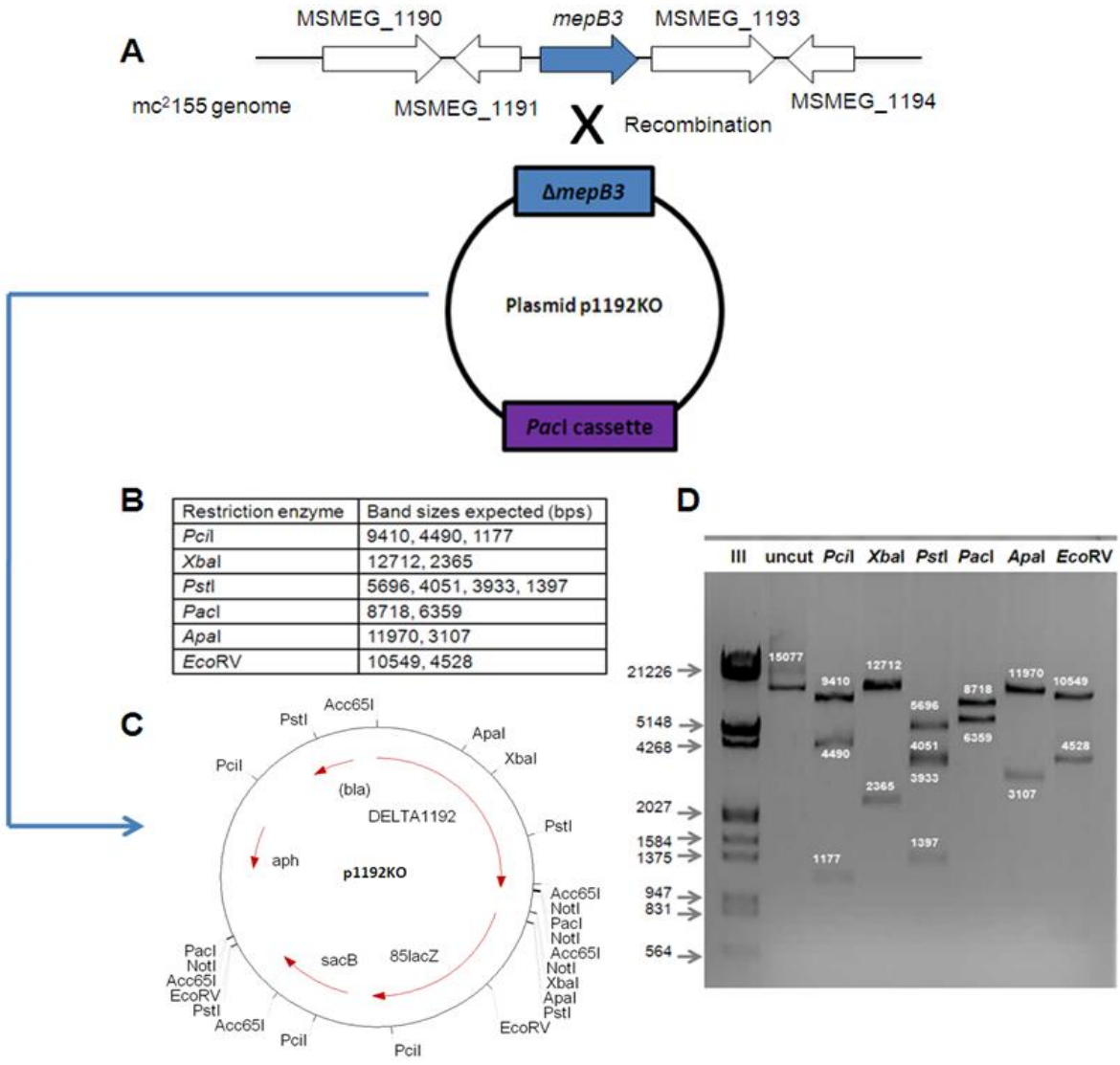


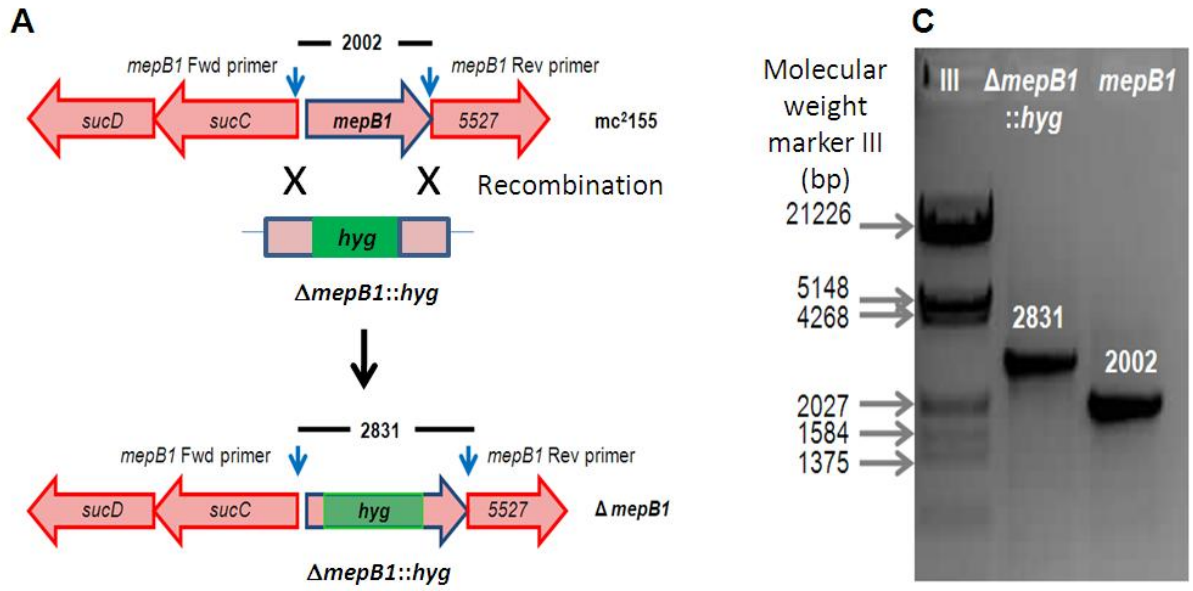
Figure 3.10: **Restriction profile of p1192KO**. (A) mc^{2}155 genome map indicating the location of the *mepB3* gene and the recombination event required for deletion of the *mepB3* gene. (B) Table indicating the restriction enzymes used for restriction analysis of p1192KO and the DNA band sizes expected. (C) Plasmid map of p1192KO. (D) Agarose gel (1%) indicating the DNA band sizes expected (labeled in base pairs).

3.2.3. Generation of the Δ*mepB1*, Δ*mepB*2 and Δ*mepB*3 deletion mutants

3.2.3.1. Generation of the Δ*mepB1* deletion mutant

For deletion of the *mepB1* gene, the *mepB1* deletion allele carrying a hygromycin resistance marker was excised from plasmid pGEM+5526::*hyg* using the restriction enzyme *Pvu*II and purified as indicated in section 2.5.5. One microgram of the *hyg*-marked *mepB1* deletion allele was co-electroporated into mc^{2}155, as indicated in section 2.6.4, with plasmid pNIT that allows the inducible expression of the phage Che9c RecET recombination system important for the recombination event. The Δ*mepB1* mutant was generated as indicated in section 2.6.5.2. PCR was used as indicated in section 2.6.5.2 to identify Δ*mepB1* mutants

(Figure 3.11). PCR revealed the deletion of the wild type *mepB1* gene by the *hyg*-marked *mepB1* deletion allele (represented by a 2831 bp band of the *hyg*-marked *mepB1* deletion allele in comparison to a 2002 bp band of the wild type *mepB1* gene [Figure 3.11 C]).



B

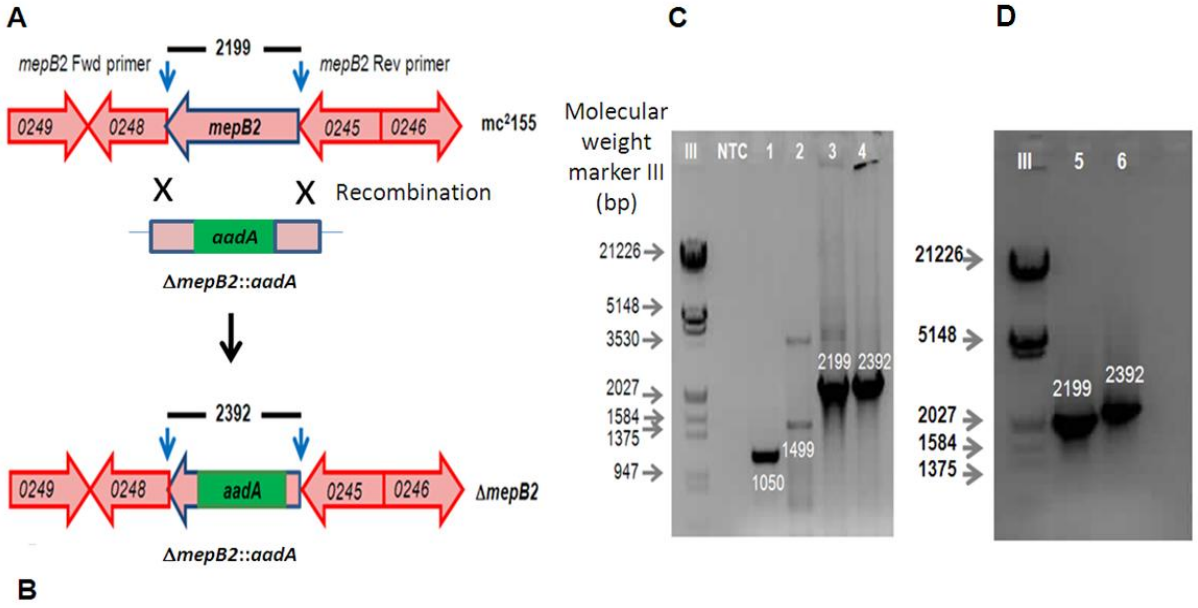
Primer set used for PCR	Band sizes expected (bp)
1. *mepB1* Fwd + *mepB1* Rev (mc^{2}155)	2002
2. *mepB1* Fwd + *mepB1* Rev (Δ*mepB1*)	2831

Figure 3.11: **Deletion of the *mepB1* gene**. (A) Schematic representation of the binding sites for primers used for screening for the Δ*mepB1* mutant, the recombination event required for deletion of the *mepB1* gene and the DNA fragment sizes expected. Blue arrows represent the primers (foward and reverse primers) as designed to bind 5′ and 3′ sequences of *mepB1* and Δ*mepB1*::*hyg*. (B) Table indicating the primer sets used for screening for the Δ*mepB1* mutant in comparison to wild type *mepB1* and the DNA fragment sizes expected. (C) Agarose gel (1%) indicating the expected band sizes (labeled in base pairs). The Δ*mepB1* gene is indicated by the 2831 bp band and mc^{2}155 was used as a control (the 2002 bp band represents the wild type *mepB1* gene).

3.2.3.2. Generation of the Δ*mepB2* deletion mutant

For deletion of the *mepB2* gene, the *mepB2* deletion allele carrying a streptomycin resistance marker was excised from plasmid p0247KO+*aadA* using the restriction enzyme *Pac*I and purified as indicated in section 2.5.5. One microgram of the *aadA*-marked *mepB2* deletion allele was co-electroporated into mc^{2}155, as indicated in section 2.6.4, with plasmid pNIT that allows the inducible expression of the phage Che9c RecET recombination system important for the recombination event. The Δ*mepB2* mutant was generated as indicated in section 2.6.5.2. PCR was used as indicated in section 2.5.1.2.2 to identify Δ*mepB2* mutants and southern blotting was used as indicated in section 2.5.9 to verify the selected Δ*mepB2*

mutant (Figure 3.12 and 3.13). PCR revealed deletion of the wild type *mepB2* gene as indiciated by a 2932 bp band of the *aadA*-marked Δ*mepB2* allele in the Δ*mepB2* mutant in comparison to a 2199 bp band of the wild type *mepB2* gene (Figure 3.12 C). However, the PCR results were not conclusive due to nearly similar band sizes of the wild type *mepB2* gene and the Δ*mepB2* allele (Figure 3.12 C). Therefore, southern blotting was conducted to confirm deletion of the *mepB2* gene. Southern blotting revealed the deletion of the *mepB2* gene (represented by the 12607 bp DNA band in mc^{2}155 [Figure 3.13 A&C]) by the *aadA*-marked Δ*mepB2* allele (represented by the 11001 bp and 2528 bp DNA bands in the Δ*mepB2* mutant [Figure 3.13 B&C]) as the restriction enzyme *Bsp*HI cuts within the *aadA*-marked Δ*mepB2* allele (see Figure 3.13 B) to produce the 11001 bp and the 2528 bp DNA bands.



Primer set used for PCR	Band sizes expected (bp)
1. *aadA* Fwd + *mepB2* Rev (Δ*mepB2*::*aadA*)	1050
2. *mepB2* Fwd + *aadA* Rev (Δ*mepB2*)	1499
3. *mepB2* Fwd + *mepB2* Rev (mc^{2}155)	2199
4. *mepB2* Fwd + *mepB2* Rev (Δ*mepB2*)	2392
5. *mepB2* Fwd + *mepB2* Rev (mc^{2}155)	2199
6. *mepB2* Fwd + *mepB2* Rev (Δ*mepB2* Δ*mepB3*)	2392

Figure 3.12: **Deletion of the *mepB2* gene**. (A) Schematic representation of the binding sites for primers used for screening for the Δ*mepB2* mutant, the recombination event required for deletion of the *mepB2* gene and the DNA fragment sizes expected. Blue arrows represent the primers (forward and reverse primers) as designed to bind 5′ and 3′ sequences of *mepB2* and Δ*mepB2*. (B) Table indicating the primer sets used for screening for the Δ*mepB2* mutant in comparison to wild type *mepB2*. (C) Agarose gel (1%) indicating the expected band sizes (labeled in base pairs). NTC: no DNA template control. (D) Agarose gel (1%) indicating the expected band sizes (labeled in base pairs) for deletion of *mepB2* from the Δ*mepB3* mutant. The 2392 bp band (lanes 4 and 6 represent the Δ*mepB2* gene, in the Δ*mepB2* mutant and the Δ*mepB2* Δ*mepB3* mutant, respectively).

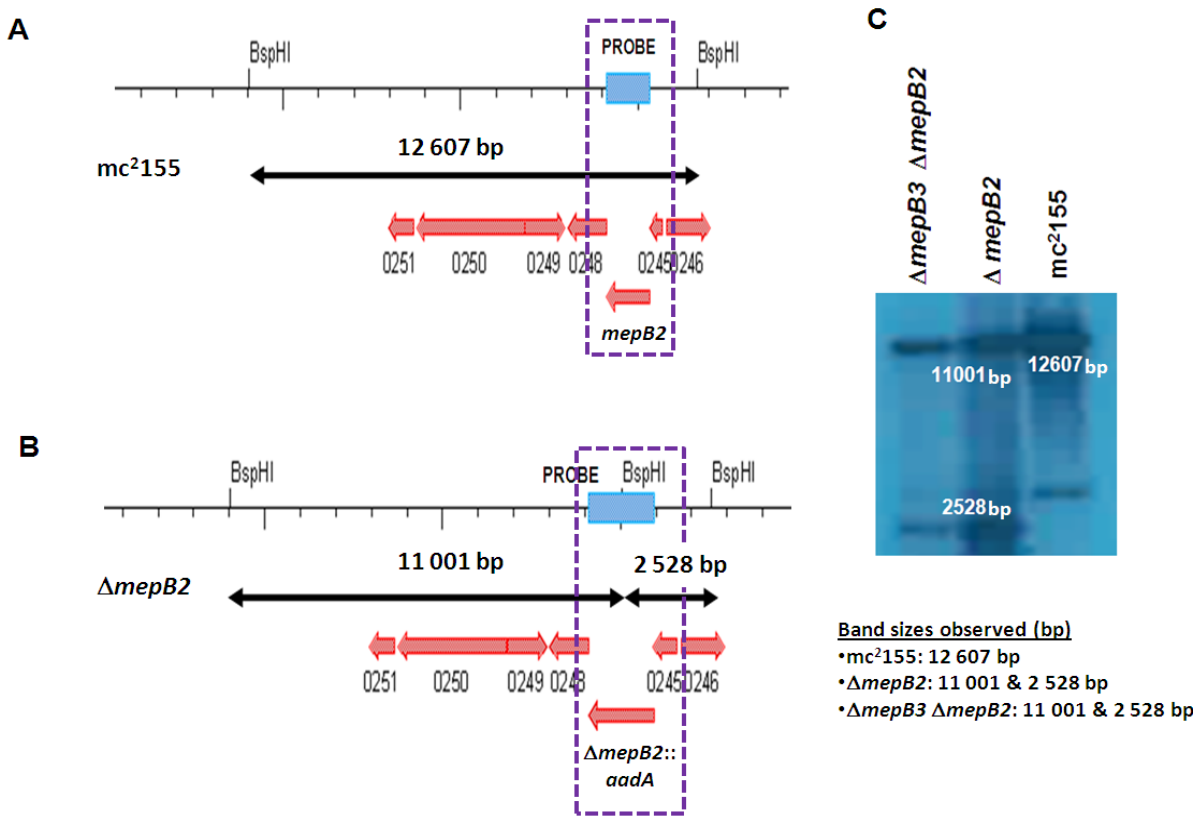
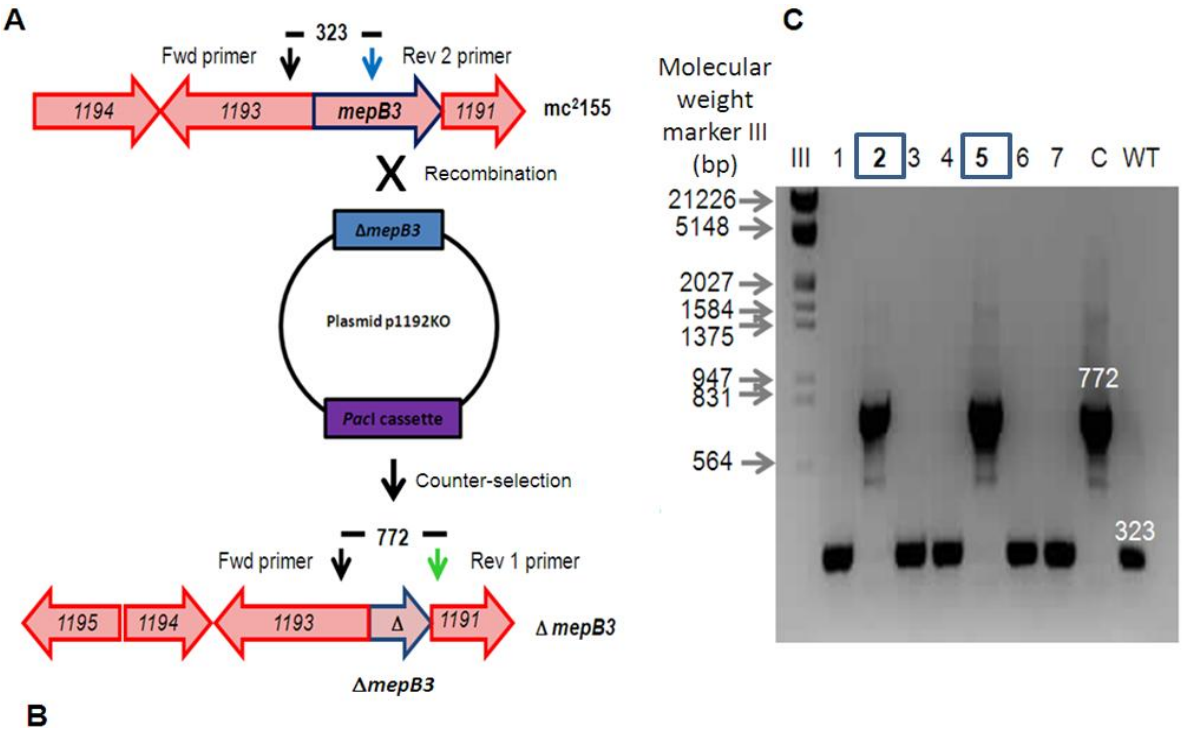


Figure 3.13: **Southern blot analysis of the Δ*mepB2* mutant**. (A) Genomic map of mc^{2}155 showing the expected DNA fragment size carrying the wild type *mepB2* gene after digestion of the genomic DNA with the restriction enzyme *Bsp*HI. (B) Genomic map of the Δ*mepB2* mutant showing the expected DNA fragment sizes carrying the Δ*mepB2* allele after digestion of the genomic DNA with the restriction enzyme *Bsp*HI. (C) Southern blot depicting the DNA fragments bound by the *mepB2* specific probe. The Δ*mepB2* allele is represented by the 11001 bp and the 2528 bp bands.

3.2.3.3. Generation of the Δ*mepB3* deletion mutant

As mentioned above, the two-step allelic exchange technique was adopted for deletion of the *mepB3* gene. This method allowed for generation of an unmarked Δ*mepB3* mutant. Plasmid p1192KO was used for deletion of *mepB3* according to the protocol outlined in section 2.6.5.1. Integration of plasmid p1192KO into the genome of mc^{2}155 resulted in the generation of 3 *mepB3* single cross-over (SCO) strains, which appeared as blue colonies on 7H10 media supplemented with 2% X-gal and Kan (25 µg/ml) (data not shown). A single *mepB3* SCO strain was processed as indicated in section 2.6.5.1 to generate the unmarked Δ*mepB3* mutant (see Figure 2.2). PCR was used as indicated in section 2.6.5.2 to identify Δ*mepB3* mutants and southern blotting was used as indicated in section 2.5.9 to verify the selected Δ*mepB3* mutant (Figure 3.14 and 3.15). PCR revealed deletion of the wild type *mepB3* gene as indiciated by a 772 bp band of the Δ*mepB3* allele in the Δ*mepB3* mutant in comparison to a 323 bp band of the wild type *mepB3* gene (Figure 3.14 C). Southern blotting

revealed the deletion of the *mepB3* gene (represented by the 4869 bp DNA band in mc^2155 [Figure 3.15 A&D]) by the Δ*mepB3* allele (represented by the 3787 bp DNA band in the Δ*mepB3* mutant [Figure 3.13 C&D]) after digestion of the genomic DNA with the restriction enzyme *Pst*I.



Primer set used for PCR	Band sizes expected (bp)
Fwd + Rev1	772
Fwd + Rev2	323

Figure 3.14: **Deletion of the *mepB3* gene**. (A) Schematic representation of the binding sites for primers used for screening for the Δ*mepB3* mutant and the recombination event required for deletion of the *mepB3* gene. Black arrows represent the forward primer (Fwd) designed to bind upstream of both the mutant gene and the wild type gene. Green arrow represents reverse primer 1 (Rev 1) designed to bind downstream of the mutated gene and the blue arrow represents reverse primer 2 (Rev 2) designed to bind within the wild type *mepB3* gene. (B) Table indicating the primer sets used for PCR screening and the expected DNA band sizes. (C) Agarose gel (1%) indicating the expected band sizes (labeled in base pairs). C: plasmid control, WT: mc^2155 control. Lanes 1 to 7 represent the samples screened. The Δ*mepB3* mutants are indicated by the blue boxes (lanes 2 and 5).

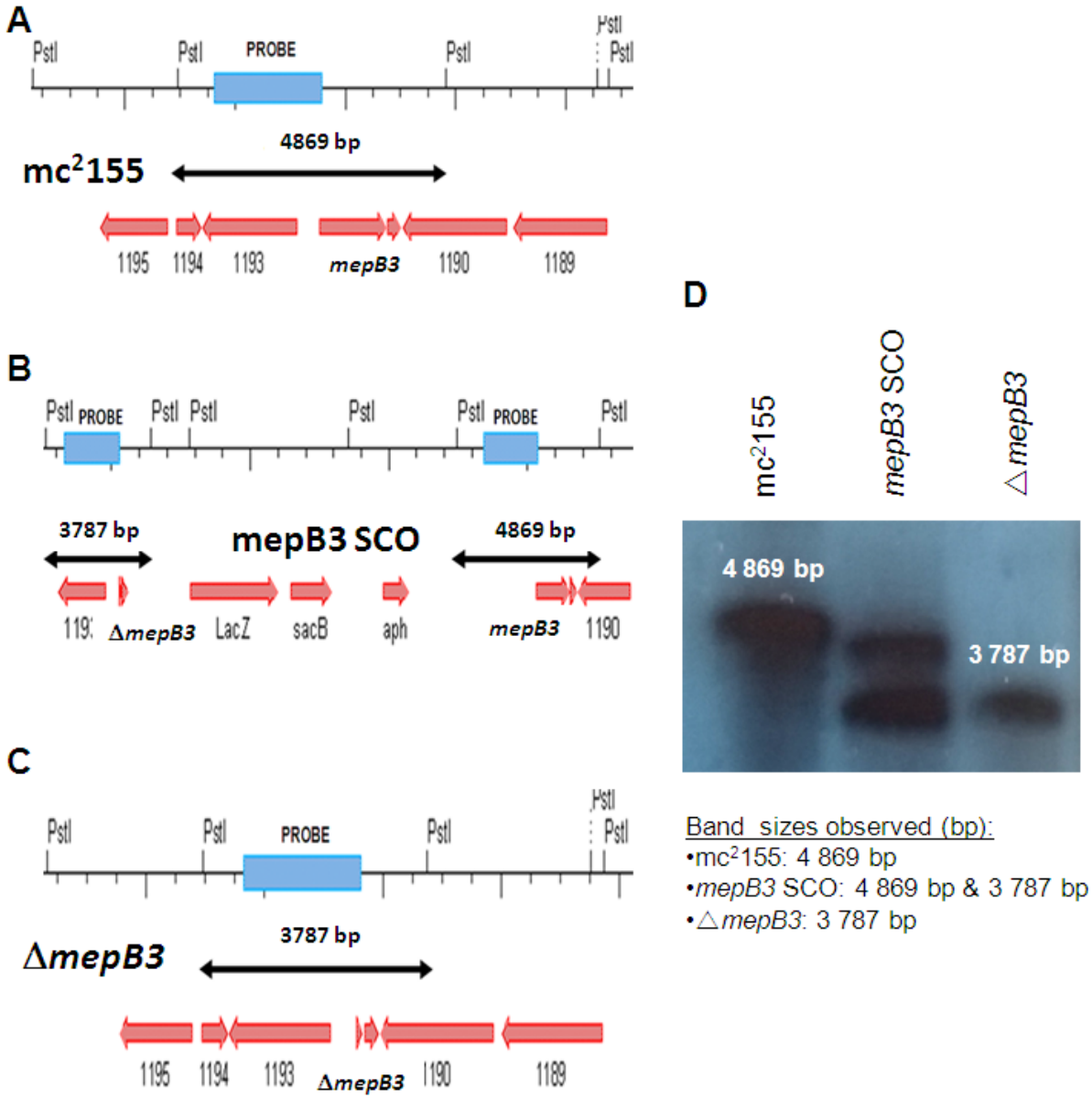


Figure 3.15: **Southern blot analysis of the Δ*mepB3* mutant**. (A) Genomic map of mc^{2}155 showing the expected DNA fragment size for the wild type *mepB3* allele. (B) Genomic map of *mepB3* SCO showing the expected DNA fragment size for the wild type *mepB3* allele and the Δ*mepB3* allele. (C) Genomic map of the Δ*mepB3* mutant showing the Δ*mepB3* allele. (D) Southern blot depicting the DNA fragments bound by the *mepB3* specific-probe. The genomic DNA was cut with the enzyme *Pst*I to produce DNA fragment sizes indicated. The Δ*mepB3* allele is represented by the 3787 bp band.

3.2.3.4. Generation of a Δ*mepB2* Δ*mepB3* double deletion mutant

As MepB2 and MepB3 share 40% sequence homology according to the NCBI BLAST tool (data not shown) and structural analysis by superimposition of the MepB2 and MepB3 protein tertiary structures (Figure 3.16), these two M23 proteins may have related biological functions. Indeed, bio-informatics analysis indicated that both MepB2 and MepB3 are related

to cell division M23 proteins of model organisms such as *V. cholerae, E. coli and P. aeruginosa* (Figure 3.1). However, these proteins also clustered closely to M23A proteins such as LasA and Pseudoalterin (Figure 3.1), which are secreted M23 proteins with PG hydrolytic activity. This suggested that both MepB2 and MepB3 belong to the M23A class of peptidases with a potential role in mycobacterial cell division. To interrogate this, a strain lacking both *mepB2* and *mepB3* was constructed by deletion of *mepB2* from the Δ*mepB3* mutant as indicated in section and 3.2.2.2. PCR was used as indicated in section 2.6.5.2 to identify the Δ*mepB2* Δ*mepB3* double deletion mutant (Figure 3.12 D) and southern blotting was used as indictated in section 2.5.9 to verify the deletion of *mepB2* from the Δ*mepB3* mutant background (Figure 3.13C). PCR revealed deletion of the wild type *mepB2* gene as indiciated by a 2932 bp band of the *aadA*-marked Δ*mepB2* allele in the Δ*mepB2* Δ*mepB3* mutant in comparison to a 2199 bp band of the wild type *mepB2* gene. Southern blotting revealed the deletion of the *mepB2* gene (represented by the 12607 bp DNA band in mc^2155 [Figure 3.13 A&C]) by the *aadA*-marked Δ*mepB2* allele (represented by the 11001 bp and 2528 bp DNA bands in the Δ*mepB2* Δ*mepB3* mutant [Figure 3.13 B&C]) as the restriction enzyme *Bsp*HI cuts within the *aadA*-marked Δ*mepB2* allele (see Figure 3.13B) to produce the 11001 bp and the 2528 bp DNA bands.

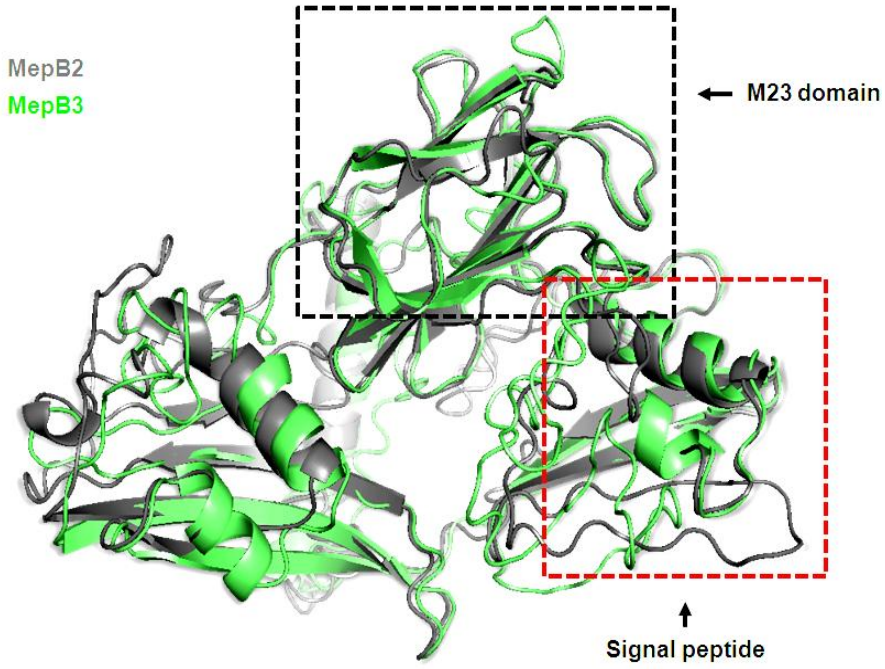


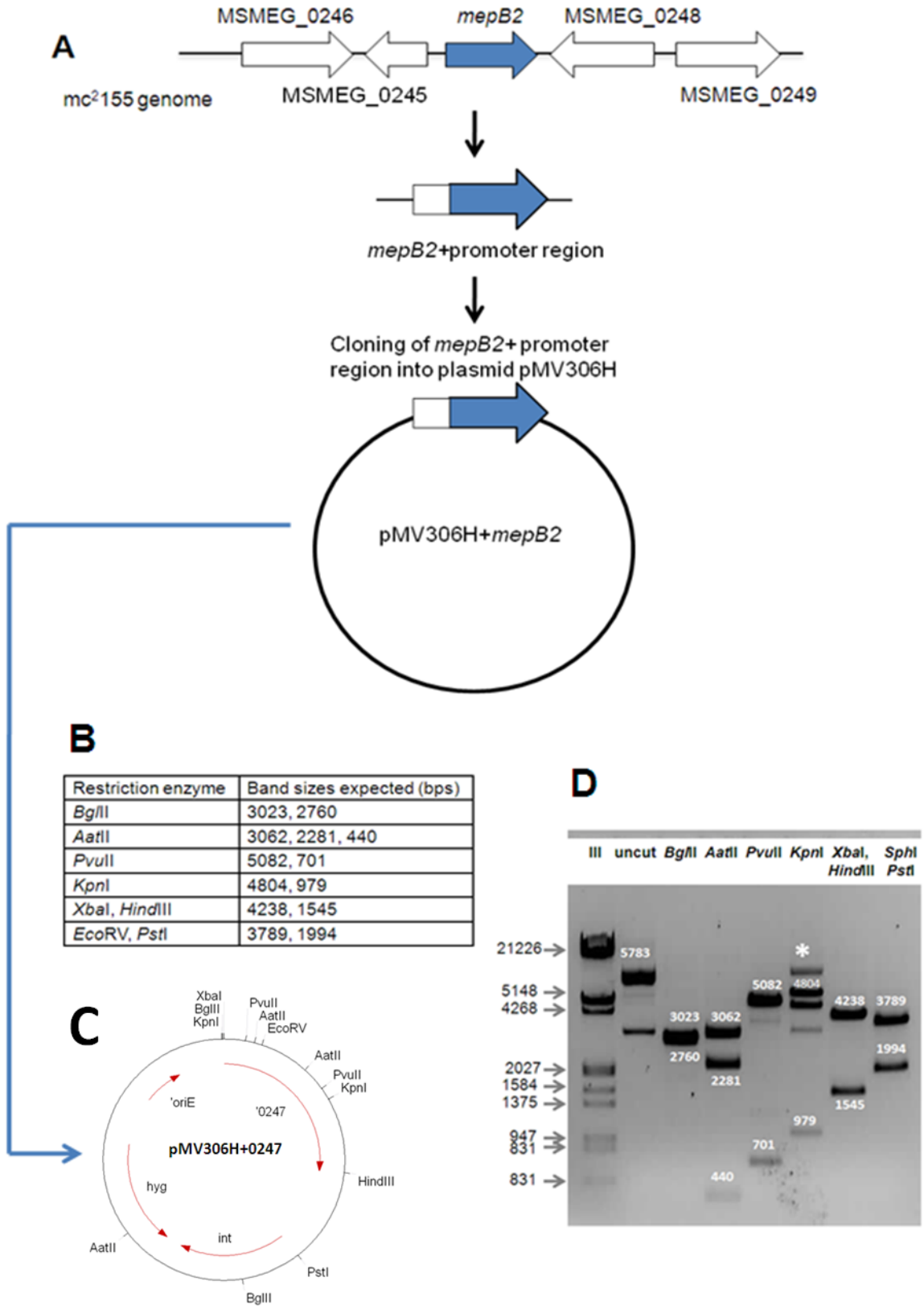
Figure 3.16: **MepB2 and MepB3 show structural similarity**. Superimposition of MepB2 (grey) and MepB3 (green) shows similar organization of both the MepB2 and MepB3 M23 domains (black box) and signal peptides (red box).

3.2.4. **Genetic complementation of the Δ*mepB2* and Δ*mepB3* deletion mutants**

Genetic complementation of mutated strains was performed to confirm that the phenotypic variation observed during the analysis of these strains was due to the inactivation of the gene of interest and not due to polar effects. The process of genetic complementation of the *mepB* mutants is detailed below (also see Figure 3.4). Genetic complementation of the Δ*mepB1* strain was not achieved. A *mepB1* complementation vector was constructed (data not shown). However, the *mepB1* complementation vector did not complement the Δ*mepB1* strain as evidenced by further analysis of the Δ*mepB1* strain. This is usually observed for strains complemented at a heterologous locus; therefore, we only show the genetic complementation of the Δ*mepB2*, Δ*mepB3* strains and the Δ*mepB2* Δ*mepB3* double deletion strain. The construction of the complementation plasmids for the *mepB2* and *mepB3* genes is detailed below.

3.2.4.1. **Construction of the *mepB2* complementation plasmid**

For the complementation of the Δ*mepB2* gene, the wild type *mepB2* allele was amplified including a 100 bp region of the native *mepB2* promoter by PCR and cloned into the plasmid pMV306H as outlined in sections 2.5.1.2.1 and 2.5.7, respectively (Figure 3.17 A). A selected clone (pMV306H+0247) was verified by restriction profiling (Figure 3.17 B,C&D) and DNA sequencing as indicated in section 2.5.3 and 2.5.8, respectively. Restriction analysis yielded the correct banding pattern (Figure 3.17 D), with the exception of products of *Kpn*I restriction analysis, which indicated partial restriction of the plasmid DNA. This was caused by the addition of slighlty more plasmid DNA for the calculated amount of restriction enzyme used. However, the plasmid was valid for use and sequencing of the plasmid DNA further confirmed the genetic integrity of the plasmid (data not shown).



Restriction enzyme	Band sizes expected (bps)
*Bgl*II	3023, 2760
*Aat*II	3062, 2281, 440
*Pvu*II	5082, 701
*Kpn*I	4804, 979
*Xba*I, *Hind*III	4238, 1545
EcoRV, *Pst*I	3789, 1994

Figure 3.17: **Construction and restriction profiling of pMV306H+0247**. (A) mc²155 genome map indicating the location of the *mepB3* gene and the construction of the *mepB2* complementation plasmid. (B) Table indicating the restriction enzymes used for restriction analysis of pMV306H+0247 and the DNA band sizes expected. (C) Plasmid map of pMV306H+0247. (D) Agarose gel (1%) indicating the DNA band sizes expected (labeled in base pairs). *: partial DNA restriction.

3.2.4.2. **Construction of the *mepB3* complementation plasmid**

For the complementation of the Δ*mepB3* gene, the wild type *mepB3* allele was amplified including a 100 bp region of the native *mepB3* promoter by PCR and cloned into the plasmid pTweety as outlined in sections 2.5.1.2.1 and 2.5.7, respectively (Figure 3.18 A). A selected clone (pTweety+1192) was verified by restriction profiling (Figure 3.18 B,C&D) and DNA sequencing as indicated in section 2.5.3 and 2.5.8, respectively. Restriction analysis yielded the correct banding pattern (Figure 3.18 D), with the exception of products of *Xba*I and *Xmn*I restriction analysis. However, sequencing of the plasmid DNA further confirmed the genetic integrity of the plasmid (data not shown).

3.2.5. **Complementation of the Δ*mepB2* mutant**

Plasmid pMV306H+0247 (Figure 3.17) was used for genetic complementation of the Δ*mepB2* mutant as indicated in section 2.6.6 (also see Figure 3.4). As mentioned above, restriction analysis yielded the correct banding pattern and sequencing further confirmed the genetic integrity of the plasmid (Figure 3.17). PCR was used to confirm the presence of the wild type *mepB2* allele after complementation of the Δ*mepB2* mutant (Appendix C).

3.2.6. **Complementation of the Δ*mepB3* mutant**

Plasmid pTweety+1192 (Figure 3.18) was used for genetic complementation of the *mepB3* mutant as indicated in section 2.6.6 (also see Figure 3.4). As mentioned above, restriction analysis yielded the correct banding pattern, except for the restriction enzyme *Xba*I (Figure 3.18). However, the restriction enzyme *Xba*I does not cut within the inserted wild type *mepB3* allele; therefore, the plasmid should express a functional MepB3 protein. Furthermore, DNA sequencing of this plasmid confirmed the genetic integrity of the plasmid (data not shown). PCR was used to confirm the presence of the wild type *mepB3* allele after complementation of the Δ*mepB3* mutant (Appendix C).

M23 proteins serve important biological roles during bacterial PG remodelling to allow efficient cell growth, cell division and maintenance of cell wall integrity and cell shape. Considering this, we investigated the role of the mycobacterial M23 proteins in bacterial biology by the following procedures (see Figure 3.4). To determine the role of the MepB proteins in mycobacterial cell growth we analysed the growth rates of the mutant strains in comparison to the wild type and the genetically complemented strains by conducting three independent growth curve experiments.

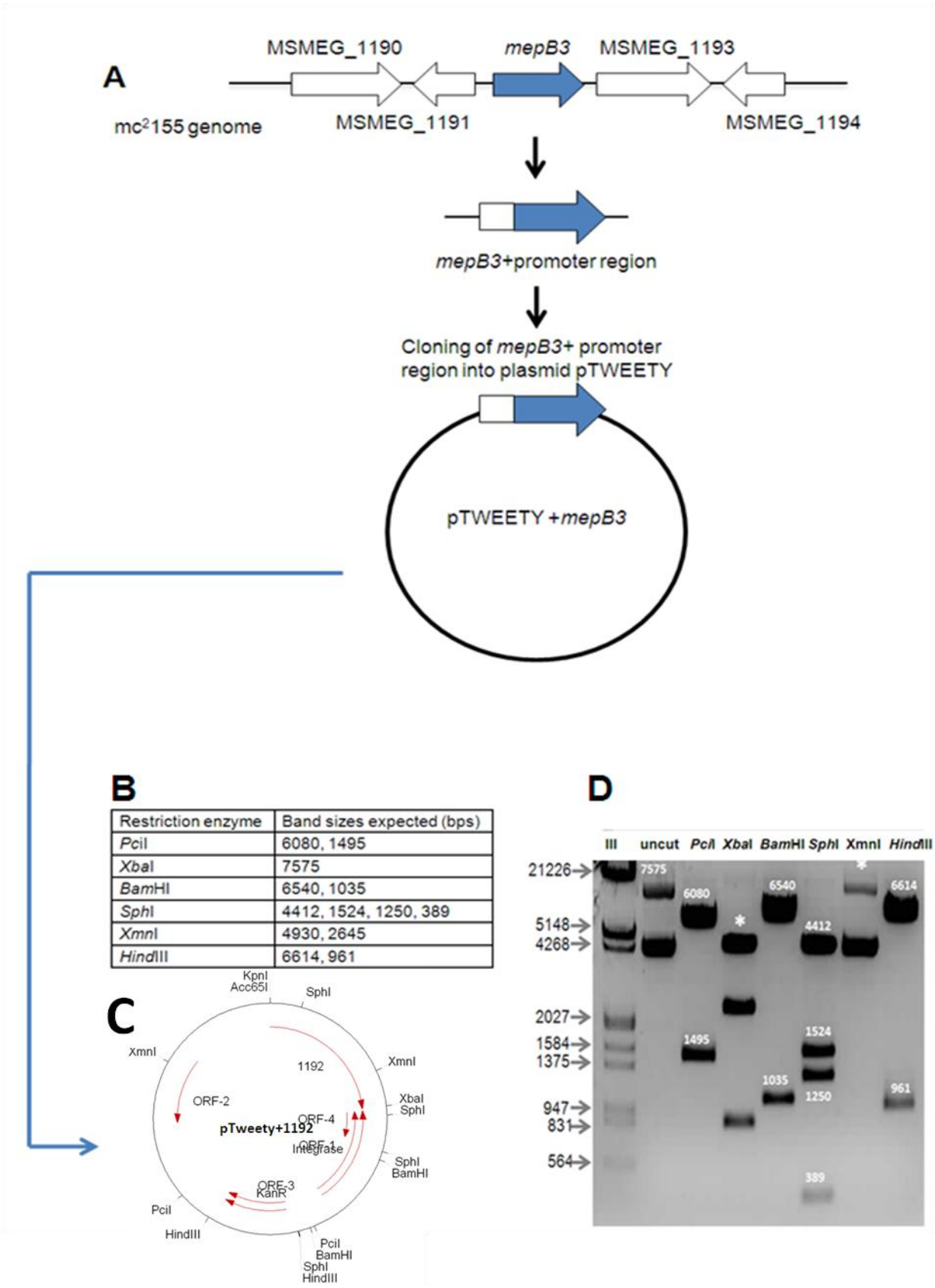


Figure 3.18: **Construction and restriction profiling of pTweety+1192**. (A) mc^{2}155 genome map indicating the location of the *mepB3* gene. (B) Table indicating the restriction enzymes used for restriction analysis of pTWEETY+1192 and the DNA band sizes expected. (C) Plasmid map of pTweety+1192. (D) Agarose gel (1%) indicating the DNA band sizes expected (labeled in base pairs).

To investigate the role of these proteins in mycobacterial cell division, we performed microscopic analysis of the mutant strains in comparison to the wild type and the genetically complemented strains with the use of cell wall staining chemical probes. Additionally, we examined the cell wall integrity of the mutant strains by exposing these strains to lysozyme and antibiotics that target the PG layer of the cell wall. Finally, protein interacting partners of these mycobacterial MepB proteins were identified and confirmed through the M-PFC assay (see Figure 3.4).

3.3. **The role of MepB1, MepB2 and MepB3 in cell growth**

To determine the role of MepB1, MepB2 and MepB3 in cell growth, the growth rate of the single deletion and double deletion mutants was analyzed in comparison to the wild type and genetically complemented strains (Figure 3.19) as detailed in section 2.9.1.1. As indicated in Figure 3.19, *mepB1, mepB2* and *mepB3* were all dispensable for growth as all Δ*mepB* mutants were able to grow without these proteins. However, the loss of *mepB1* caused slightly delayed growth kinetics, particularly during the exponential growth phase. This suggested that MepB1 could be involved in cytosolic PG biosynthesis, cell division or cell growth associated processes as MepB1 does not have a signal peptide for translocation to the periplasm. The pertubation of PG biosynthesis often results in defects in cell division or cell growth. To assess the role of the MepB proteins in cell division or growth, we employed flow cytometry and fluorescence microscopy with the use of fluorescent chemical probes which stain the mycobacterial cell wall (see Figure 3.4). The flow cytometry and fluorescence microscopy results are detailed below.

3.4. **Flow cytometry analysis of the Δ*mepB2*, Δ*mepB3* mutants and the Δ*mepB2* Δ*mepB3* double mutant**

Flow cytometry was used to assess the cell morphology of the mutant strains because this system analyzes a large number of the sample compared to conventional microscopy for analysis of cell morphology. The morphology of the mutant strains was assessed by flow cytometry side scatter. The individual loss of *mepB2* and *mepB3* did not significantly affect the morphology of the mutant strains, as evidenced by a slight shift in side scatter (Figure 3.20). Interestingly, concurrent inactivation of both *mepB2* and *mepB3* resulted in a change in cell morphology (Figure 3.21). This analysis indicated the formation of larger cells of the Δ*mepB2* Δ*mepB3* double mutant suggesting that the cells were impaired in cell division processes.

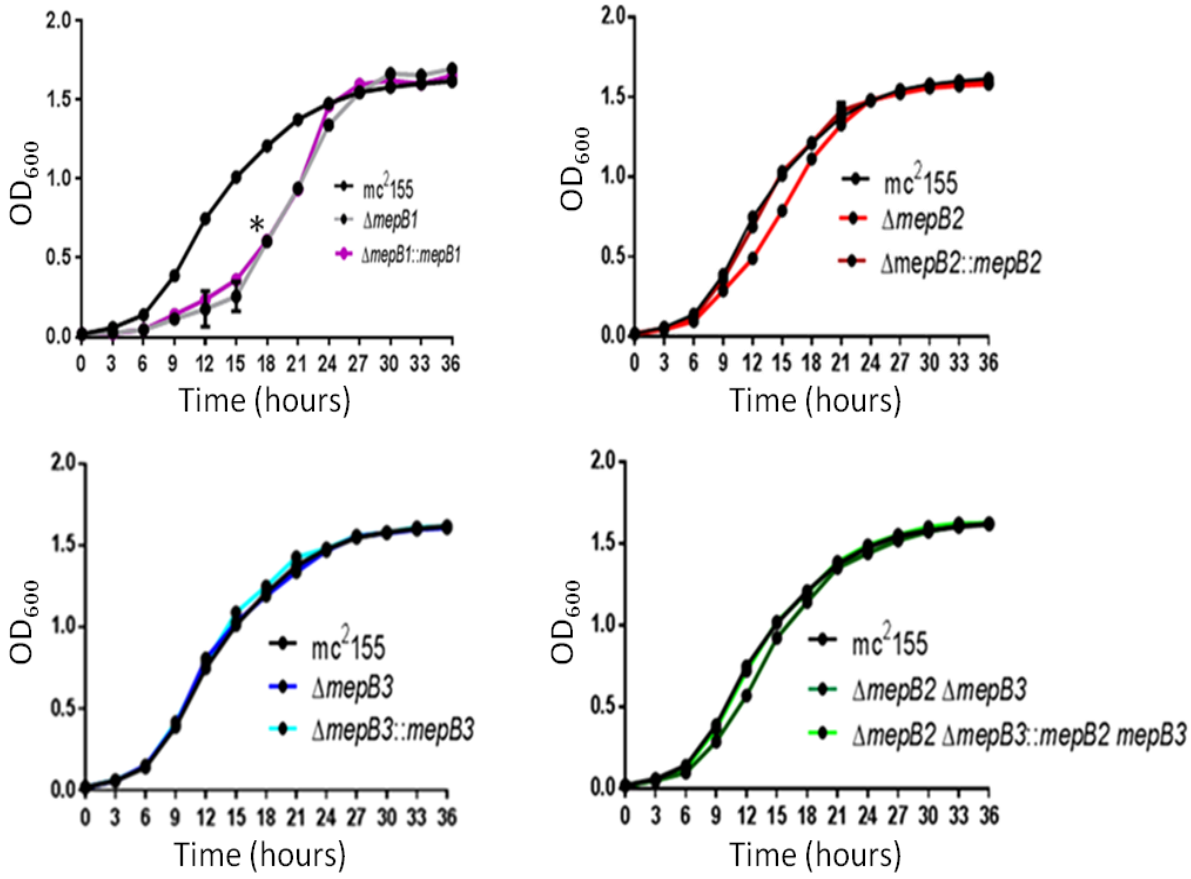


Figure 3.19: **Loss of MepB1 causes delayed growth kinetics**. Growth kinetics of the Δ*mepB1*, Δ*mepB2*, Δ*mepB3* and Δ*mepB2* Δ*mepB3* mutants in comparison to mc^2155 and the complemented strains were conducted by measuring the increase in culture optical density (OD_{600}) over 36 hours. *: p-value <0.0001(by the unpaired Student's *t*-test). The data indicated represents three independent experiments for all strains analyzed.

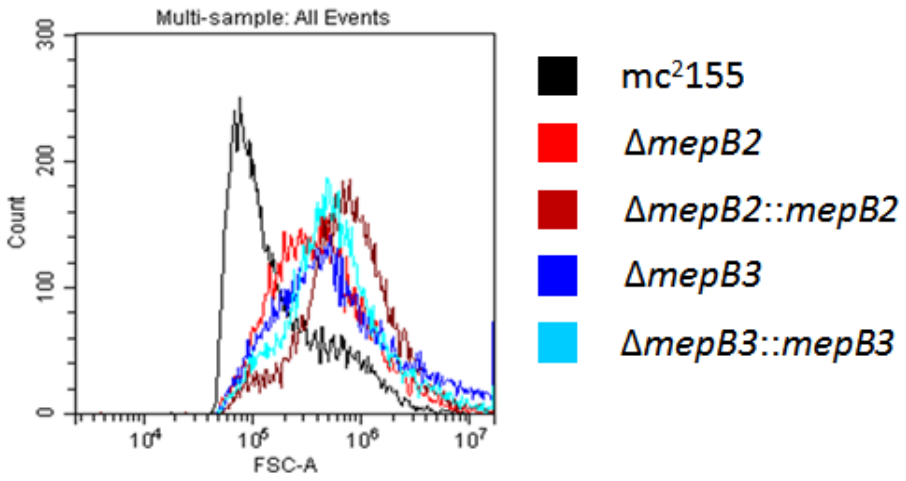


Figure 3.20: **Flow cytometry analysis of the morphology of Δ*mepB2* and Δ*mepB3* in comparison to mc²155 and the complemented strains**. Δ*mepB2* and Δ*mepB3* display a slightly different cell morphology.

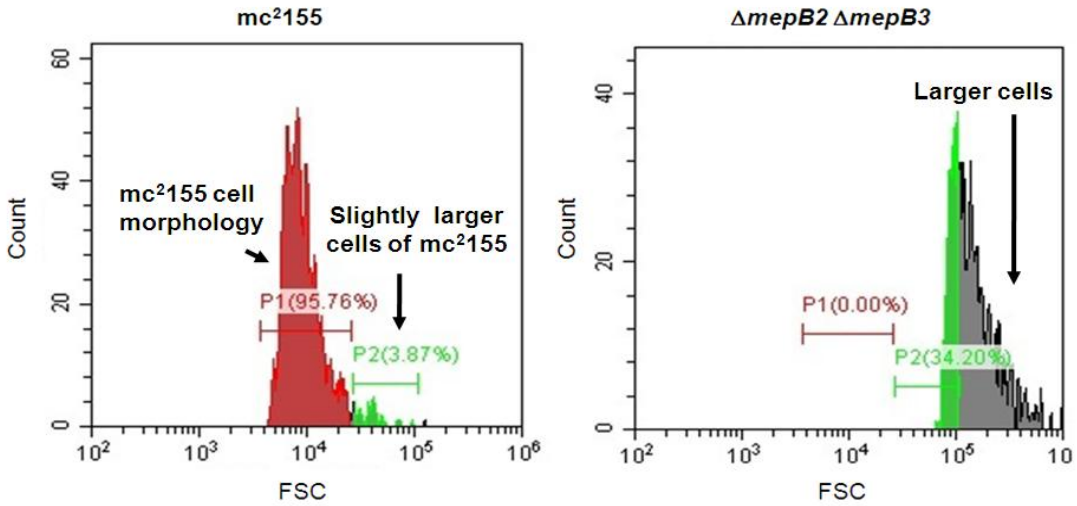


Figure 3.21: **Loss of MepB2 and MepB3 collectively affects cell morphology**. Flow cytometry analysis of the Δ*mepB2* Δ*mepB3* mutant in comparison to wild type indicated a change in cell morphology (forward scatter [FSC] analysis determines the approximate size of the sample). The wild type cell size (indicated in red and green) was used to gate for the Δ*mepB2* Δ*mepB3* sample. The grey population indicates a larger Δ*mepB2* Δ*mepB3* cell size in comparison to mc²155.

3.5. **Microscopic analysis of the Δ*mepB1*, Δ*mepB2*, Δ*mepB*3 and the Δ*mepB2* Δ*mepB3* strains**

The Δ*mepB1*, Δ*mepB2*, Δ*mepB3* and Δ*mepB2* Δ*mepB3* strains were prepared for microscopy as indicated in section 2.9.2 together with mc^{2}155 and the genetically complemented strains. Interestingly, microscopic analysis of the fluorescent BODIPY Vancomycin stained Δ*mepB1* cells revealed septal and cell pole buldging cells (Figure 3.22 B) as compared to rod-shaped cells of the wild type mc^{2}155 strain (Figure 3.22 A). The frequency of the polar buldging cells of the Δ*mepB1* strain was quantified in comparison to mc^{2}155 cells after staining of the cells with a cell membrane stain FM4/64 as indicated in section 2.9.2.4 (Figure 3.22 C). Strikingly, 87% of the Δ*mepB1* cells displayed a polar buldging phenotype indicating pertubations in cell growth processes. This is supported by the observation that the Δ*mepB1* displays reduced growth kinetics (Figure 3.19). Microscopic analysis of the Δ*mepB2* Δ*mepB3* double mutant revealed a defect in cell division (Figure 3.23). This is evidenced by the presence of chains of cells that are linked by septal bridges, indicating arrested cell separation. DNA staining also confirmed a failure in cell separation as evidenced by the presence of multiple DNA foci within a chain of cells in comparison to mc^{2}155 (Figure 3.24).

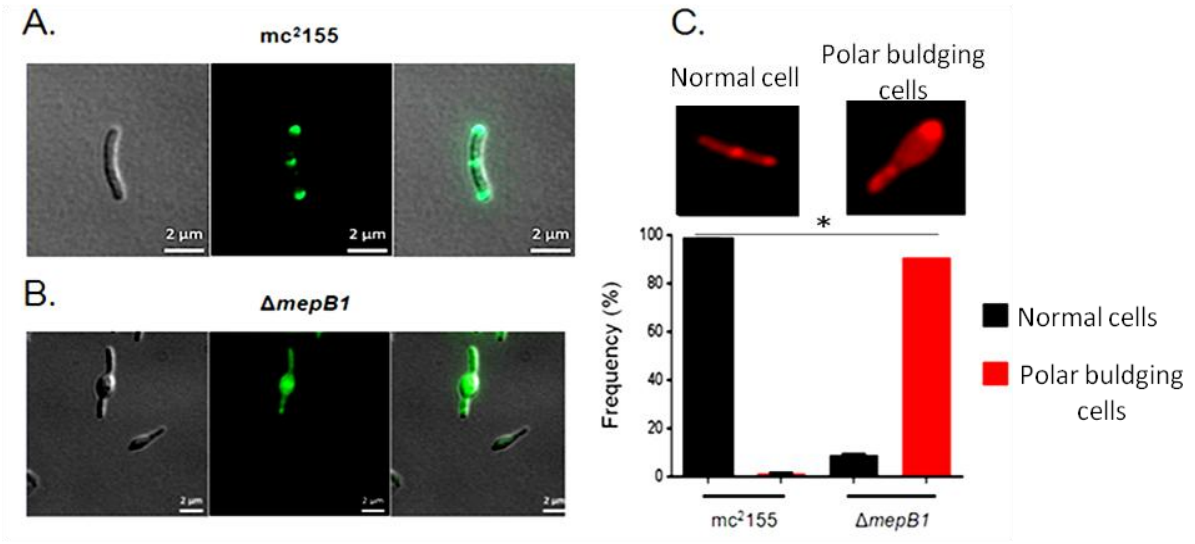


Figure 3.22**: Loss of MepB1 causes septum formation and cell pole buldging**. (A & B) mc^{2}155 and Δ*mepB1* stained with the Fluorescent BODIPY Vancomycin stain (Life Technologies). (C) Quantification of the Δ*mepB1* cell buldging phenotype in comparison to mc^{2}155. *: p-value <0.0001 (by the unpaired Student's *t*-test). The data indicated represents three independent experiments for all strains analyzed.

The Δ*mepB2* Δ*mepB3* mutant cell length was measured in relation to mc^{2}155 and the complemented strains (Figure 3.25). This analysis revealed the formation of longer cells by the Δ*mepB2* Δ*mepB3* double mutant. This confirmed the flow cytometry analysis of the

Δ*mepB2* Δ*mepB3* double mutant. The complemented strain displayed partial reduction in cell length to wild type levels. To further analyse the cell division defect caused by the inactivation of MepB2 and MepB3, staining of PG was used to investigate septal PG biosynthesis in the Δ*mepB2*, Δ*mepB3* and Δ*mepB2* Δ*mepB3* mutants. For this experiment, the mutants were prepared together with mc^2155 as indicated in sections 2.9.2.1 and 2.9.2.2. PG staining revealed the formation of mutiple septa between cells that were unable to separate (Figure 3.26). These observations confirmed that the Δ*mepB2* Δ*mepB3* mutant was able to synthesize the septum, but thereafter required MepB2 and MepB3 as PG hydrolases for the cleavage of septal PG to allow cell division. The absence of these proteins resulted in the chaining of cells.

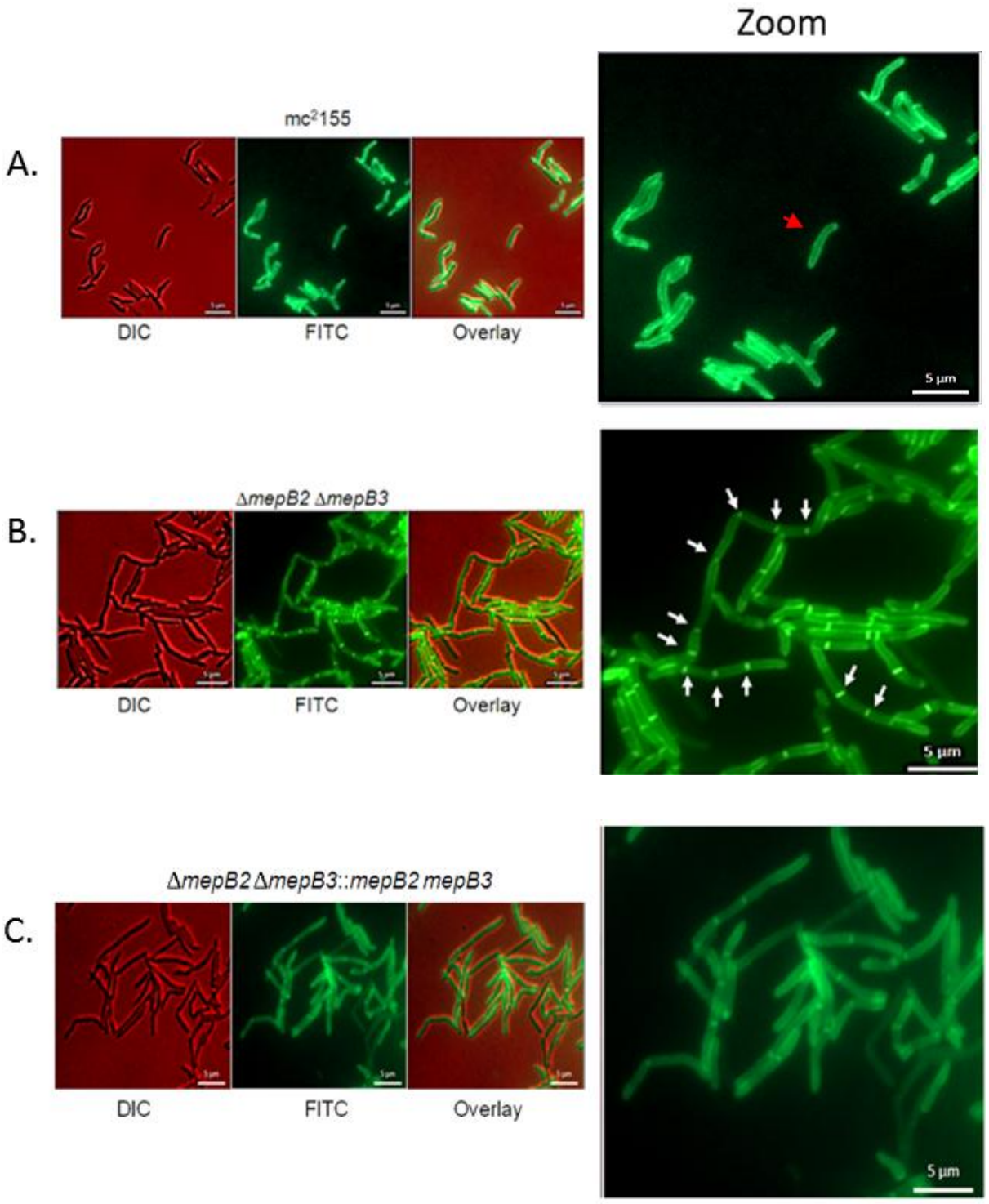


Figure 3.23: **Microscopic analysis of the DMN-trehalose stained Δ*mepB1* Δ*mepB2* mutant.** (A) DMN-trehalose stained mc^{2}155. (B) DMN-trehalose stained *ΔmepB1 ΔmepB2* mutant. (C) DMN-trehalose stained complemented strain. White arrows indicate sites of failure of cell division (chaining cells). Scale bar: 5 µm.

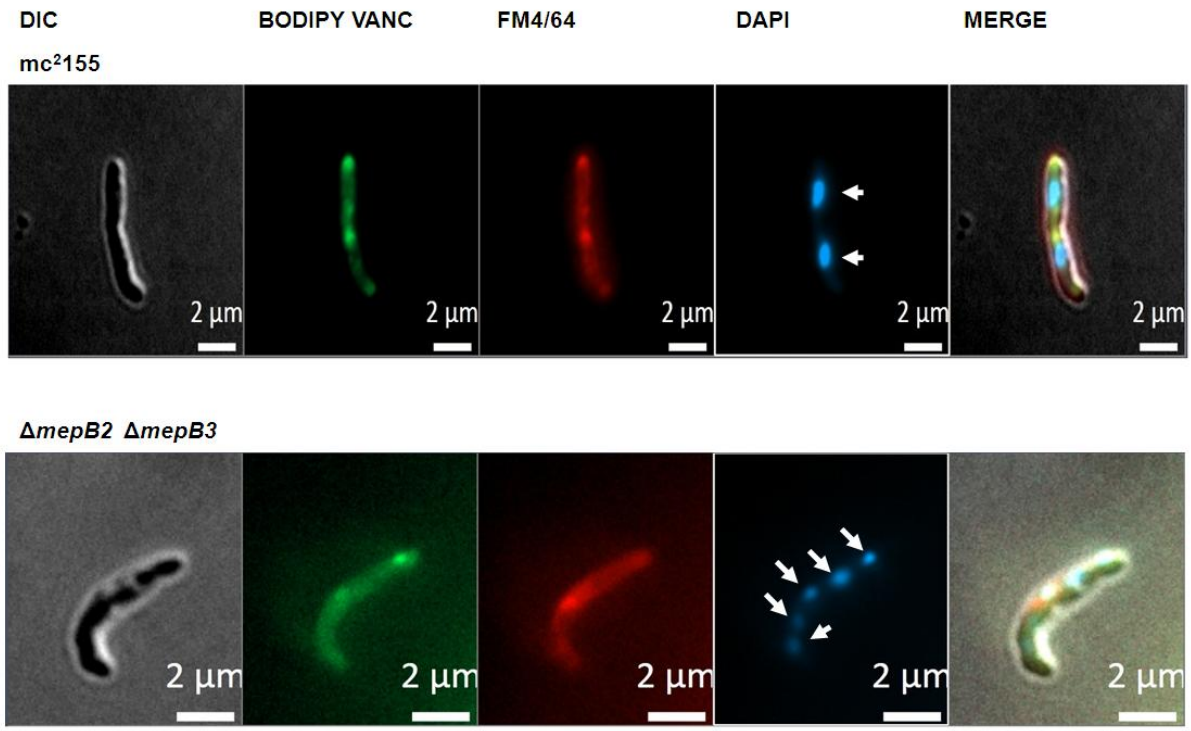


Figure 3.24: **DNA staining of the Δ*mepB2* Δ*mepB3* mutant reveals multiple DNA foci**. Multiple DNA foci are observed in the Δ*mepB2* Δ*mepB3* strain indicating a cell division defect in comparison to mc^{2}155.

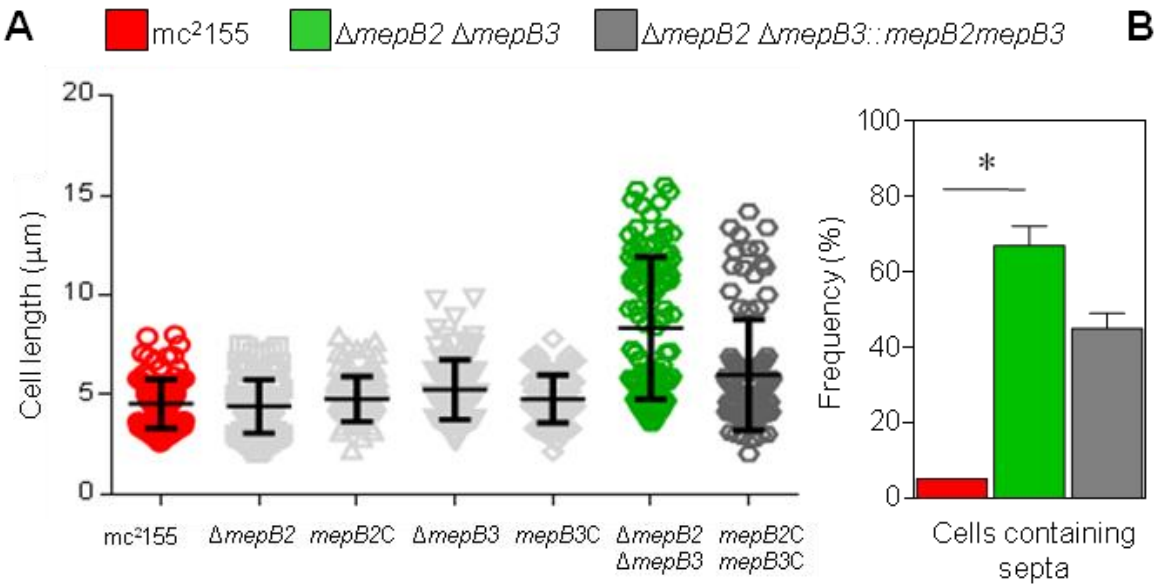


Figure 3.25: **The Δ*mepB2* Δ*mepB3* mutant forms chains of cells**. (A) Cell length measurements of the Δ*mepB1*, Δ*mepB2*, Δ*mepB3*, Δ*mepB2* Δ*mepB3* in comparison to mc^{2}155 and the complemented strains. Δ*mepB2* Δ*mepB3* cells (271 cells measured) are longer than mc^{2}155 (269 cells measured). The mc^{2}155 mean cell length is: 4.5 µm and the Δ*mepB2* Δ*mepB3* mean cell length is: 8.3 µm. ***: p-value <0.0001 (by the unpaired Student's *t*-test). (B) Histogram indicating the proportion of cells with multiple septa (n=300). *:p < 0.0001. The data indicated represents three independent experiments for all strains analyzed.

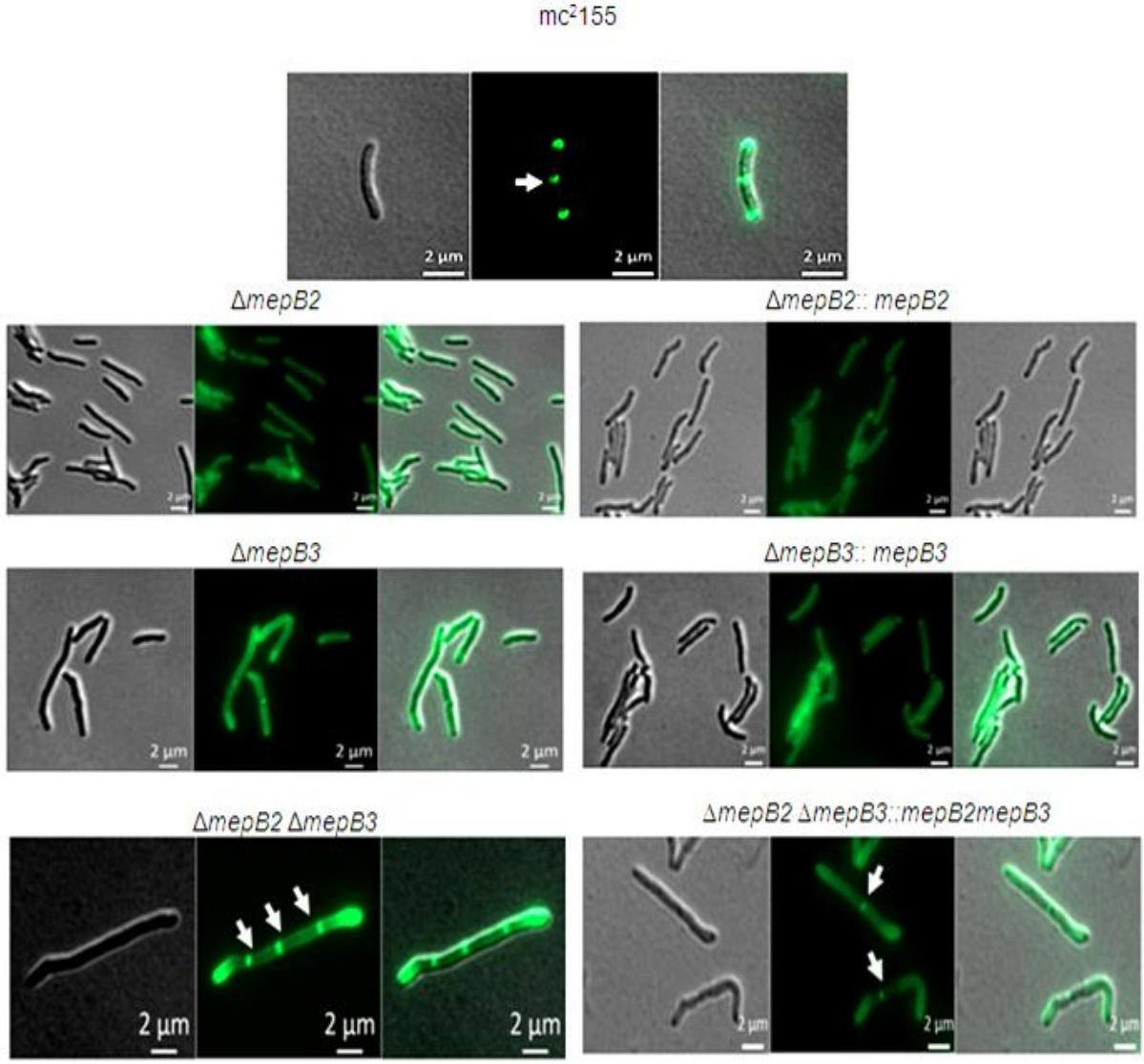


Figure 3.26: **MepB2 and MepB3 are required for cleavage of septal PG to allow cell division**. PG staining with the Click Chemistry D-alanine analogue. Staining of Δ*mepB2* Δ*mepB3* cells displayed multiple septa (white arrows) indicating a cell division defect.

3.6. **Localization of DivIVA-GFP and FtsZ-GFP in Δ*mepB2* Δ*mepB3* mutant**

Furthermore, to analyze septal PG synthesis, we conducted protein localization studies in the Δ*mepB2* Δ*mepB3* mutant. DivIVA, a marker of polar growth and septal PG synthesis; and FtsZ, a marker of the divisome were tagged to GFP (green fluorescent protein) as indicated in section 2.7 and used as markers of septal PG synthesis and localization of the divisome, respectively. DivIVA-GFP and FtsZ-GFP localization in the Δ*mepB2* Δ*mepB3* mutant

displayed multiple foci (Figure 3.27), which, in both cases, represented multiple septa further confirming the presence of chains of cells that were unable to divide. Collectively, these results identify the role of MepB1 in cell growth and of MepB2 and MepB3 in mycobacterial cell division. Scanning electron microscopic analysis of the mutant strains was conducted in comparison to mc^{2}155 and the complemented strains to assess changes in the cell wall surface due to the loss of MepB2 and MepB3 (Appendix D). No significant changes in the surface morphology of the cell wall of the mutant strains were observed relative to mc^{2}155 and the complemented strains.

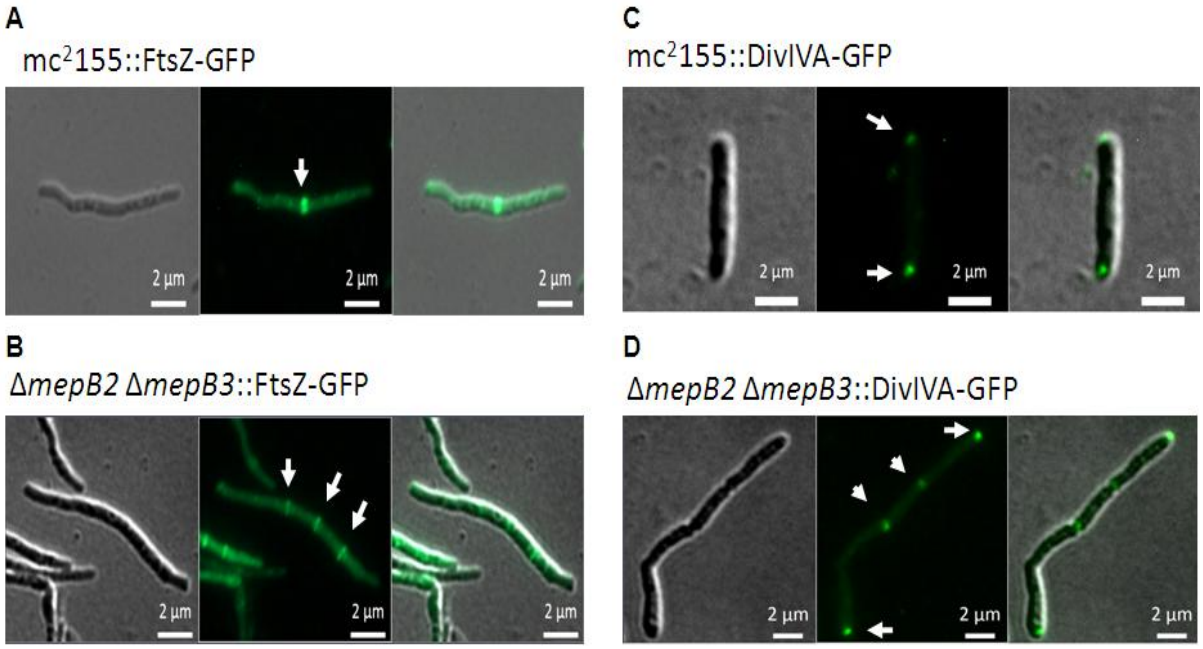


Figure 3.27: ***In vivo* localization of DivIVA-GFP and FtsZ-GFP in Δ*mepB2* Δ*mepB3***. (A) mc^{2}155::FtsZ-GFP displaying midcell localization of FtsZ-GFP (white arrow). (B) Δ*mepB2* Δ*mepB3*::FtsZ-GFP displaying multiseptal FtsZ-GFP foci (white arrows). (C) mc^{2}155::DivIVA-GFP displaying polar localization of DivIVA-GFP (white arrows). (D) Δ*mepB2* Δ*mepB3*::DivIVA-GFP displaying multiple DivIVA-GFP foci (white arrows).

3.7. **Time-lapse microscopic analysis of the Δ*mepB2* Δ*mepB3* mutant**

To further analyse the growth patterns of the Δ*mepB2* Δ*mepB3* mutant, time-lapse microscopic analysis of the Δ*mepB2* Δ*mepB3* mutant was conducted as indicated in section 2.11. Time-lapse microscopic analysis of the mc^2155 strain revealed the typical V-snapping cell division phenotype of mycobacteria indicated by red arrows in Figure 3.28 A. Strikingly, time-lapse microscopic analysis of the Δ*mepB2* Δ*mepB3* mutant revealed an aberrant cell growth phenotype, characterized by the formation of long cells. Defective cell division in the Δ*mepB2* Δ*mepB3* mutant also caused lateral budding (indicated by green arrows in Figure 3.28 B) as a mechanism to escape defects in cell division.

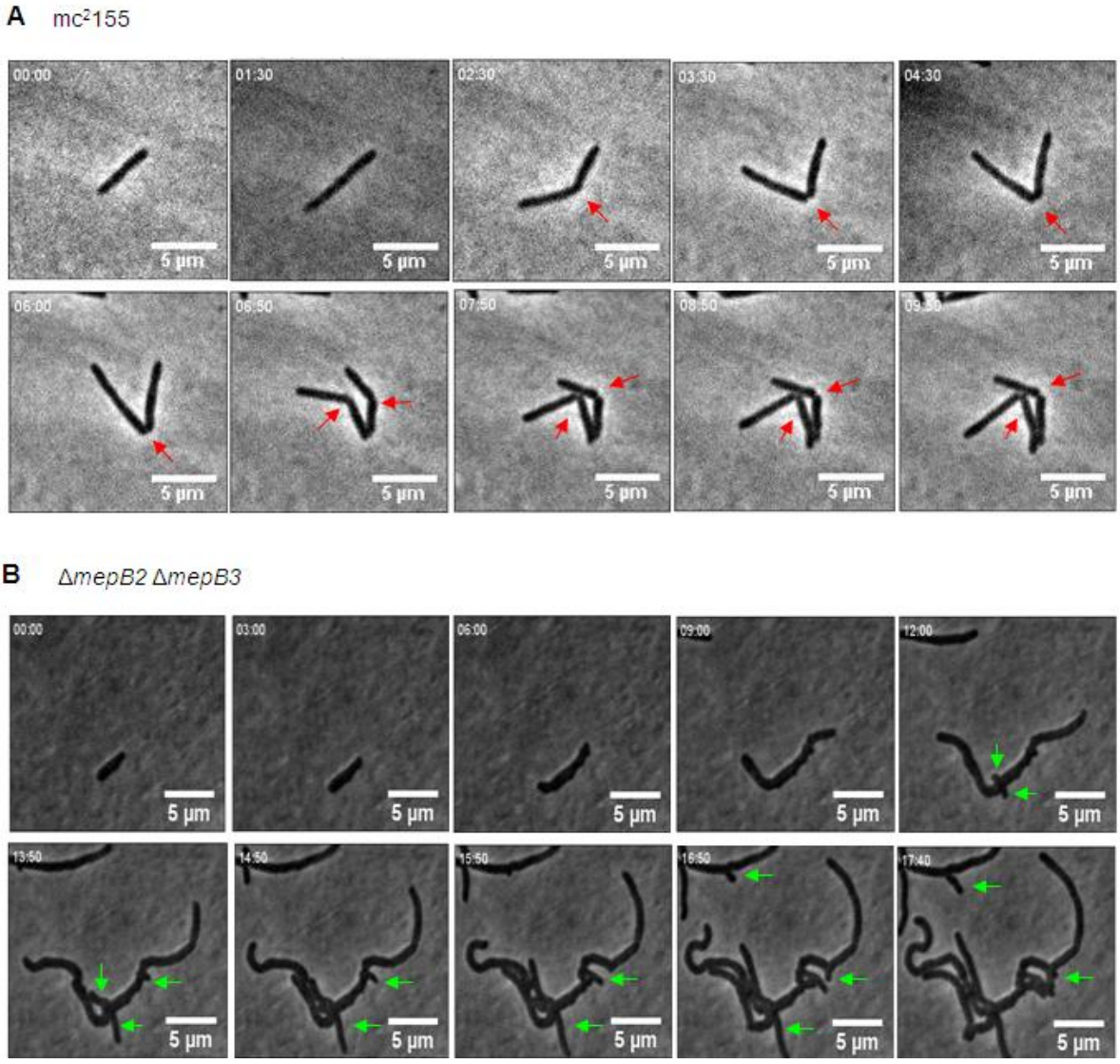


Figure 3.28. **Time-lapse microscopic analysis of the Δ*mepB2* Δ*mepB3* strain**. (A) Time-lapse micrographs of mc^2155, displaying typical cell division patterns of mc^2155 (red arrows). (B) Time lapse micrographs of the Δ*mepB2* Δ*mepB3* strain displaying an aberrant growth pattern and a lateral budding phenotype (green arrows). Scale = 5 µm. Time frame is in hours.

3.8. **Time-lapse microscopic analysis of the localization of DivIVA-GFP in the Δ*mepB2* Δ*mepB3* mutant**

As DivIVA is the coordinator of mycobacterial cell growth, we investigated whether the lateral budding caused by cell division defects is due to DivIVA mislocalization. To investigate this, time-lapse microscopic analysis of the localization patterns of DivIVA-GFP in the Δ*mepB2* Δ*mepB3* mutant were conducted as indicated in section 2.11. This revealed that the cell division defect caused by the loss of both MepB2 and MepB3 caused multiple DivIVA-GFP foci (white arrows) which resulted in lateral budding (blue arows) (Figure 3.29).

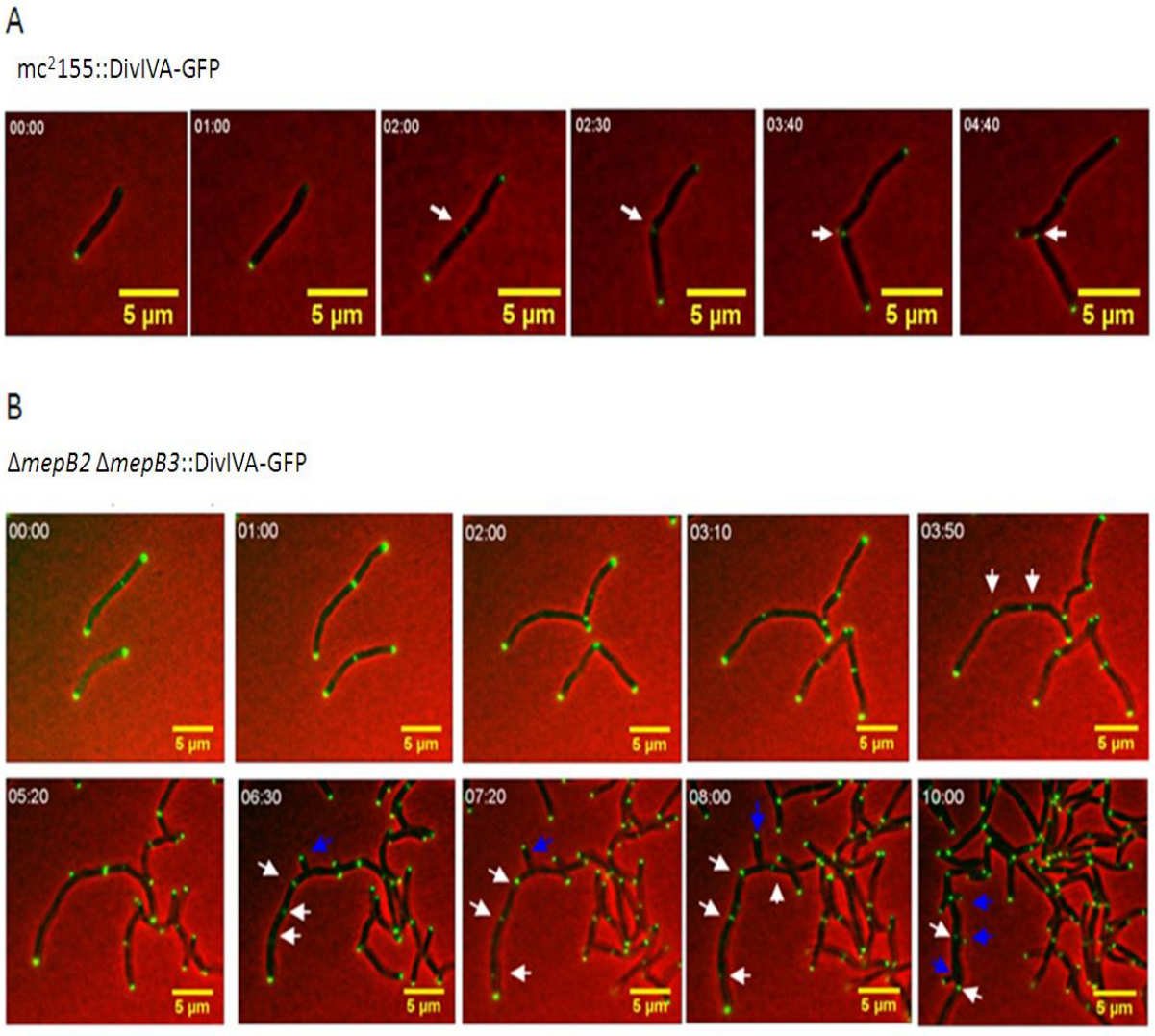


Figure 3.29. **Time-lapse microscopic analysis the Δ*mepB2* Δ*mepB3* DivIVA-GFP strain**. (A) Time-lapse micrographs of mc^{2}155 DivIVA-GFP, displaying typical cell division patterns of mc^{2}155 and localization of DivIVA-GFP (white arrows). (B) Time-lapse micrographs of the Δ*mepB2* Δ*mepB3* DivIVA-GFP strain displaying aberrant cell division patterns and lateral budding (blue arrows) and multiple DivIVA-GFP foci (white arrows). Scale = 5 µm. Time frame is in hours

3.9. The Δ*mepB2* Δ*mepB3* mutant is hypersensitive to lysozyme

The loss of PG endopeptidases RipA and RipC has been shown to alter PG turnover /remodelling and this defect was evidenced by the sensitivity of the mutants to lysozyme (Martinelli and Pavelka, 2016). As MepB2 and MepB3 are predicted to also have PG endopeptidase activity, the Δ*mepB1*, Δ*mepB2*, Δ*mepB3* deletion mutants and the Δ*mepB2* Δ*mepB3* double deletion mutant were assayed for lysozyme sensitivity as detailed in section 2.9.1.2. The Δ*mepB1*, Δ*mepB2* and Δ*mepB3* deletion mutants had increased sensitivity to lysozyme. Loss of MepB2 increased lysozyme sensitivity by 2-fold and the loss of MepB1 and MepB3 increased lysozyme sensitivity by 3-fold (Figure 3.30). The double deletion mutant was hypersensitive to lysozyme with a lysozyme MIC of 0.0625 μg/ml in comparison to mc^{2}155 with an MIC of 1.4 μg/ml (Figure 3.30). Lysozyme sensitivity suggests that the mutant strains had defects in the maintenance of cell wall integrity. The complementation of the mutants resulted in partial reversal of the lysozyme sensitivity (Figure 3.30).

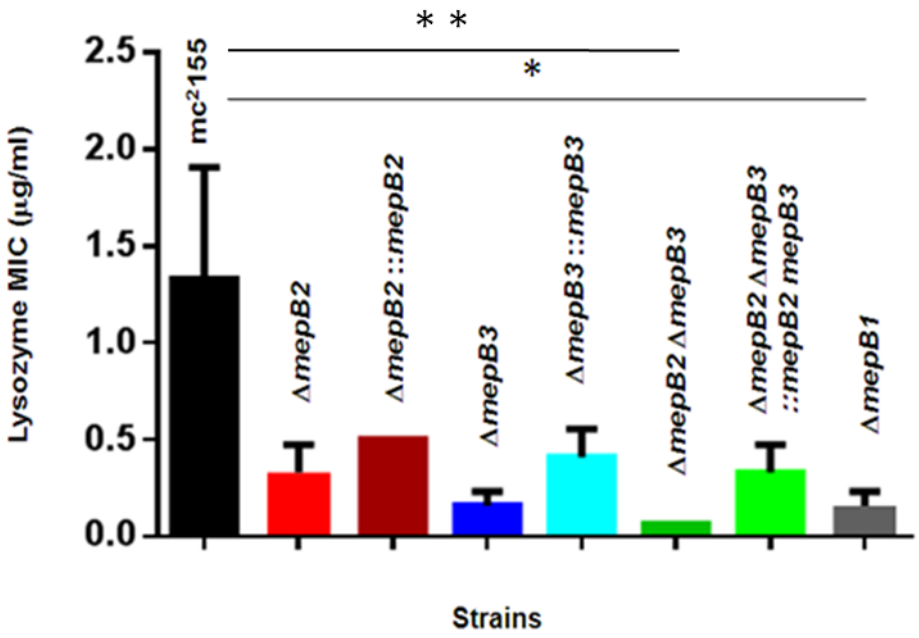


Figure 3.30: **The Δ*mepB2* Δ*mepB3* mutant is hypersensitive to lysozyme**. Lysozyme sensitivity of the Δ*mepB1*, Δ*mepB2*, Δ*mepB3* and Δ*mepB2* Δ*mepB3* mutants in comparison to the mc^{2}155 and the complemented strains. * p-value: <0.001, ** p-value: <0.0001 (by the unpaired Student's *t*-test). The data indicated represents three independent experiments for all strains analyzed.

These results indicate that MepB1 and MepB2 have a role in maintenance of cell wall integrity. The sensitivity of the mutant strains to the antibiotics; RIF, INH, Amoxicillin, daptomycin, teicoplanin, EMB, vancomycin and imipenem was also assayed in an attempt to further probe PG and cell wall biology in these mutants. The Δ*mepB1* and Δ*mepB3* mutant

strains were found to have increased sensitivity to RIF with an MIC of 0.4 μg/ml and 0.09 μg/ml, respectively, in comparison to mc^2155 with an MIC of 1.6 μg/ml. We hypothesize that the MepB proteins are required for PG biosynthesis. The sensitivity of the *mepB1*, *mepB2* and *mepB3* deletion mutants to the other antibiotics tested remained similar to mc^2155 levels (data not shown).

Our studies of the mycobacterial M23 peptidases, thus far, indicate that these are novel cell division proteins with an important role in degradation of septal PG to allow cell separation during the concluding stages of cell division. The sensitivity of the mutant strains to lysozyme suggests that these proteins also have a role in maintenance of mycobacterial cell wall integrity. To further investigate the roles of these PG endopeptidases at the mycobacterial cell division site, protein interaction studies were conducted using the bacterial two-hybrid mycobacterial protein fragment complementation (M-PFC) assay (also see Figure 3.4) and the results of this experiment are detailed below.

3.10. **MepB2 and MepB3 are components of the mycobacterial divisome**

M23 proteins (EnvC and NlpD) of the model organisms *E. coli* and *V. cholerae* interact with different components of the divisome (Figure 3.31). EnvC interacts with an ATP-binding cassette transporter-like complex FtsEX to specifically activate cell separation amidases AmiA and AmiB. FtsE (the nucleotide-binding domain of the FtsEX complex) serves as a cytoplasmic ATPase receiving signals from FtsZ (the cytoskeleton of the divisome) to induce conformational changes in FtsX (the transmembrane membrane domain of the FtsEX complex). FtsEX recruits EnvC to the cell division septum by interaction of EnvC with a large periplasmic loop of FtsX. Conformational changes in FtsX induced by FtsE, activate the bound EnvC, which in turn activates AmiA and AmiB to degrade the septal PG and allow cell separation (Figure 3.31).

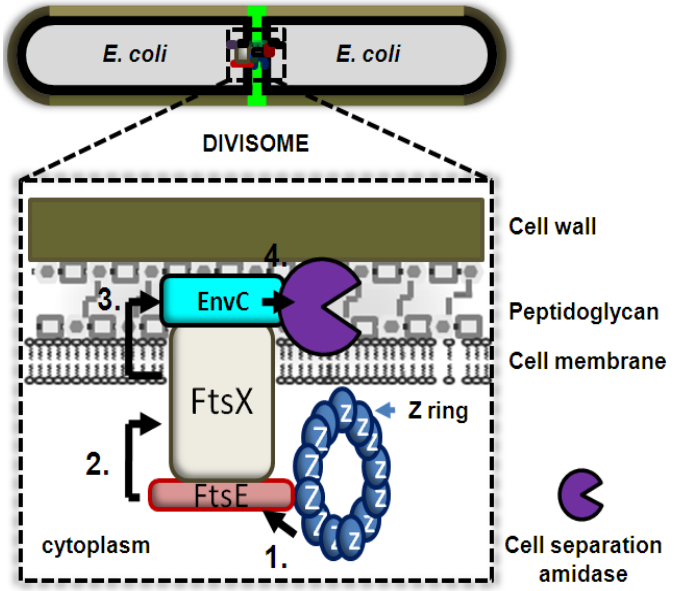
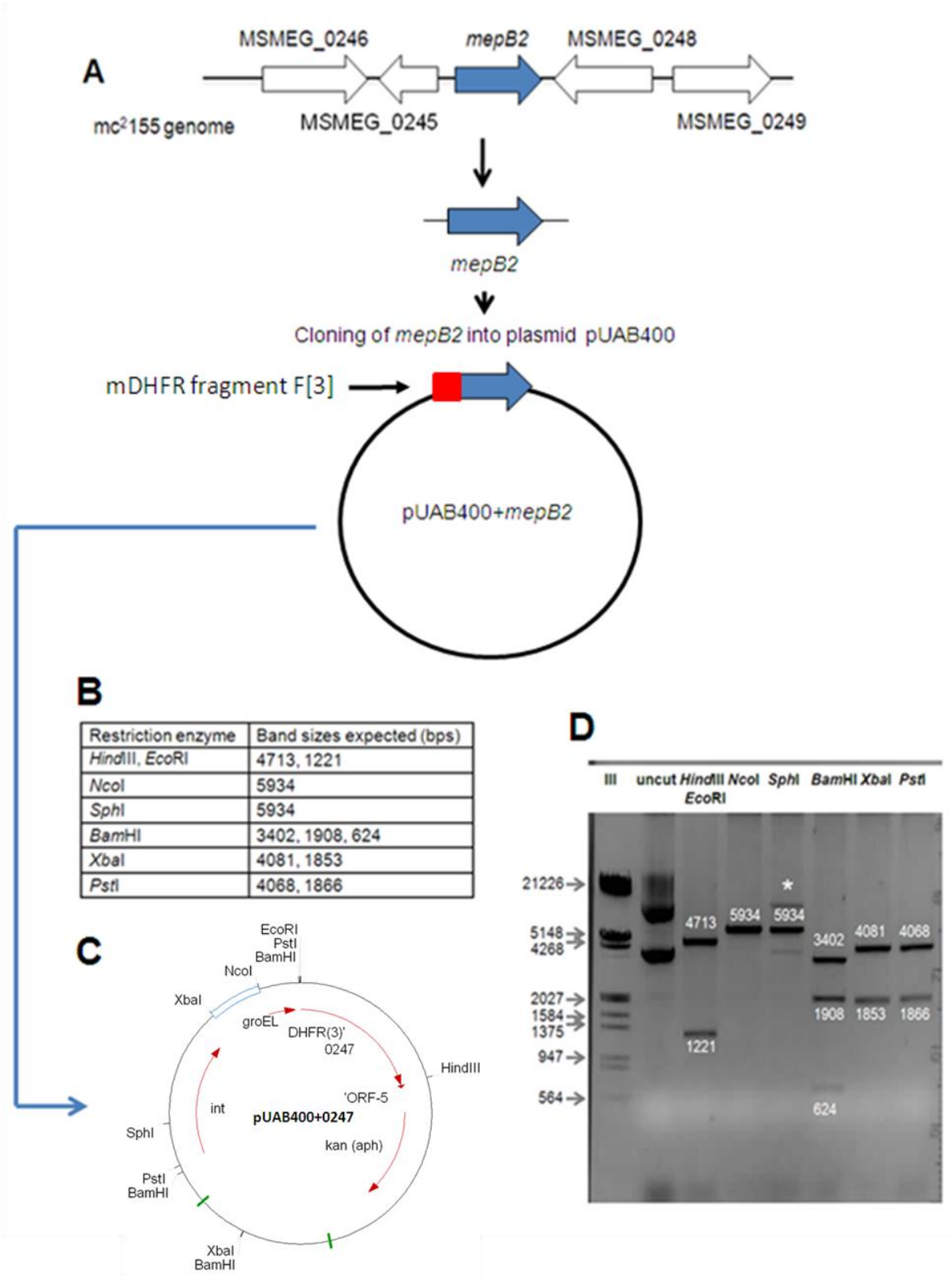


Figure 3.31: **Schematic diagram illustrating the activation of cell separation amidases by the FtsEX complex in *E. coli***. (1) Z-ring sends a signal to FtsE and (2) FtsE induces conformational changes in FtsX. (3) FtsX recruits EnvC which activates cell separation amidases (4). Black arrows indicate the relay of signals from the FtsZ ring to the cell separation amidase.

Mycobacteria also encode a similar FtsEX complex, however, no EnvC orthologs are found in the mycobacterial proteome (Mavrici et al., 2014). To probe the role of MepB proteins in the mycobacterial divisome, we conducted *in silico* predictions of mycobacterial FtsEX interacting proteins and this revealed M23 proteins; MepB2 (MSMEG_0247) and MepB3 (MSMEG_1192) as potential interacting partners (Appendix B). *In vivo* analysis of the interaction of FtsX with MepB2 and MepB3 was tested with the M-PFC assay as detailed in section 2.8. The construction of the M-PFC vectors and the results of this experiment are detailed below.

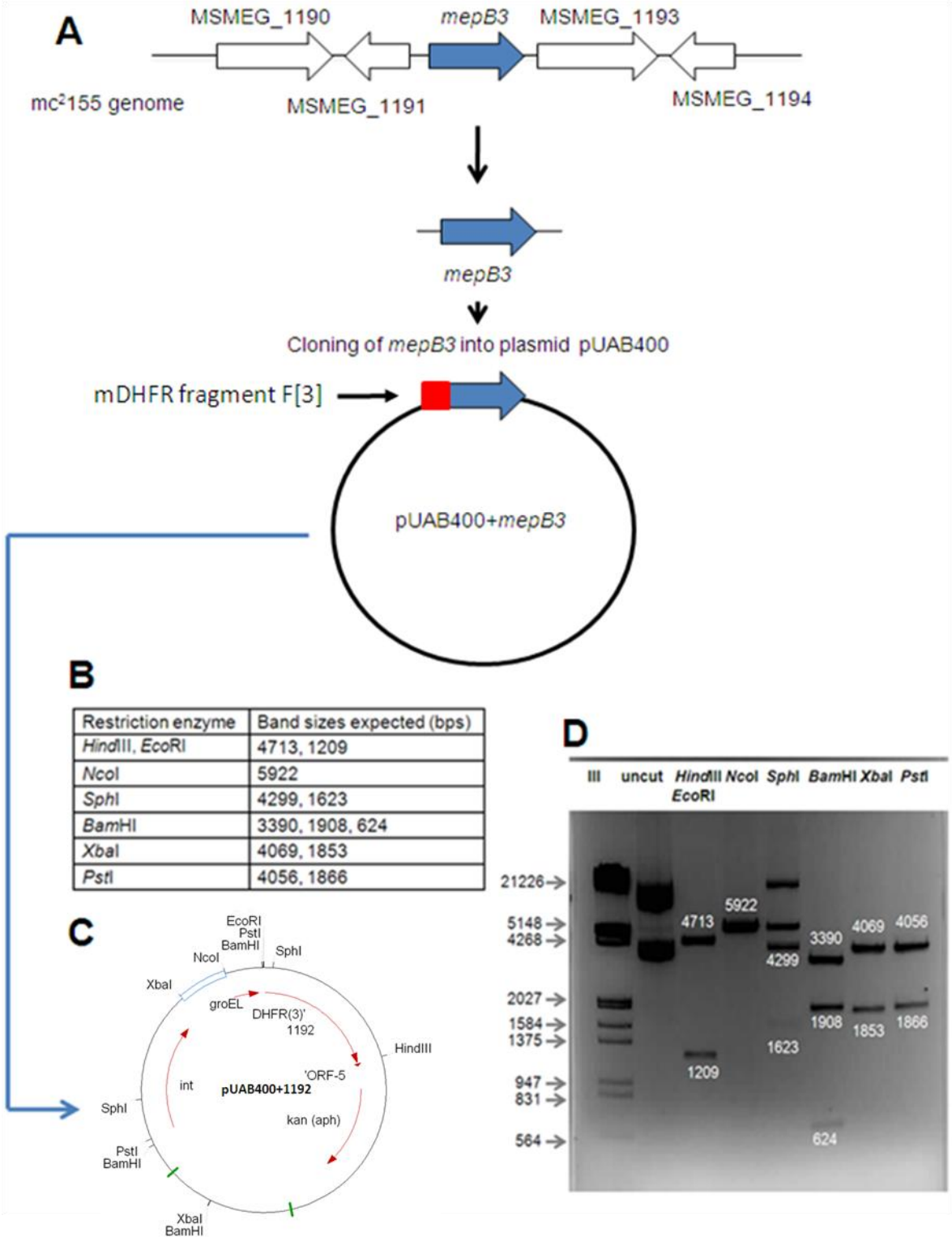
3.11. Construction of the M-PFC plasmids for analysis of FtsX - MepB interactions

For this experiment, both MepB2 and MepB3 were tagged on the N-terminus with the murine dehydrofolate reductase (mDHFR) fragment F[3]) on plasmid pUAB400 (Figure 3.32 and 3.33). Restriction analysis yielded the correct banding pattern (Figure 3.32 and 3.33) and sequencing further confirmed the genetic integrity of the plasmids (data not shown).



Restriction enzyme	Band sizes expected (bps)
*Hind*III, *Eco*RI	4713, 1221
*Nco*I	5934
*Sph*I	5934
*Bam*HI	3402, 1908, 624
*Xba*I	4081, 1853
*Pst*I	4068, 1866

Figure 3.32: **Construction and restriction profiling of pUAB400+0247**. (A) mc^{2}155 genome map indicating the location of the *mepB2* gene. (B) Table indicating the restriction enzymes used for restriction analysis of pUAB400+0247 and the DNA band sizes expected. (C) Plasmid map of pUAB400+0247. (D) Agarose gel (1%) indicating the DNA band sizes expected (labeled in base pairs). *: partial DNA restriction.



Restriction enzyme	Band sizes expected (bps)
*Hind*III, *Eco*RI	4713, 1209
*Nco*I	5922
*Sph*I	4299, 1623
*Bam*HI	3390, 1908, 624
*Xba*I	4069, 1853
*Pst*I	4056, 1866

Figure 3.33: **Construction and restriction profiling of pUAB400+1192**. (A) mc^{2}155 genome map indicating the location of the *mepB3* gene. (B) Table indicating the restriction enzymes used for restriction analysis of pUAB400+1192 and the DNA band sizes expected. (C) Plasmid map of pUAB400+1192. (D) Agarose gel (1%) indicating the DNA band sizes expected (labeled in base pairs).

3.12. **M-PFC assay for analysis of FtsX, MepB2 and MepB3 interactions**

The large periplasmic loop of FtsX has been shown to interact with RipC, a PG hydrolase (Mavrici et al., 2014). Therefore, we hypothesized that FtsX could similarly interact with MepB2 and MepB3. To test this, FtsX was tagged at the N-terminus (close to the large periplasmic loop) with the murine dehydrofolate reductase (mDHFR) fragment F[1,2] (Figure 3.34) and restriction analysis yielded the correct banding pattern (Figure 3.34 D). Sequencing of the plasmid DNA further confirmed the genetic integrity of the plasmid (data not shown). Tagging of the N-terminus of FtsX with the mDHFR fragment F[1,2] allowed the assembly of a functional mDHFR when MepB2 or MepB3 tagged with the mDHFR fragment F[3] interacted with the mDHFR fragment F[1,2] tagged FtsX (Figure 3.35). This is evidenced by the resistance of the mc^2155::FtsX+MepB2 and mc^2155::FtsX+MepB3 strains to the antibiotic trimethoprim (Figure 3.36 B and 3.37 B).

These results indicate that MepB2 and MepB3 indeed interact with FtsX and are components of the mycobacterial divisome (Figure 3.38). Furthermore, these observations also suggest that the ATP-binding cassette transporter-like complex FtsEX is evolved for regulation of PG hydrolases in mycobacteria.

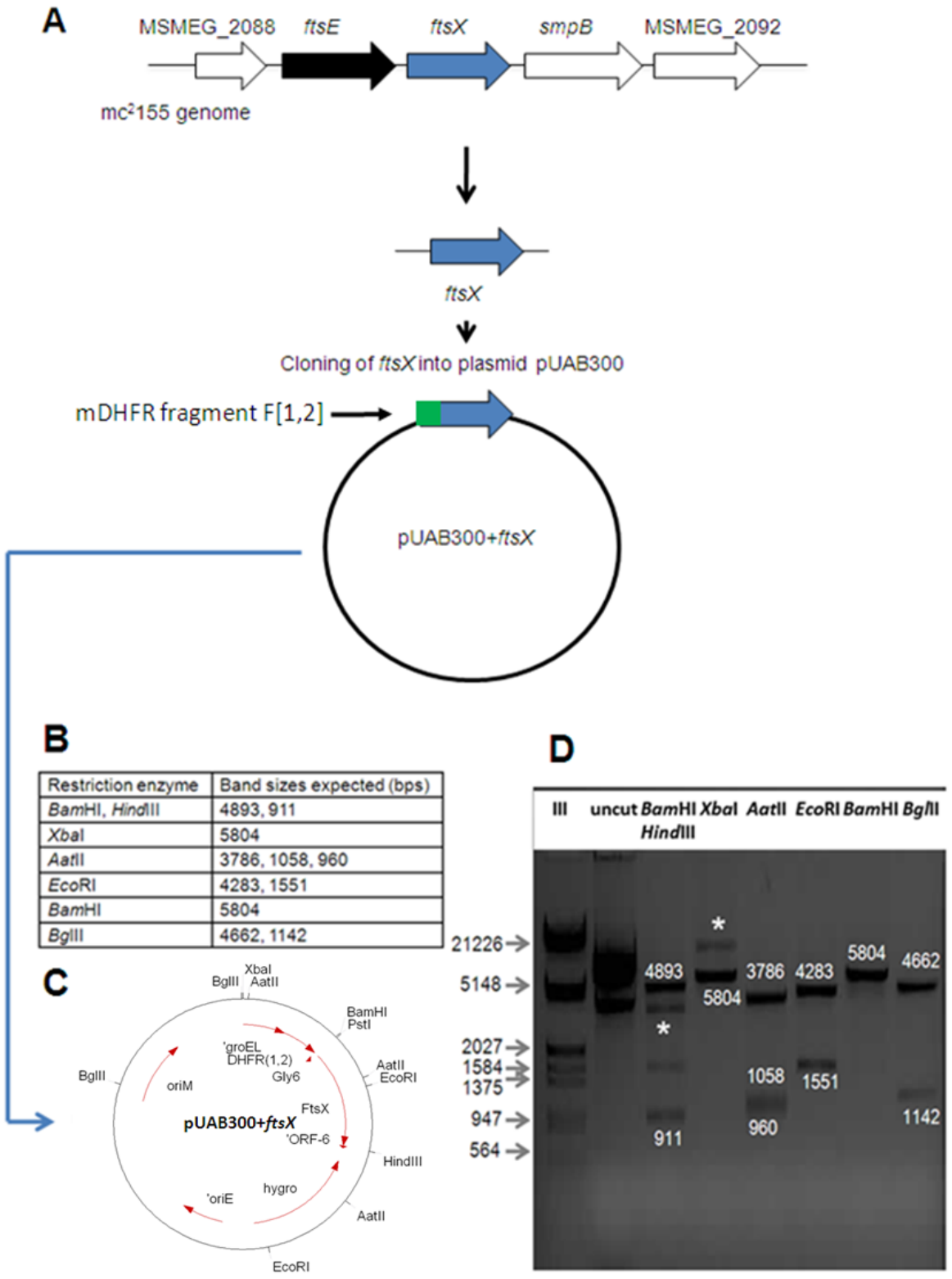


Figure 3.34: **Construction and restriction profiling of pUAB300+FtsX**. (A) mc^{2}155 genome map indicating the location of the *ftsX* gene. (B) Table indicating the restriction enzymes used for restriction analysis of pUAB300+FtsX and the DNA band sizes expected. (C) Plasmid map of pUAB300+FtsX. (D) Agarose gel (1%) indicating the DNA band sizes expected (labeled in base pairs). *: partial DNA restriction.

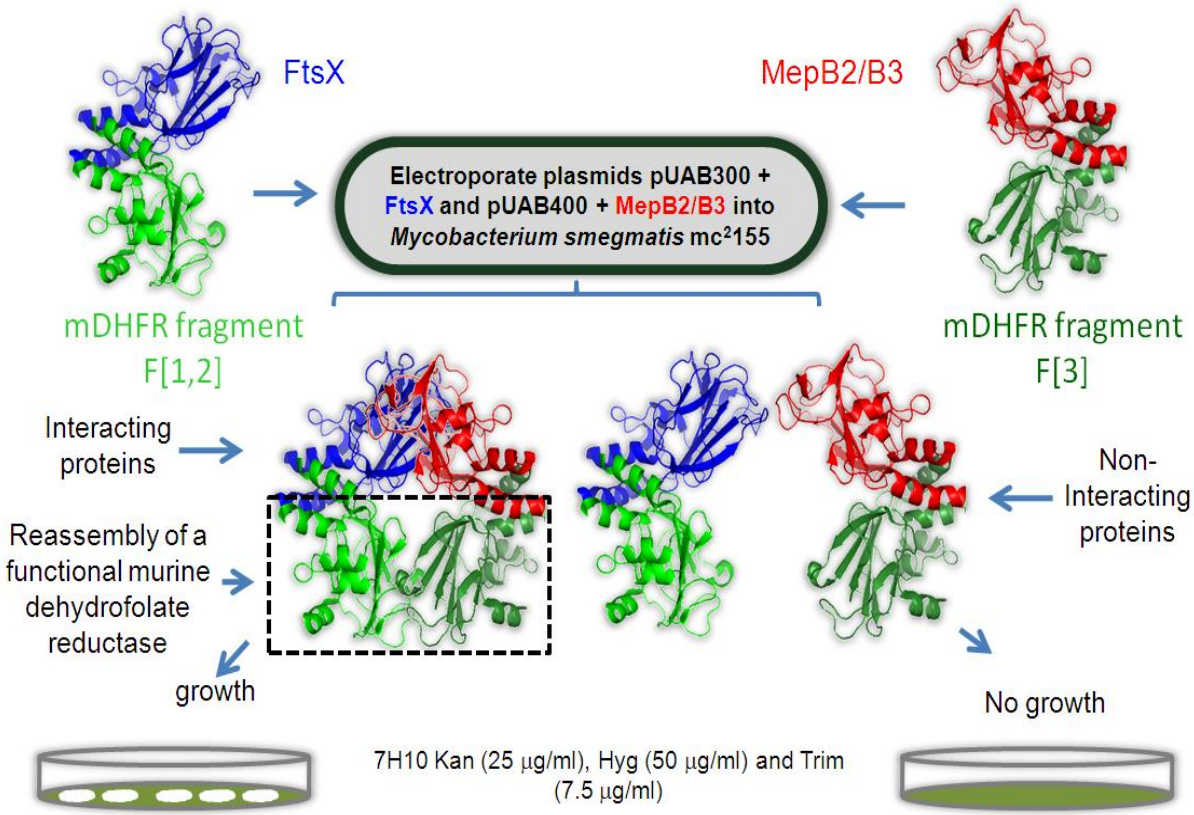
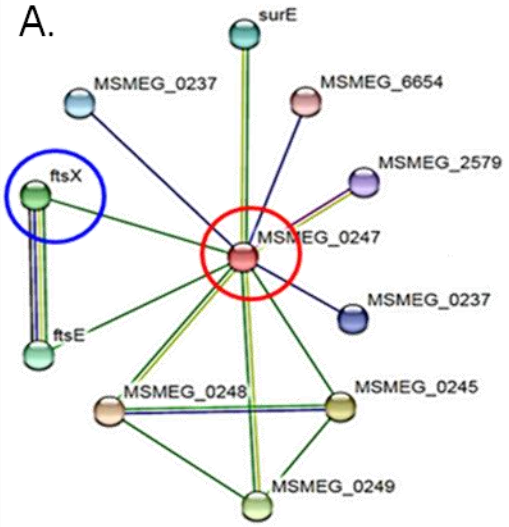
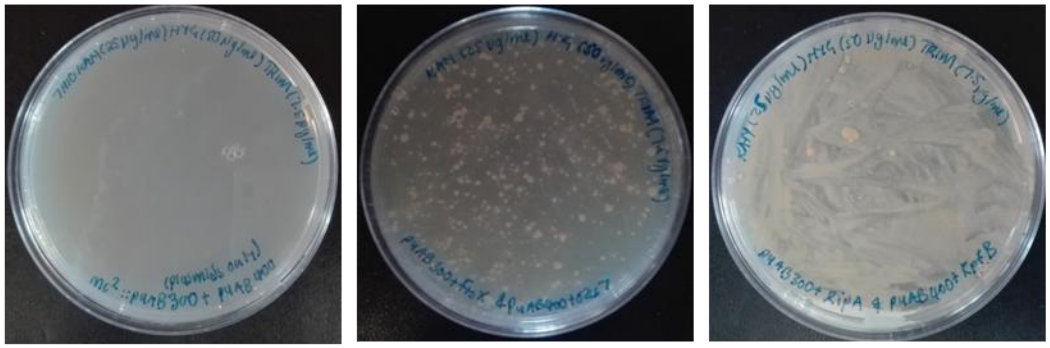


Figure 3.35: **Schematic diagram illustrating the M-PFC assay for FtsX-MepB2/B3 interactions**. MepB2/B3 and FtsX are fused to complementary mDHFR fragments F[3] and F[1,2], respectively. Co-transformation of *M. smegmatis* mc^{2}155 with plasmids encoding the MepB2/B3 and FtsX fused with the complementary mDHFR fragments results in the reconstitution of a functional mDHFR and subsequent growth of the strain on Middlebrook 7H10 broth supplemented with Trim (7.5 µg/ml), Kan (25 µg/ml), Hyg (50 µg/ml) only if MepB2/B3 and FtsX are interacting partners. Diagram adapted from (Singh et al., 2006).

A.



B.



mc²155::pUAB400+ pUAB300 (plasmids only control)

mc²155::FtsX+ MepB1

RipA+RpfB (positive control)

C.

Your Input:

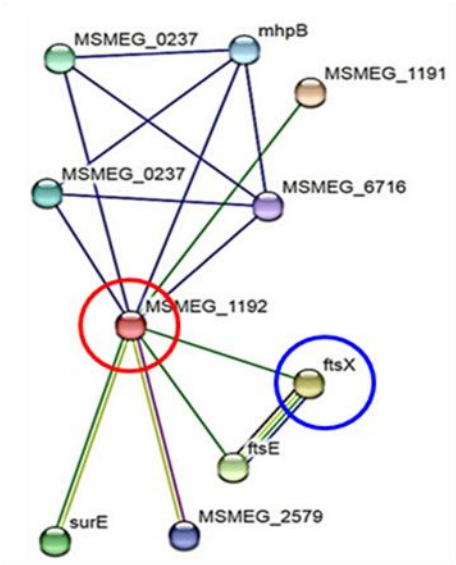
		Neighborhood	Gene Fusion	Cooccurence	Coexpression	Experiments	Databases	Textmining	[Homology]	Score
MSMEG_0247	*secreted peptidase (404 aa)*									

Predicted Functional Partners:

MSMEG_0248	*hypothetical protein (363 aa)*	●								0.869
MSMEG_0245	*transmembrane protein (122 aa)*	●								0.866
MSMEG_0249	*integral membrane protein (379 aa)*	●								0.679
ftsX	*cell division protein FtsX; Part of the ABC transporter FtsEX involved in cellular division (By similarity) (298 aa)*	●								0.656
ftsE	*cell division ATP-binding protein FtsE (229 aa)*	●								0.656
surE	*acid phosphatase SurE (259 aa)*	●							●	0.606
MSMEG_0237	*ISMsm3, transposase (468 aa)*			●						0.546
MSMEG_0237	*ISMsm3, transposase (468 aa)*			●						0.546
MSMEG_2579	*zinc metalloprotease (406 aa)*					●			●	0.450
MSMEG_6654	*TnpC protein (467 aa)*			●						0.423

Figure 3.36: **FtsX interacts with MepB2**. (A) Potential MepB2 interacting proteins identified by STRING analysis. (B) FtsX-MepB2 interaction by M-PFC analysis. (C) Table indicating the potential MepB2 interacting proteins identified by STRING analysis. FtsE and FtsX are indicated by the red box.

A.



B.



mc²155::pUAB400+ pUAB300 (plasmids only control)

mc²155:: FtsX+ MepB2

RipA+RpfB (positive control)

C.

Your Input:

		Neighborhood	Gene Fusion	Cooccurence	Coexpression	Experiments	Databases	Textmining	[Homology]	Score
MSMEG_1192	*M23 peptidase domain-containing protein (400 aa)*									

Predicted Functional Partners:

MSMEG_1191	*hypothetical protein (73 aa)*	●								0.715
ftsX	*cell division protein FtsX; Part of the ABC transporter FtsEX involved in cellular division (By similarity) (298 aa)*	●								0.656
ftsE	*cell division ATP-binding protein FtsE (229 aa)*	●								0.656
surE	*acid phosphatase SurE (259 aa)*	●							●	0.606
MSMEG_0237	*ISMsm3, transposase (468 aa)*			●						0.584
MSMEG_0237	*ISMsm3, transposase (468 aa)*			●						0.584
mhpB	*3-(2,3-dihydroxyphenyl)propionate dioxygenase; Catalyzes the non-heme iron(II)-dependent oxidative cleavage of...*			●						0.484
MSMEG_2579	*zinc metalloprotease (406 aa)*					●			●	0.450
MSMEG_6716	*AP endonuclease, family protein 2 (273 aa)*			●						0.426

Figure 3.37: **FtsX interacts with MepB3**. (A) Potential MepB3 interacting proteins identified by STRING analysis. (B) FtsX-MepB3 interaction by M-PFC analysis. (C) Table indicating the Identified potential MepB3 interacting proteins identified by STRING analysis. FtsE and FtsX are indicated by the red box.

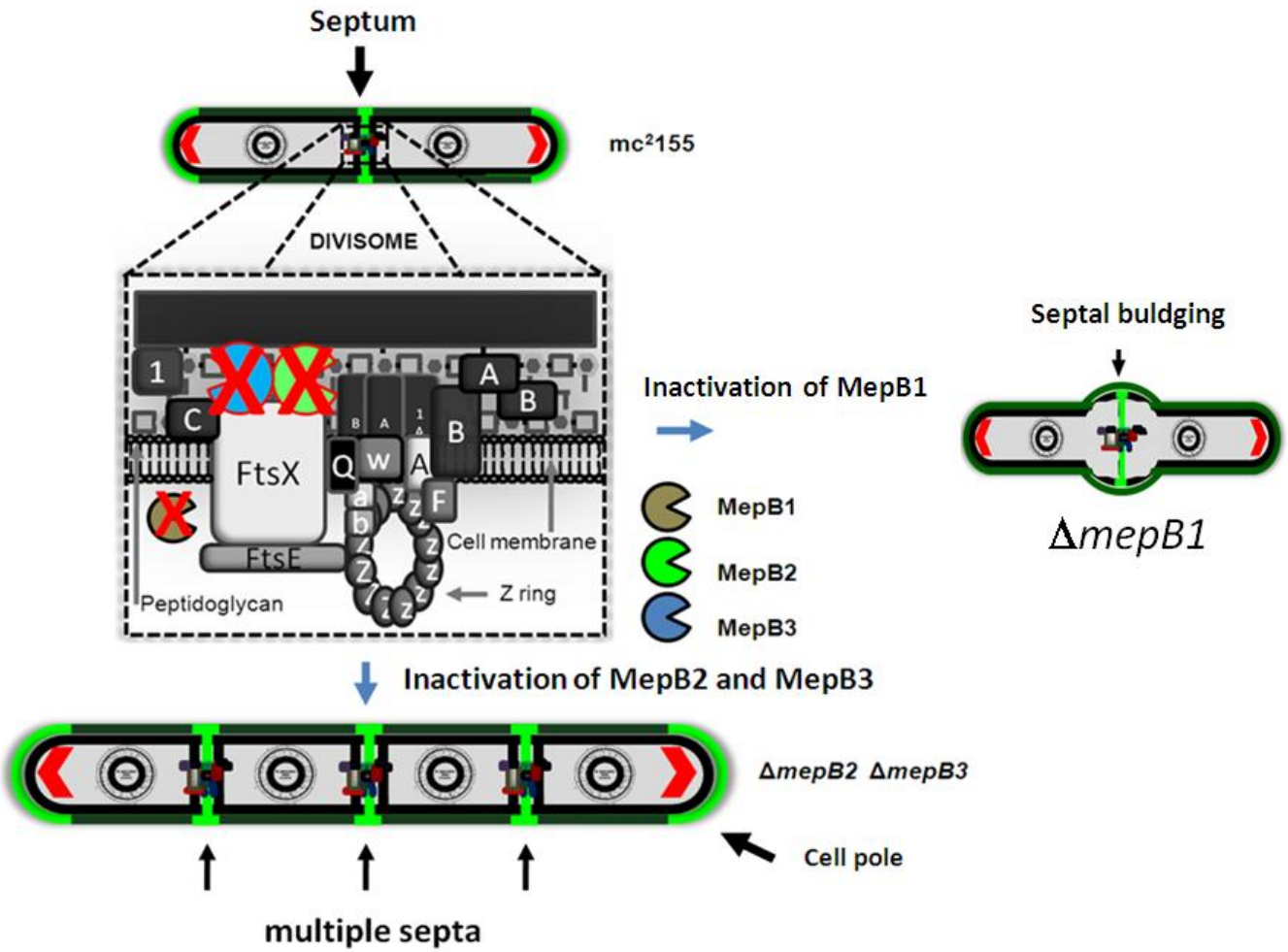


Figure 3.38: **Schematic diagram illustrating the role of mycobacterial MepB proteins in mycobacterial cell division**. Red crosses indicate the inactivation of the proteins. Inactivation of MepB1 causes septal buldging resulting in delayed cell proliferation and concurrent inactivation of MepB2 and MepB3 causes inhibition of cell division resulting in cell chaining.

4. Discussion

Treatment of drug susceptible TB requires the administration of a prolonged multi-drug regimen whereas other bacterial infections can be cured within a week of monotherapy (Zumla et al., 2013b). There are several factors responsible for this protracted TB treatment course. These include: the complex TB lung pathology presumed to cause sub-optimal exposure of infected pulmonary sites to some of the anti-TB drugs, development of drug resistance, the emergence of bacterial sub-populations that tolerate otherwise lethal drug concentrations and the inherent impermeability of the mycobacterial cell wall (Prideaux et al., 2015). The latter factors have provided impetus for studies aimed at increasing the efficacy of the current anti-TB drug regimen. Accordingly, cell wall targeted efforts continually highlight the biosynthesis of essential components of the mycobacterial cell wall as potential drug targets, the inhibition of which compromises cell wall integrity and eventually causes increased susceptibility to antibiotics (Kieser et al., 2015). Therefore, in the context of the soaring global prevalence of TB, understanding the biochemistry and the biosynthesis of the mycobacterial cell wall and identifying key cell wall biosynthesis pathways will guide the rational development of novel anti-TB drugs. This is anticipated to reduce the prolonged treatment course of TB and the incidence of drug resistance.

Structure and localization of mycobacterial MepB proteins

This MSc focused on the biosynthesis of the PG layer, an essential component of the mycobacterial cell wall providing support for the outer cell wall layers and endurance to osmotic pressure. Herein, the role of mycobacterial M23 peptidase class of PG hydrolyzing enzymes predicted to play an important role in PG remodelling during growth and cell division in mycobacteria is investigated. The M23 peptidases display pivotal roles in cell biology in other organisms and herein it is demonstrated that these proteins have a role in mycobacterial cell division processes and maintenance of mycobacterial cell wall integrity. This is evidenced by the observation of cell division defects and the sensitivity of the mutant strains to cell wall targeting agents after inactivation of these proteins. The structure of the M23 peptidases studied herein display similar architectural traits to PG remodelling M23 peptidases. MepB2 and MepB3 both have signal peptides for translocation to the periplasm and are composed of a C-terminal M23 domain with the typical HXH motif for coordination of the catalytic Zn^{2+}. MepB1 does not have a signal peptide for translocation to the cell wall and this suggests that MepB1 participates in cytosolic PG biosynthesis. Interestingly, CwlM

(a mycobacterial PG biosynthesis associated enzyme), was recently found to be sequestered from the cell wall, by cytosolic localization (Boutte et al., 2016). This study identifies MepB1 as another example of a PG hydrolase sequestered from the PG matrix for cytosolic PG biosynthesis. The tertiary structure of MepB1 displays a canonical mode of Zn^{2+} coordination of M23 peptidases while both MepB2 and MepB3 tertiary structures display a non-canonical motif 1 for Zn^{2+} coordination. The Zn^{2+} coordinating motif 1 is usually composed of the following amino acid sequence: HXXXD (with X representing any amino acid). The non-canonical Zn^{2+} coordinating motif 1 is usually observed in the M23A class of peptidases (Spencer et al., 2009). *In silico* analysis of MepB1, MepB2 and MepB3 indicates that these M23 proteins are catalytically active in contrast to the well-studied *E. coli* homologs; EnvC and NlpD, which are degenerate. Catalytically active M23 peptidases are usually components of the PG remodelling class of PG hydrolases involved in essential processes such as cell division and PG turnover during growth (Dorr et al., 2013). The PG hydrolytic potential of MepB1, MepB2 and MepB3 suggests a role for these proteins in PG remodelling. The demonstrated cell division and cell wall defects in the mutant strains that lack these proteins, provides preliminary evidence to support this hypothesis.

Mycobacterial MepB proteins have important roles during cell growth and division

The delayed mc^2155 growth kinetics caused by the loss of MepB1 suggests an important role for MepB1 in coordination of cell growth while the loss of both MepB2 and MepB3 from mc^2155 resulted in a defect in cell separation characterized by the chaining of cells held together by a PG layer between individual cells. PG hydrolases of the class NlpC/p60 (e.g. RipA) were the first to be implicated in the final stages of mycobacterial cell division (Hett and Rubin, 2008). RipA localizes to the division site and cleaves sepal PG to allow cell separation (Hett et al., 2008). Recently, RipA was shown to be expressed from a bicistronic operon also encoding for RipB, another NlpC/p60 PG endopeptidases (Martinelli and Pavelka, 2016). The depletion of RipA by replacement of the *ripA* promoter with an inducible tetracycline promoter resulted in a severe cell division defect characterized by the chaining of cells (Hett et al., 2008). This is suggested to be due to the lack of expression of *ripB* as well, as these two genes occur in an operon, indicating that both PG endopeptidases are required for cleavage of septal PG (Martinelli and Pavelka, 2016). Cleavage of septal PG in model organisms such as *E. coli*, *V. cholerae* and *P. aeruginosa* is facilitated by cell separation amidases (Uehara et al., 2010, Moll et al., 2014, Yakhnina et al., 2015). Accordingly, a recent study in our laboratory indicates that the mycobacterial PG amidase termed Ami1 with

homology to *E. coli* AmiA is similarly required for mycobacterial cell division (Senzani et al., 2017). *E. coli* encodes three cell division amidases; this indicates a significant level of functional redundancy for these enzymes (Uehara et al., 2010). The role of MepB2 and MepB3 in mycobacterial cell division suggests that mycobacteria employ a number of PG hydrolases for septal PG hydrolysis during cell division. In the model organism *E. coli*, other classes of PG hydrolases such as the endopeptidases and lytic transglycosylases have minor but significant roles in cell division (Yahashiri et al., 2015). This suggests that septal PG hydrolysis during bacterial cell division is facilitated by a range of PG hydrolases. In the model organisms *E. coli*, *V. cholerae* and *P. aeruginosa*, cell division M23 proteins have evolved for activation of cell separation amidases at the expense of their own PG hydrolytic activity (Uehara et al., 2009, Peters et al., 2013, Moll et al., 2014, Yakhnina et al., 2015, Yang et al., 2011).

Mycobacterial MepB proteins are part of the mycobacterial divisome

The event of septal PG hydrolysis appears to be highly regulated to prevent an unexpected burst of PG hydrolysis by the cell division associated PG hydrolases (Yang et al., 2011). These mechanisms of regulation range from transcriptional levels of regulation to post transcriptional levels of regulation (Singh et al., 2015). In mycobacteria, RipA is shown to be produced in an inactive form (Kieser and Rubin, 2014). RipA is suggested to be activated through interactions with RpfB and these interactions result in the generation of a RipA variant with enhanced PG hydrolytic activity (Hett and Rubin, 2008, Chao et al., 2013). Recently, a mycobacterial periplasmic protease, MarP, was identified as the activator of RipA during acid stress (Botella et al., 2017). A similar mechanism of activation of Ami1 remains to be demonstrated.

A recent study on RipC indicates that RipC also requires activation for enhanced PG hydrolytic activity (Mavrici et al., 2014). RipC interacts with the FtsEX complex through a conserved coiled coil domain which interacts with a large periplasmic loop formed by FtsX (Mavrici et al., 2014). Similarly, CwlO (a NlpC/p60 endopeptidase of *B. subtilis*), PcsB (a cell separation PG amidase of *S. pneumoniae*) and EnvC (in *E. coli*), also interact with the FtsEX complex through a conserved coiled-coil domain (Meisner et al., 2013, Sham et al., 2013, Yang et al., 2011). CwlO is required for cell elongation rather than cell division in *B. subtilis*; therefore, this indicates that the regulation of the hydrolytic activity of PG hydrolases

is also essential for cell growth as CwlO and FtsEX mutants of *B. subtilis* were found to be defective for cell elongation (Meisner et al., 2013).

The mycobacterial FtsEX complex is also suggested to regulate PG remodelling through recruiting and activating PG hydrolases at the site of PG biosynthesis (Kieser and Rubin, 2014). In this study, *in silico* analysis of the potential interacting partners of the mycobacterial FtsEX complex identified MepB2 and MepB3 as potential interacting partners. The interaction between FtsX and both MepB2 and MepB3 was assessed through the use of the M-PFC assay. This assay is demonstrated to be effective for testing the interaction between transmembrane protein complexes with either periplasmic or cytoplasmic partners (Singh et al., 2006). Both MepB2 and MepB3 were found to interact with FtsX although sequence analysis of the proteins does not indicate the presence of the coiled-coil domain in both proteins (Appendix F). Interestingly, through the bacterial adenylate cyclase two-hybrid assay used to assess protein interactions, Moll et al. and Domínguez-Cuevas et al., confirmed the ability of the FtsEX complex to interact with divisome components such as NlpD and elongasome components such as penicilin binding proteins of *B. subtilis,* that do not have the coiled-coil domain (Moll et al., 2014, Meisner et al., 2013). This suggested that this domain is not compulsory for FtsX interactions. As both MepB2 and MepB3 do not have PG binding domains, the FtsEX complex could recruit these cell division enzymes to the cell division septum for septal PG processing. The interaction of FtsX with both MepB2 and MepB3, and the cell division defect observed after inactivation of *mepB2* and *mepB3,* suggest that mycobacterial periplasmic M23 proteins are novel divisome components identified by this study to be involved in septal PG hydrolysis during the concluding stages of cell division (Figure 4.1).

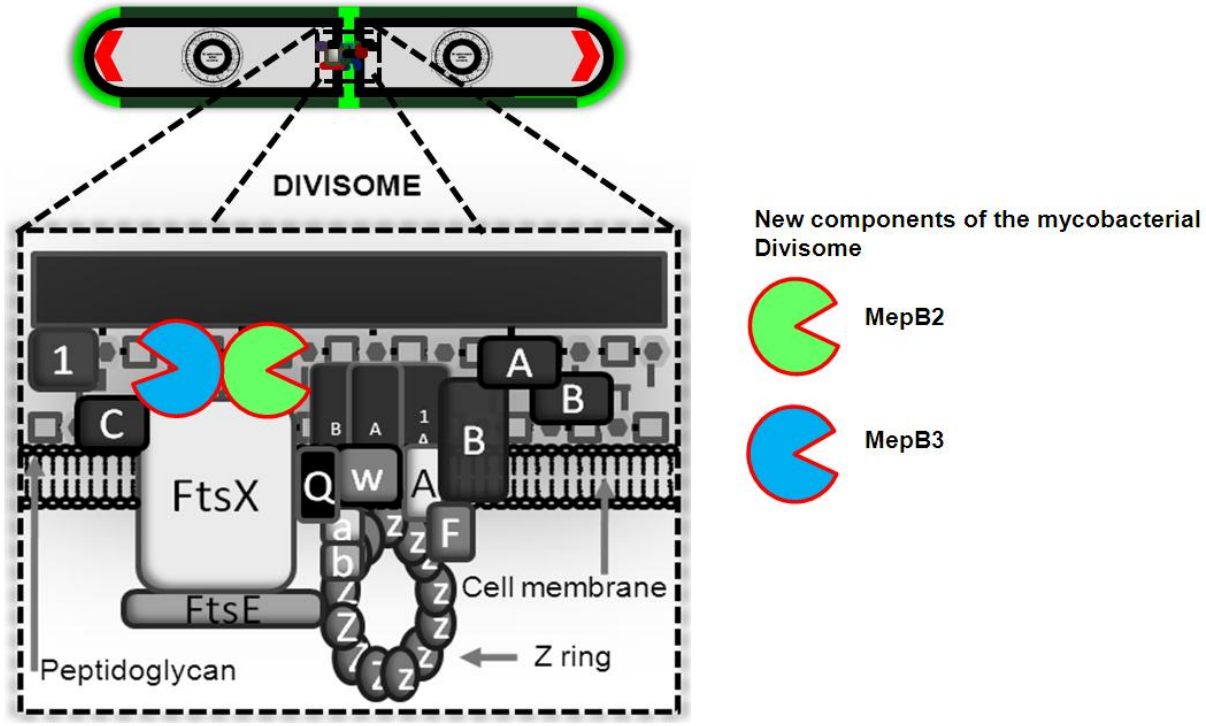


Figure 4.1: **MepB2 and MepB3 are identified as new components of the mycobacterial divisome**. MepB2 and MepB3 interact with the FtsEX complex and function together with the cell separation amidase Ami1 and the NlpC/p60 endopeptidases RipA and RipB to degrade septal PG during mycobaterial cell division.

Loss of both MepB2 and MepB3 causes aberrant cell division and localization of DivIVA

To further explore the cell division defect caused by the loss of MepB1 and MepB2, DivIVA and FtsZ localization studies were performed. DivIVA is an essential component of the mycobacterial elongasome (Meniche et al., 2014). It directs cell wall synthesis by recruiting the cell wall biosynthetic machinery to the poles in mycobacteria. The GFP-tagged DivIVA allele expressed in the Δ*mepB1* Δ*mepB2* mutant localized at the cell poles and also at the sites connecting cells unable to separate. Since DivIVA is known to require membrane curvature for localization, this indicates that at these sites of failed cell division, all the initial stages of cell division were accomplished including the invagination of the cytoplasmic membrane, to create curvature. This confirmed that the cell division defect is due to inefficient cleavage of septal PG rather than defects in septal PG synthesis. The GFP-tagged FtsZ allele expressed in the Δ*mepB2* Δ*mepB3* mutant revealed the formation of multiple FtsZ-rings. The FtsZ-ring serves as a scaffold for septal PG synthesis and generates the energy required for membrane

invagination during cell division (Hett and Rubin, 2008). The formation of multiple FtsZ rings confirmed the failure of coordinated cell division.

In contrast to model organisms such as *E. coli*, mycobacteria employ rather unique divisome components such as CrgA, CwsA and FhaB which are required for FtsZ ring stabilization (Kieser and Rubin, 2014). The role of catalytically active M23 proteins in cell division is only thus far demonstrated with DipM, a periplasmic PG binding M23 peptidase only observed in the genus *Caulobacter* (Moll et al., 2010, Goley et al., 2010). The mycobacterial M23 proteins studied herein display a similar role.

Mycobacterial MepB proteins have important roles in maintenance of cell wall integrity

The loss of the D,L-endopeptidase activity of RipA and RipC increases the susceptibility of mycobacteria to lysozyme (Martinelli and Pavelka, 2016, Parthasarathy et al., 2012). Lysozyme is a glycosidase which cleaves the β(1→4) glycosidic bonds of the PG matrix. The sensitivity of the Δ*ripA* and Δ*ripC* strains to lysozyme is presumed to be due to secondary effects on the structure of the cell wall as a result of defective PG remodelling in the absence of RipA or RipC (Hett et al., 2008, Mavrici et al., 2014). The pertubation of cell wall integrity is thought to increase the permeability of the cell wall. This also causes increased sensitivity to antibiotics and immune stresses. The Δ*ripC* strain is hypersusceptible to RIF while deletion of *ripA* and *ripB* causes increased sensitivity to RIF, erythromycin and vancomycin (Mavrici et al., 2014, Martinelli and Pavelka, 2016). Disturbance of mycobacterial PG synthesis biosynthesis and spatial localization also causes sensitivity to antibiotics. The inactivation of *ponA2* and *ldtMt2* causes increased sensitivity to meropenem and teicoplanin. Futhermore, deletion of *ponA1* increases sensitivity to ethambutol (Kieser et al., 2015). As a result, cell wall targeted studies indicate that cell wall biosynthesis remains an attractive target for enhancing the efficiency of the current anti-TB drug regimen or for the development of new anti-TB drugs (Kieser and Rubin, 2014).

In this study, the deletion of *mepB1* or *mepB2* and *mepB3* either individually or in combination causes increased sensitivity to lysozyme. This suggests a role for these mycobacterial M23 proteins in the maintenance of cell wall integrity. The loss of these proteins could also cause secondary defects in the cell wall causing increased permeability of the cell wall. The hypersensitivity of the Δ*mepB2* strain to RIF was expected as a mc^2155 FtsX mutant is also hypersusceptible to RIF. This suggests that the FtsEX complex is required for the regulation of PG hydrolases for effective PG remodelling.

4.1. **Limitations**

The prediction of the 3D tertiary structures of the mycobacterial MepB proteins was one of the limiting factors in this study because the protein modelling software are based on prediction algorithms. However, this study will guide structure-based functional characterization of these proteins. Genetic complementation of the mutant strains did not fully revert the phenotypic variations observed in the mutant strains to wild type levels. This is usually observed for strains complemented at a heterologous locus. Localization of the MepB2-GFP and MepB3-GFP fusion proteins was also not successful. This could be due to the instability of the GFP-tag used. The variant of the GFP used may not withstand the mycobacterial cell wall periplasmic space conditions. A fluorescent protein tag that is stable in the mycobacterial cell wall periplasmic space would be useful to study the localization of these MepB proteins. Live cell imaging of the mutant strains expressing DivIVA-GFP and FtsZ-GFP fusion proteins would also be a useful tool to further analyse the cell division defects caused by the loss of the MepB proteins.

4.2. **Future studies**

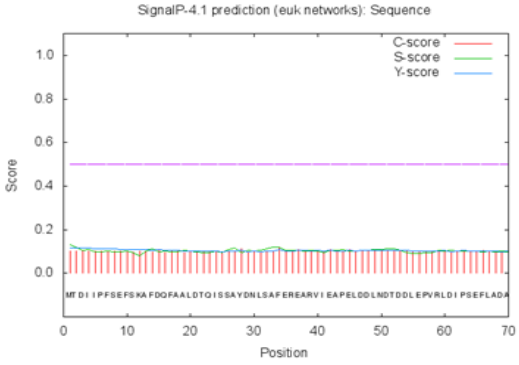
Future work on the mycobacterial M23 peptidases will include further characterization of MepB1 which lacks a signal peptide, suggesting a cytoplasmic role for this M23 peptidase. Preliminary studies on a mutant strain lacking this enzyme displays delayed cell growth suggesting a rather unique role for this enzyme in contrast to its periplasmic counterparts. The PG hydrolytic activity of the M23 peptidases is also a subject of investigation in order to determine the PG cleavage site of these proteins. Protein localization studies for the mycobacterial M23 peptidases were not successful due to the low fluorescence intensity observed for the GFP-tagged variants of MepB2 and MepB3 (data not shown). This could be due to proteolytic processing of both MepB2 and MepB3 by proteases regulating PG hydrolases. Interestingly, during the identification of potential interacting partners for both MepB2 and MepB3, an intramembrane zinc metalloprotease (MSMEG_2579) termed Rip1 was also identified (Appendix B). Rip1 regulates PG biosynthesis during oxidative stress, by cleaving FtsI (a septal PG biosynthesis enzyme) (Mukherjee et al., 2009). Since PG hydrolases are also subject to proteolytic processing, MepB2 and MepB3 PG hydrolytic activity could also be regulated at this level. The potential interaction of both MepB2 and MepB3 with Rip1 could identify a novel role for Rip1.

4.3. **Concluding remarks**

The mycobacterial cell wall remains an interesting area of anti-TB drug target identification. Unravelling the networks regulating mycobacterial growth and cell wall integrity will enhance cell wall targeted efforts as this will identify essential pathways orchestrating TB pathology. Furthermore, during infection, *Mtb* is believed to reside for prolonged periods of non- or slow replication. To transmit itself from one host to another, *Mtb* undergoes periods of active replication which require an operational cell division machinery. Therefore, targeting cell division pathways of *Mtb* represents an ideal alternative to curb *Mtb* transmission and proliferation. This study identified a novel class of PG hydrolases important for mycobacterial growth and proliferation as putative TB drug targets. Our work will guide further investigation of the mycobacterial M23 class of PG remodelling enzymes.

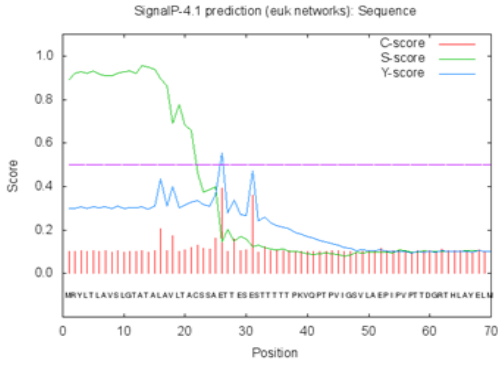
5. Appendices

MSMEG_5526 (MepB1)



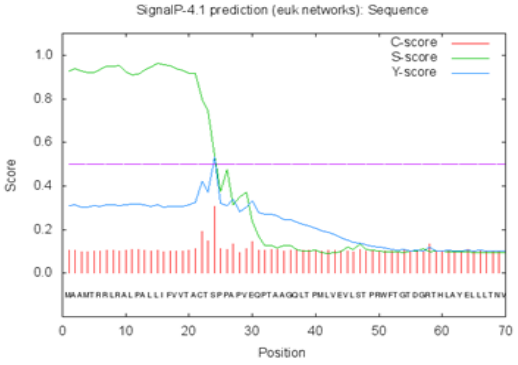
No Signal peptide.

MSMEG_0247 (MepB2)



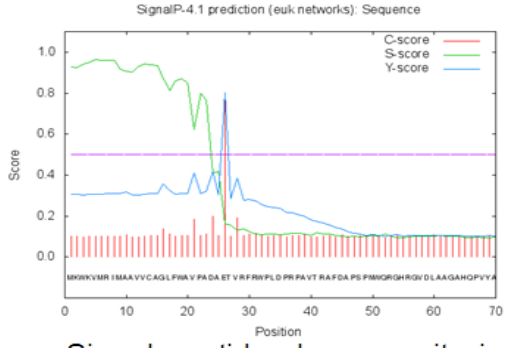
Signal peptide cleavage site is between amino acid 25 and 26.

MSMEG_1192 (MepB3)



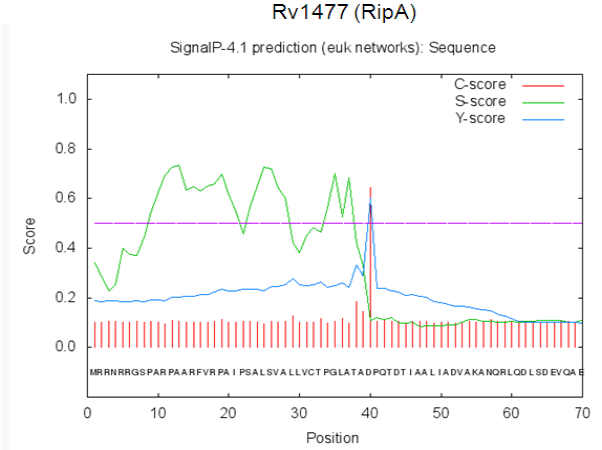
Signal peptide cleavage site is between amino acid 23 and 24.

MSMEG_2518



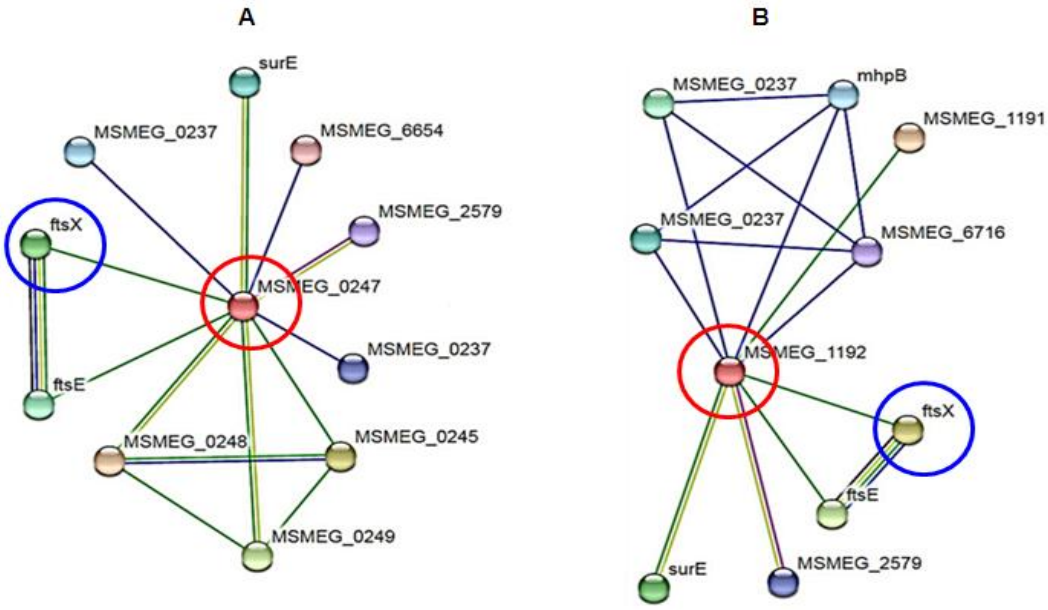
Signal peptide cleavage site is between amino acid 25 and 26.

Rv1477 (RipA)

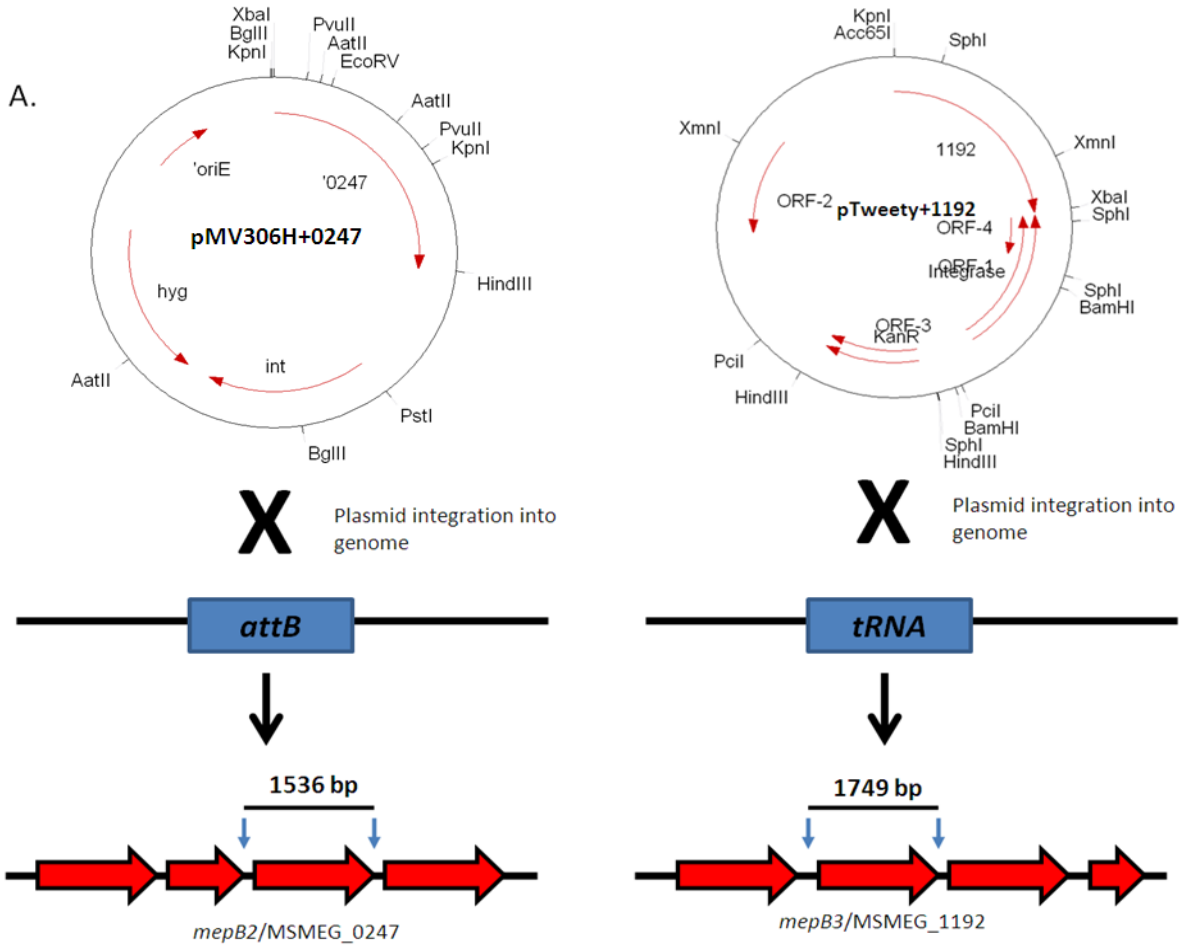



```
# Measure  Position  Value    Cutoff   signal peptide?
  max. C    40        0.643
  max. Y    40        0.600
  max. S    13        0.732
  mean S     1-39     0.536
       D     1-39     0.565   0.450   YES
```

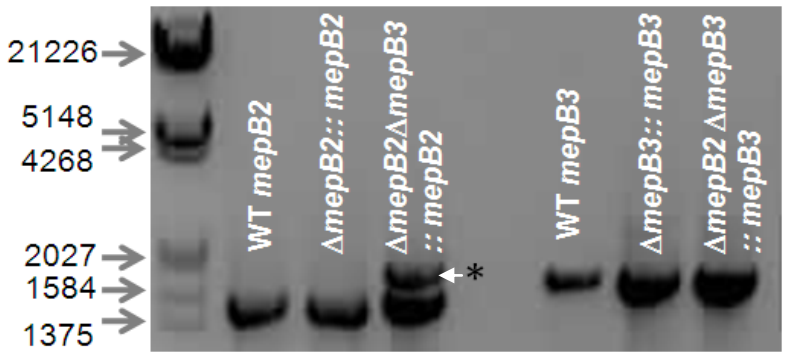
Appendix A: **SignalP analysis of the four *M. smegmatis* M23 protein sequence to identify signal peptides for translocation the cell wall**. RipA which has been biochemically characterized was used as positive control. MepB2 and MepB3 have signal peptides, and MepB1 does not have a signal peptide.



Appendix B**: STRING prediction of MepB2 and MepB3 potential interacting partners.** (A & B) Potential MepB2 (MSMEG_0247) and MepB3 (MSMEG_1192) interacting proteins identified by STRING analysis, respectively.



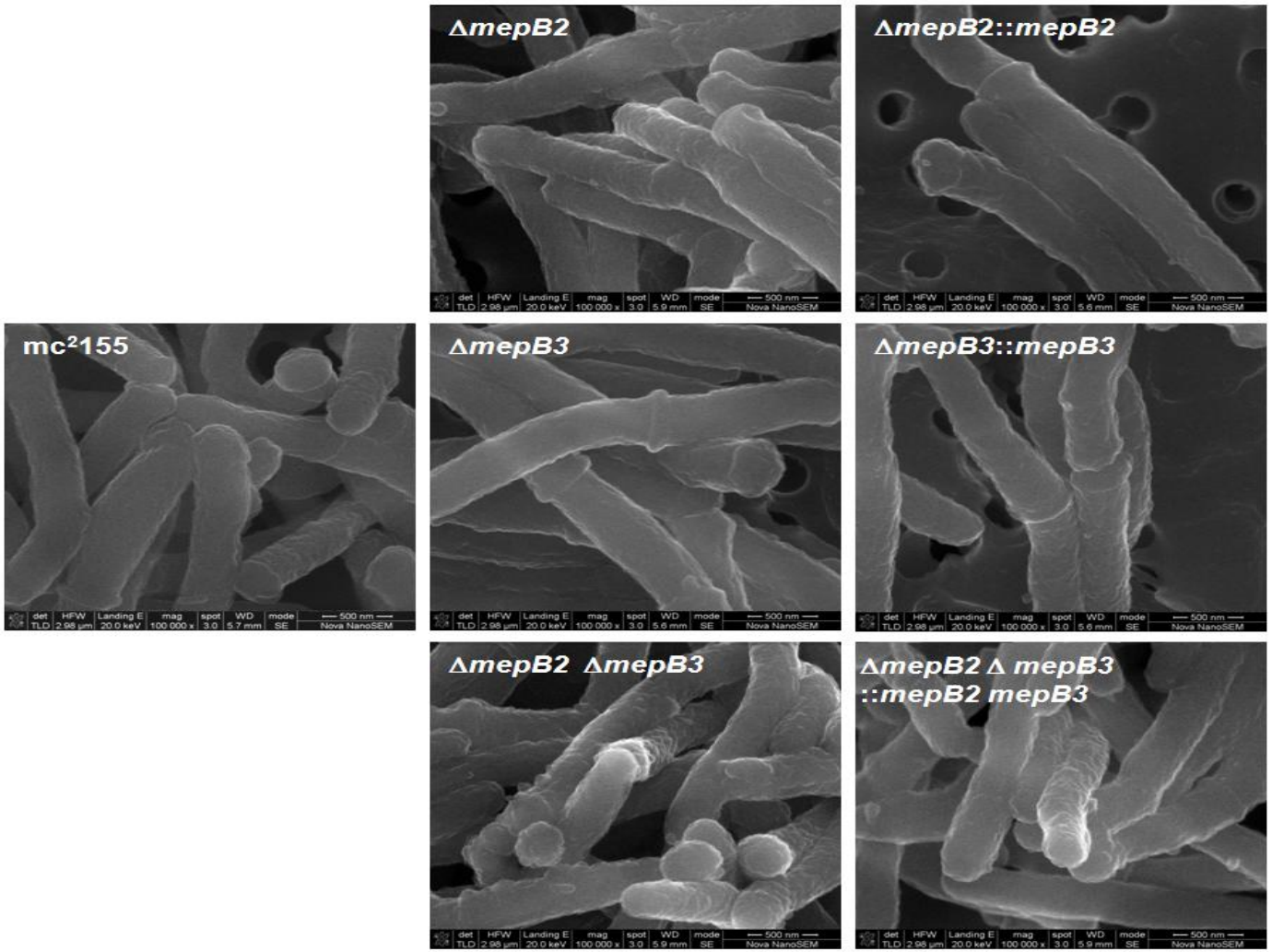
B.



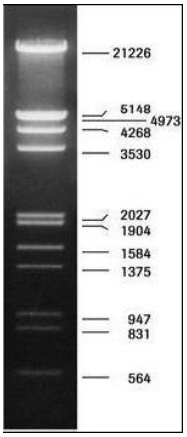
C.

Allele	Band sizes expected (bps)
mepB2	1536
MepB3	1749

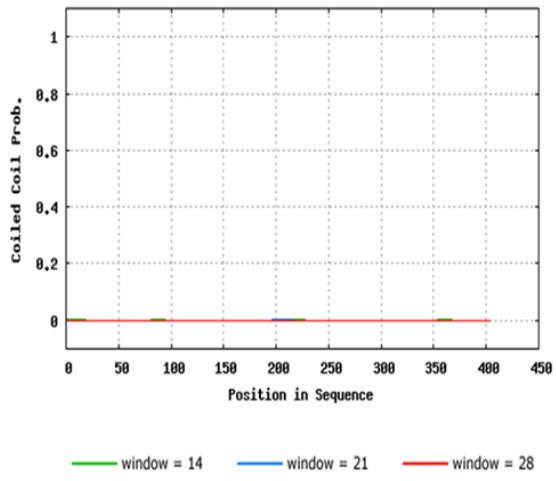
Appendix C: **Genetic complementation of the Δ*mepB2* and Δ*mepB3* single mutants and the double deletion mutant**. (A) Schematic representation of the gene complementation process. (B) PCR results for confirmation of the complementation of *mepB2* and *mepB3* in both the Δ*mepB2* and Δ*mepB3* single mutants and the double deletion mutant. (C) Table indicating the expected band sizes after PCR. *: amplification of Δ*mepB2*::*aadA* in the Δ*mepB2*::*aadA*Δ*mepB3*::*mepB2* strain because the PCR primers used bind both genes (Δ*mepB2*::*aadA* and *mepB2*). Complementation of the *mepB* proteins was achieved.



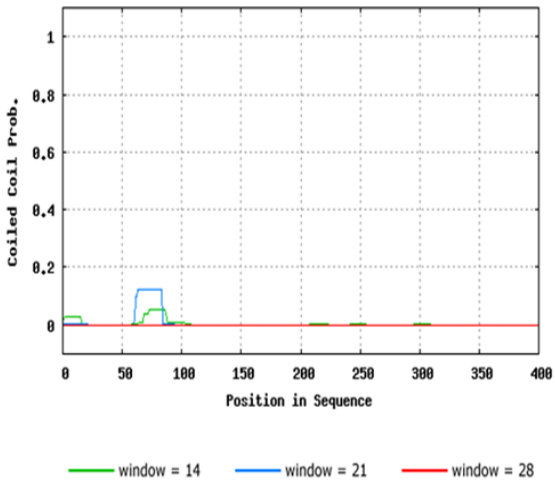
Appendix D: **Scanning electron micrographs of Δ*mepB2*, Δ*mepB3*, Δ*mepB2* Δ*mepB3* in comparison to mc^{2}155 and the complemented strains**. Scale bar: 500 nm. No significant changes in the surface of the cell wall of the mutant strains were observed.



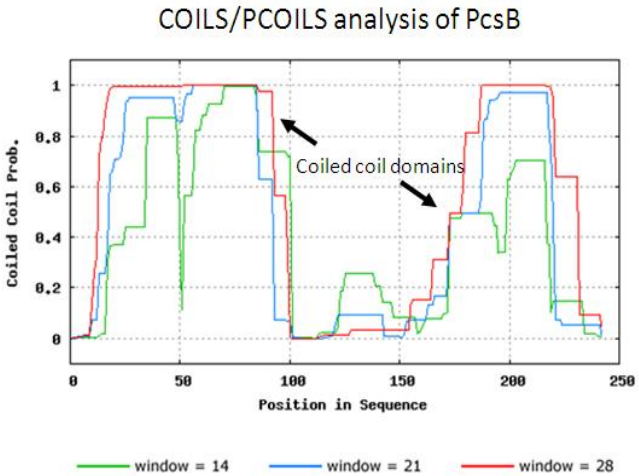
Appendix E: **Roche marker III (molecular weight marker used in this study).**

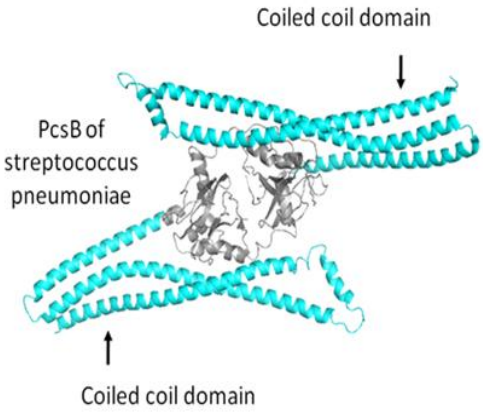


MepB2



MepB3





Appendix F: **COILS/PCOILS analysis of MepB2 and MepB3**. PcsB (PDB ID: 4CGK) which has been biochemically characterized was used as positive control. The coiled-coil domains of PcsB are indicated in cyan. Both MepB2 and MepB3 do not have the coiled-coil domain.

Table 4: **Primers used for screening for the Δ*mepB2::aadA* strain.**

Primer name	Sequence (5′-3′)
mepB2 Fwd	gtgggtaccctgatgaactgcgtgacga
mepB2 Rev	gtgggtacccagcgcggtttccaacttc
aadA Fwd	cccagcttctgtatggaacgg
aadA Rev	ttatttgccgactaccttggt

Table 5**:** **Primers used for PCR synthesis of the Δ*mepB3* allele.**

Primer name	Sequence (5′-3′)
mepB3 USF	gtgggtaccgtcggtgtagatgtggaacgt
mepB3 USR	gtgtctagacaccacgaagatcagcagtg
mepB3 DSF	gtgtctagagtgctcacgtttcctgcg
mepB3 DSR	gtggcggccgcatccacgatcgaggcaagc

Table 6: **Primers used for screening for the Δ*mepB2* strain.**

Primer name	Sequence (5′-3′)
mepB3 Fwd	catcaccaagcgaagagaacg
mepB3 Rev1	tggtcagcagcaactcgtag
mepB3 Rev2	ccagaattctcgaccagcaca

Table 7: **Primers used for PCR synthesis of the *mepB2* and *mepB3* alleles for gene complementation studies.**

Primer name	Sequence (5′-3′)
mepB2 Fwd	gtgtctagaggggtcacggtggcatac
mepB2 Rev	gtgaagcttcaccaccacacagaccagatc
mepB3 Fwd	gtgggtaccaagttgtgagctcggtgatgt
mepB3 Rev	gtgtctagaaaaactccacaaacgcctggg

Table 8: **Primers used for PCR synthesis of the *mepB2*, *mepB3* and *ftsX* alleles for protein interaction studies.**

Primer name	Sequence (5′-3′)
mepB2 Fwd	gtggaattctgtacaatgcgatatctgaccctc
mepB2 Rev	gtgaagctttgtacactagtcgctcgcatacgt
mepB3 Fwd	gtggaattctgtacaatggccgccatgacgcgg
mepB3 Rev	gtgaagctttgtacattaaccgtcagccgcagg
ftsX Fwd	gtgctgcaggtgcgcttcggctttctc
ftsX Rev	gtgaagcttctacctacgtacgtacag

6. References

ADAMS, D. W. & ERRINGTON, J. (2009) Bacterial cell division: assembly, maintenance and disassembly of the Z ring. *Nat Rev Microbiol,* 7**,** 642-53.

ALDRIDGE, B. B., KEREN, I. & FORTUNE, S. M. (2014) The spectrum of drug susceptibility in mycobacteria. *Microbiol Spectr,* 2.

AN, D. R., IM, H. N., JANG, J. Y., KIM, H. S., KIM, J., YOON, H. J., HESEK, D., LEE, M., MOBASHERY, S., KIM, S. J. & SUH, S. W. (2016) Structural basis of the heterodimer formation between cell shape-determining proteins Csd1 and Csd2 from *Helicobacter pylori*. *PLoS One,* 11**,** e0164243.

ANGALA, S. K., BELARDINELLI, J. M., HUC-CLAUSTRE, E., WHEAT, W. H. & JACKSON, M. (2014) The cell envelope glycoconjugates of *Mycobacterium tuberculosis*. *Crit Rev Biochem Mol Biol,* 49**,** 361-99.

BAMFORD, C. V., FRANCESCUTTI, T., CAMERON, C. E., JENKINSON, H. F. & DYMOCK, D. (2010) Characterization of a novel family of fibronectin-binding proteins with M23 peptidase domains from *Treponema denticola*. *Mol Oral Microbiol,* 25**,** 369-83.

BARANOWSKI, C. & RUBIN, E. J. (2016) Could killing bacterial subpopulations hit tuberculosis out of the park? *J Med Chem,* 59**,** 6025-6.

BARRY, C. E., 3RD, BOSHOFF, H. I., DARTOIS, V., DICK, T., EHRT, S., FLYNN, J., SCHNAPPINGER, D., WILKINSON, R. J. & YOUNG, D. (2009) The spectrum of latent tuberculosis: rethinking the biology and intervention strategies. *Nat Rev Microbiol,* 7**,** 845-55.

BATEMAN, A., BIRNEY, E., CERRUTI, L., DURBIN, R., ETWILLER, L., EDDY, S. R., GRIFFITHS-JONES, S., HOWE, K. L., MARSHALL, M. & SONNHAMMER, E. L. (2002) The Pfam protein families database. *Nucleic Acids Res,* 30**,** 276-80.

BENSEN, D., RODRIGUEZ, S., NIX, J., CUNNINGHAM, M. & TARI, L. (2012) Structure of MurA (UDP-N-acetylglucosamine enolpyruvyl transferase) from *Vibrio fischeri* in complex with substrate UDP-N-acetylglucosamine and the drug fosfomycin. *Acta Cryst Sec F: Struct Biol and Crystal Commun,* 68**,** 382-385.

BLAYLOCK, B., JIANG, X., RUBIO, A., MORAN, C. P., JR. & POGLIANO, K. (2004) Zipper-like interaction between proteins in adjacent daughter cells mediates protein localization. *Genes Dev,* 18**,** 2916-28.

BOCHTLER, M., ODINTSOV, S. G., MARCYJANIAK, M. & SABALA, I. (2004) Similar active sites in lysostaphins and D-Ala-D-Ala metallopeptidases. *Protein Sci,* 13**,** 854-61.

BONECA, I. G. (2005) The role of peptidoglycan in pathogenesis. *Curr Opin Microbiol,* 8**,** 46-53.

BONIS, M., ECOBICHON, C., GUADAGNINI, S., PREVOST, M. C. & BONECA, I. G. (2010) A M23B family metallopeptidase of *Helicobacter pylori* required for cell shape, pole formation and virulence. *Mol Microbiol,* 78**,** 809-19.

BOSHOFF, H. I. & BARRY, C. E. (2005) Tuberculosis-metabolism and respiration in the absence of growth. *Nat Rev Microbiol,* 3**,** 70-80.

BOTELLA, H., VAUBOURGEIX, J., LEE, M. H., SONG, N., XU, W., MAKINOSHIMA, H., GLICKMAN, M. S. & EHRT, S. (2017) Mycobacterium tuberculosis protease MarP activates a peptidoglycan hydrolase during acid stress. *The EMBO Journal***,** e201695028.

BOUTTE, C. C., BAER, C. E., PAPAVINASASUNDARAM, K., LIU, W., CHASE, M. R., MENICHE, X., FORTUNE, S. M., SASSETTI, C. M., IOERGER, T. R. & RUBIN, E. J. (2016) A cytoplasmic peptidoglycan amidase homologue controls mycobacterial cell wall synthesis. *Elife,* 5.

BROCKER, M., MACK, C. & BOTT, M. (2010) The response regulator MtrA of *Corynebacterium glutamicum*: target genes, consensus binding site and role of phosphorylation. *J of Bacteriol*.

BROSSIER, F., VEZIRIS, N., TRUFFOT-PERNOT, C., JARLIER, V. & SOUGAKOFF, W. (2011) Molecular investigation of resistance to the antituberculous drug ethionamide in multidrug-resistant clinical isolates of *Mycobacterium tuberculosis*. *Antimicrob agents and chemo,* 55**,** 355-360.

CABEEN, M. T. & JACOBS-WAGNER, C. (2005) Bacterial cell shape. *Nat Rev Microbiol,* 3**,** 601-10.

CAMERON, C. E., BROWN, E. L., KUROIWA, J. M., SCHNAPP, L. M. & BROUWER, N. L. (2004) *Treponema pallidum* fibronectin-binding proteins. *J Bacteriol,* 186**,** 7019-22.

CAMP, A. H. & LOSICK, R. (2008) A novel pathway of intercellular signalling in *Bacillus subtilis* involves a protein with similarity to a component of type III secretion channels. *Mol Microbiol,* 69**,** 402-17.

CELLINI, L. (2014) *Helicobacter pylori*: a chameleon-like approach to life. *World J Gastroenterol,* 20**,** 5575-82.

CHAO, M. C., KIESER, K. J., MINAMI, S., MAVRICI, D., ALDRIDGE, B. B., FORTUNE, S. M., ALBER, T. & RUBIN, E. J. (2013) Protein complexes and proteolytic activation of the cell wall hydrolase RipA regulate septal resolution in mycobacteria. *PLoS Pathog,* 9**,** e1003197.

COHEN, D. N., SHAM, Y. Y., HAUGSTAD, G. D., XIANG, Y., ROSSMANN, M. G., ANDERSON, D. L. & POPHAM, D. L. (2009) Shared catalysis in virus entry and bacterial cell wall depolymerization. *J Mol Biol,* 387**,** 607-18.

COSTA, K., BACHER, G., ALLMAIER, G., DOMINGUEZ-BELLO, M. G., ENGSTRAND, L., FALK, P., DE PEDRO, M. A. & GARCIA-DEL PORTILLO, F. (1999) The morphological transition of *Helicobacter pylori* cells from spiral to coccoid is preceded by a substantial modification of the cell wall. *J Bacteriol,* 181**,** 3710-5.

CRAWSHAW, A. D., SERRANO, M., STANLEY, W. A., HENRIQUES, A. O. & SALGADO, P. S. (2014) A mother cell-to-forespore channel: current understanding and future challenges. *FEMS Microbiol Lett,* 358**,** 129-36.

DARTOIS, V. (2014) The path of anti-tuberculosis drugs: from blood to lesions to mycobacterial cells. *Nat Rev Microbiol,* 12**,** 159-67.

DHAR, N. & MANINA, G. (2015) Single-cell analysis of mycobacteria using microfluidics and time-lapse microscopy. *Mycobacteria Protocols***,** 241-256.

DIACON, A. H., VAN DER MERWE, L., BARNARD, M., VON GROOTE-BIDLINGMAIER, F., LANGE, C., GARCÃA-BASTEIRO, A. L., SEVENE, E. A., BALLELL, L. & BARROS-AGUIRRE, D. (2016) B-lactams against tuberculosis-new trick for an old dog? *N Engl J of Med,* 375**,** 393-394.

DOMINGUEZ-GIL, T., LEE, M., ACEBRAN-AVALOS, I., MAHASENAN, K. V., HESEK, D., DIK, D. A., BYUN, B., LASTOCHKIN, E., FISHER, J. F. & MOBASHERY, S. (2016) Activation by allostery in cell-wall remodeling by a modular membrane-bound lytic transglycosylase from *Pseudomonas aeruginosa*. *Structure,* 24**,** 1729-1741.

DORR, T., CAVA, F., LAM, H., DAVIS, B. M. & WALDOR, M. K. (2013) Substrate specificity of an elongation-specific peptidoglycan endopeptidase and its implications for cell wall architecture and growth of *Vibrio cholerae*. *Mol Microbiol,* 89**,** 949-62.

DORR, T., DAVIS, B. M. & WALDOR, M. K. (2015) Endopeptidase-mediated beta lactam tolerance. *PLoS Pathog,* 11**,** e1004850.

DOWNING, K. J., MISCHENKO, V. V., SHLEEVA, M. O., YOUNG, D. I., YOUNG, M., KAPRELYANTS, A. S., APT, A. S. & MIZRAHI, V. (2005) Mutants of *Mycobacterium tuberculosis* lacking three of the five rpf-like genes are defective for growth *in vivo* and for resuscitation *in vitro*. *Infec and immun,* 73**,** 3038-3043.

ERCOLI, G., TANI, C., PEZZICOLI, A., VACCA, I., MARTINELLI, M., PECETTA, S., PETRACCA, R., RAPPUOLI, R., PIZZA, M., NORAIS, N., SORIANI, M. & ARICO, B. (2015) LytM proteins play a crucial role in cell separation, outer membrane composition, and pathogenesis in nontypeable *Haemophilus influenzae*. *MBio,* 6**,** e02575.

FAVROT, L. & RONNING, D. R. (2012) Targeting the mycobacterial envelope for tuberculosis drug development. *Expert Rev Anti Infect Ther,* 10**,** 1023-36.

FIRCZUK, M. & BOCHTLER, M. (2007) Folds and activities of peptidoglycan amidases. *FEMS Microbiol Rev,* 31**,** 676-91.

FORTUNE, S. M. & RUBIN, E. J. (2007) The complex relationship between mycobacteria and macrophages: it's not all bliss. *Cell Host Microbe,* 2**,** 5-6.

GALPERIN, M. Y., MEKHEDOV, S. L., PUIGBO, P., SMIRNOV, S., WOLF, Y. I. & RIGDEN, D. J. (2012) Genomic determinants of sporulation in Bacilli and Clostridia: towards the minimal set of sporulation-specific genes. *Environ Microbiol,* 14**,** 2870-90.

GOLD, B., SMITH, R., NGUYEN, Q., ROBERTS, J., LING, Y., LOPEZ QUEZADA, L., SOMERSAN, S., WARRIER, T., LITTLE, D., PINGLE, M., ZHANG, D., BALLINGER, E., ZIMMERMAN, M., DARTOIS, V., HANSON, P., MITSCHER, L. A., PORUBSKY, P., ROGERS, S., SCHOENEN, F. J., NATHAN, C. & AUBE, J. (2016) Novel cephalosporins selectively active on nonreplicating *Mycobacterium tuberculosis*. *J Med Chem,* 59**,** 6027-44.

GOLEY, E. D., COMOLLI, L. R., FERO, K. E., DOWNING, K. H. & SHAPIRO, L. (2010) DipM links peptidoglycan remodelling to outer membrane organization in *Caulobacter*. *Mol Microbiol,* 77**,** 56-73.

GORDHAN, B. G. & PARISH, T. (2001) Gene Replacement using Pretreated DNA. *Methods Mol Med,* 54**,** 77-92.

HEIDRICH, C., TEMPLIN, M. F., URSINUS, A., MERDANOVIC, M., BERGER, J., SCHWARZ, H., DE PEDRO, M. A. & HOLTJE, J. V. (2001) Involvement of N-acetylmuramyl-L-alanine amidases in cell separation and antibiotic-induced autolysis of *Escherichia coli*. *Mol Microbiol,* 41**,** 167-78.

HEIDRICH, C., URSINUS, A., BERGER, J., SCHWARZ, H. & HOLTJE, J. V. (2002) Effects of multiple deletions of murein hydrolases on viability, septum cleavage, and sensitivity to large toxic molecules in *Escherichia coli*. *J Bacteriol,* 184**,** 6093-9.

HETT, E. C., CHAO, M. C., DENG, L. L. & RUBIN, E. J. (2008) A mycobacterial enzyme essential for cell division synergizes with resuscitation-promoting factor. *PLoS Pathog,* 4**,** e1000001.

HETT, E. C., CHAO, M. C., STEYN, A. J., FORTUNE, S. M., DENG, L. L. & RUBIN, E. J. (2007) A partner for the resuscitation-promoting factors of *Mycobacterium tuberculosis*. *Mol Microbiol,* 66**,** 658-68.

HETT, E. C. & RUBIN, E. J. (2008) Bacterial growth and cell division: a mycobacterial perspective. *Microbiol Mol Biol Rev,* 72**,** 126-56.

HIGGINS, D. & DWORKIN, J. (2012) Recent progress in *Bacillus subtilis* sporulation. *FEMS Microbiol Rev,* 36**,** 131-48.

HOAGLAND, D. T., LIU, J., LEE, R. B. & LEE, R. E. (2016) New agents for the treatment of drug-resistant Mycobacterium tuberculosis. *Adv Drug Deliv Rev,* 102**,** 55-72.

HOLTJE, J. V. (1998) Growth of the stress-bearing and shape-maintaining murein sacculus of *Escherichia col*i. *Microbiol Mol Biol Rev,* 62**,** 181-203.

HORSBURGH, G. J., ATRIH, A. & FOSTER, S. J. (2003) Characterization of LytH, a differentiation-associated peptidoglycan hydrolase of *Bacillus subtilis* involved in endospore cortex maturation. *J Bacteriol,* 185**,** 3813-20.

HUANG, K. C., MUKHOPADHYAY, R., WEN, B., GITAI, Z. & WINGREEN, N. S. (2008) Cell shape and cell-wall organization in Gram-negative bacteria. *Proc Natl Acad Sci U S A,* 105**,** 19282-7.

HUGONNET, J. E., TREMBLAY, L. W., BOSHOFF, H. I., BARRY, C. E., 3RD & BLANCHARD, J. S. (2009) Meropenem-clavulanate is effective against extensively drug-resistant *Mycobacterium tuberculosis*. *Science,* 323**,** 1215-8.

JANKUTE, M., COX, J. A., HARRISON, J. & BESRA, G. S. (2015) Assembly of the Mycobacterial cell wall. *Annu Rev Microbiol,* 69**,** 405-23.

JERABEK-WILLEMSEN, M., WIENKEN, C. J., BRAUN, D., BAASKE, P. & DUHR, S. (2011) Molecular interaction studies using microscale thermophoresis. *Assay Drug Dev Technol,* 9**,** 342-53.

KANA, B. D., GORDHAN, B. G., DOWNING, K. J., SUNG, N., VOSTROKTUNOVA, G., MACHOWSKI, E. E., TSENOVA, L., YOUNG, M., KAPRELYANTS, A. & KAPLAN, G. (2008) The resuscitation promoting factors of *Mycobacterium tuberculosis* are required for virulence and resuscitation from dormancy but are collectively dispensable for growth *in vitro*. *Mol microbiol,* 67**,** 672-684.

KANA, B. D. & MIZRAHI, V. (2010) Resuscitation-promoting factors as lytic enzymes for bacterial growth and signaling. *FEMS Immunol Med Microbiol,* 58**,** 39-50.

KIESER, K. J., BARANOWSKI, C., CHAO, M. C., LONG, J. E., SASSETTI, C. M., WALDOR, M. K., SACCHETTINI, J. C., IOERGER, T. R. & RUBIN, E. J. (2015) Peptidoglycan synthesis in *Mycobacterium tuberculosis* is organized into networks with varying drug susceptibility. *Proc Natl Acad Sci U S A,* 112**,** 13087-92.

KIESER, K. J. & RUBIN, E. J. (2014) How sisters grow apart: mycobacterial growth and division. *Nat Rev Microbiol,* 12**,** 550-62.

KONDRATIEVA, T., RUBAKOVA, E., KANA, B. D., BIKETOV, S., POTAPOV, V., KAPRELYANTS, A. & APT, A. (2011) *Mycobacterium tuberculosis* attenuated by multiple deletions of rpf genes effectively protects mice against TB infection. *Tuberculosis,* 91**,** 219-223.

KOUL, A., ARNOULT, E., LOUNIS, N., GUILLEMONT, J. & ANDRIES, K. (2011) The challenge of new drug discovery for tuberculosis. *Nature,* 469**,** 483-90.

KUMAR, A., KUMAR, S., KUMAR, D., MISHRA, A., DEWANGAN, R. P., SHRIVASTAVA, P., RAMACHANDRAN, S. & TANEJA, B. (2013) The structure of Rv3717 reveals a novel amidase from *Mycobacterium tuberculosis*. *Acta Crystallogr D Biol Crystallogr,* 69**,** 2543-54.

LARROUY-MAUMUS, G., MARINO, L. B., MADDURI, A. V., RAGAN, T. J., HUNT, D. M., BASSANO, L., GUTIERREZ, M. G., MOODY, D. B., PAVAN, F. R. & DE CARVALHO, L. P. (2016) Cell-envelope remodeling as a determinant of phenotypic antibacterial tolerance in *Mycobacterium tuberculosis*. *ACS Infect Dis,* 2**,** 352-360.

LIENHARDT, C., GLAZIOU, P., UPLEKAR, M., LONNROTH, K., GETAHUN, H. & RAVIGLIONE, M. (2012) Global tuberculosis control: lessons learnt and future prospects. *Nat Rev Microbiol,* 10**,** 407-16.

LIN, Y., ZHU, N., HAN, Y., JIANG, J. & SI, S. (2014) Identification of anti-tuberculosis agents that target the cell-division protein FtsZ. *J Antibiot (Tokyo),* 67**,** 671-6.

LOCK, R. L. & HARRY, E. J. (2008) Cell-division inhibitors: new insights for future antibiotics. *Nat Rev Drug Discov,* 7**,** 324-38.

MACHOWSKI, E. E., SENZANI, S., EALAND, C. & KANA, B. D. (2014) Comparative genomics for mycobacterial peptidoglycan remodelling enzymes reveals extensive genetic multiplicity. *BMC Microbiol,* 14**,** 75.

MAITRA, A., BATES, S., SHAIK, M., EVANGELOPOULOS, D., ABUBAKAR, I., MCHUGH, T. D., LIPMAN, M. & BHAKTA, S. (2016) Repurposing drugs for treatment of tuberculosis: a role for non-steroidal anti-inflammatory drugs. *Br Med Bull,* 118**,** 138-48.

MARAKALALA, M. J., RAJU, R. M., SHARMA, K., ZHANG, Y. J., EUGENIN, E. A., PRIDEAUX, B., DAUDELIN, I. B., CHEN, P. Y., BOOTY, M. G., KIM, J. H., EUM, S. Y., VIA, L. E., BEHAR, S. M., BARRY, C. E., 3RD, MANN, M., DARTOIS, V. & RUBIN, E. J. (2016) Inflammatory signaling in human tuberculosis granulomas is spatially organized. *Nat Med,* 22**,** 531-8.

MARTINELLI, D. J. & PAVELKA, M. S., JR. (2016) The RipA and RipB peptidoglycan endopeptidases are individually nonessential to *Mycobacterium smegmatis*. *J Bacteriol,* 198**,** 1464-75.

MAVRICI, D., MARAKALALA, M. J., HOLTON, J. M., PRIGOZHIN, D. M., GEE, C. L., ZHANG, Y. J., RUBIN, E. J. & ALBER, T. (2014) *Mycobacterium tuberculosis* FtsX extracellular domain activates the peptidoglycan hydrolase, RipC. *Proc Natl Acad Sci U S A,* 111**,** 8037-42.

MCSHANE, H. (2011) Tuberculosis vaccines: beyond bacille Calmette-Guerin. *Philos Trans R Soc Lond B Biol Sci,* 366**,** 2782-9.

MEISNER, J., MAEHIGASHI, T., ANDRE, I., DUNHAM, C. M. & MORAN, C. P., JR. (2012) Structure of the basal components of a bacterial transporter. *Proc Natl Acad Sci U S A,* 109**,** 5446-51.

MEISNER, J., MONTERO LLOPIS, P., SHAM, L. T., GARNER, E., BERNHARDT, T. G. & RUDNER, D. Z. (2013) FtsEX is required for CwlO peptidoglycan hydrolase activity during cell wall elongation in *Bacillus subtilis*. *Mol microbiol,* 89**,** 1069-1083.

MEISNER, J. & MORAN, C. P., JR. (2011) A LytM domain dictates the localization of proteins to the mother cell-forespore interface during bacterial endospore formation. *J Bacteriol,* 193**,** 591-8.

MENICHE, X., OTTEN, R., SIEGRIST, M. S., BAER, C. E., MURPHY, K. C., BERTOZZI, C. R. & SASSETTI, C. M. (2014) Subpolar addition of new cell wall is directed by DivIVA in mycobacteria. *Proc Natl Acad Sci U S A,* 111**,** E3243-51.

MIYAGISHIMA, S. Y., KABEYA, Y., SUGITA, C., SUGITA, M. & FUJIWARA, T. (2014) DipM is required for peptidoglycan hydrolysis during chloroplast division. *BMC Plant Biol,* 14**,** 57.

MOLL, A., DORR, T., ALVAREZ, L., CHAO, M. C., DAVIS, B. M., CAVA, F. & WALDOR, M. K. (2014) Cell separation in *Vibrio cholerae* is mediated by a single amidase whose action is modulated by two nonredundant activators. *J Bacteriol,* 196**,** 3937-48.

MOLL, A., SCHLIMPERT, S., BRIEGEL, A., JENSEN, G. J. & THANBICHLER, M. (2010) DipM, a new factor required for peptidoglycan remodelling during cell division in *Caulobacter crescentus*. *Mol Microbiol,* 77**,** 90-107.

MUKHERJEE, P., SUREKA, K., DATTA, P., HOSSAIN, T., BARIK, S., DAS, K. P., KUNDU, M. & BASU, J. (2009) Novel role of Wag31 in protection of mycobacteria under oxidative stress. *Mol microbiol,* 73**,** 103-119.

MURPHY, K. C., PAPAVINASASUNDARAM, K. & SASSETTI, C. M. (2015) Mycobacterial recombineering. *Mycobacteria Protocols***,** 177-199.

PAI, M., BEHR, M. A., DOWDY, D., DHEDA, K., DIVANGAHI, M., BOEHME, C. C., GINSBERG, A., SWAMINATHAN, S., SPIGELMAN, M., GETAHUN, H.,

MENZIES, D. & RAVIGLIONE, M. (2016) Tuberculosis. *Nat Rev Dis Primers,* 2**,** 16076.

PAREDES-SABJA, D., SHEN, A. & SORG, J. A. (2014) *Clostridium difficile* spore biology: sporulation, germination, and spore structural proteins. *Trends Microbiol,* 22**,** 406-16.

PARISH, T. & STOKER, N. G. (2000) Use of a flexible cassette method to generate a double unmarked *Mycobacterium tuberculosis* tlyA plcABC mutant by gene replacement. *Microbiology,* 146 (Pt 8)**,** 1969-75.

PARTHASARATHY, G., LUN, S., GUO, H., AMMERMAN, N. C., GEIMAN, D. E. & BISHAI, W. R. (2012) Rv2190c, an NlpC/P60 family protein, is required for full virulence of *Mycobacterium tuberculosis*. *PLoS One,* 7**,** e43429.

PETERS, N. T., DINH, T. & BERNHARDT, T. G. (2011) A fail-safe mechanism in the septal ring assembly pathway generated by the sequential recruitment of cell separation amidases and their activators. *J Bacteriol,* 193**,** 4973-83.

PETERS, N. T., MORLOT, C., YANG, D. C., UEHARA, T., VERNET, T. & BERNHARDT, T. G. (2013) Structure-function analysis of the LytM domain of EnvC, an activator of cell wall remodelling at the *Escherichia coli* division site. *Mol Microbiol,* 89**,** 690-701.

PHAM, T. T., JACOBS-SERA, D., PEDULLA, M. L., HENDRIX, R. W. & HATFULL, G. F. (2007) Comparative genomic analysis of mycobacteriophage Tweety: evolutionary insights and construction of compatible site-specific integration vectors for mycobacteria. *Microbiology,* 153**,** 2711-23.

PRIDEAUX, B., VIA, L. E., ZIMMERMAN, M. D., EUM, S., SARATHY, J., O'BRIEN, P., CHEN, C., KAYA, F., WEINER, D. M. & CHEN, P.-Y. (2015) The association between sterilizing activity and drug distribution into tuberculosis lesions. *Nat Med,* 21**,** 1223-1227.

PRIYADARSHINI, R., DE PEDRO, M. A. & YOUNG, K. D. (2007) Role of peptidoglycan amidases in the development and morphology of the division septum in *Escherichia coli*. *J Bacteriol,* 189**,** 5334-47.

RAGUMANI, S., KUMARAN, D., BURLEY, S. K. & SWAMINATHAN, S. (2008) Crystal structure of a putative lysostaphin peptidase from *Vibrio cholerae*. *Proteins,* 72**,** 1096-103.

RAMAKRISHNAN, L. (2012) Revisiting the role of the granuloma in tuberculosis. *Nat Rev Immunol,* 12**,** 352-66.

RAVIGLIONE, M., MARAIS, B., FLOYD, K., LONNROTH, K., GETAHUN, H., MIGLIORI, G. B., HARRIES, A. D., NUNN, P., LIENHARDT, C., GRAHAM, S., CHAKAYA, J., WEYER, K., COLE, S., KAUFMANN, S. H. & ZUMLA, A. (2012) Scaling up interventions to achieve global tuberculosis control: progress and new developments. *Lancet,* 379**,** 1902-13.

RAVIGLIONE, M. C. (2008) Facing extensively drug-resistant tuberculosis--a hope and a challenge. *N Engl J Med,* 359**,** 636-8.

RAWLINGS, N. D., MORTON, F. R., KOK, C. Y., KONG, J. & BARRETT, A. J. (2008) MEROPS: the peptidase database. *Nucleic Acids Res,* 36**,** D320-5.

ROCABOY, M., HERMAN, R., SAUVAGE, E., REMAUT, H., MOONENS, K., TERRAK, M., CHARLIER, P. & KERFF, F. (2013) The crystal structure of the cell division amidase AmiC reveals the fold of the AMIN domain, a new peptidoglycan binding domain. *Mol Microbiol,* 90**,** 267-77.

RODRIGUES, C. D., MARQUIS, K. A., MEISNER, J. & RUDNER, D. Z. (2013) Peptidoglycan hydrolysis is required for assembly and activity of the transenvelope secretion complex during sporulation in *Bacillus subtilis*. *Mol Microbiol,* 89**,** 1039-52.

SACCHETTINI, J. C., RUBIN, E. J. & FREUNDLICH, J. S. (2008) Drugs versus bugs: in pursuit of the persistent predator *Mycobacterium tuberculosis*. *Nat Rev Microbiol,* 6**,** 41-52.

SENZANI, S., LI, D., BHASKAR, A., EALAND, C., CHANG, J., RIMAL, B., LIU, C., JOON, K. S., DHAR, N. & KANA, B. (2017) An Amidase_3 domain-containing N-acetylmuramyl-L-alanine amidase is required for mycobacterial cell division. *Scientific reports,* 7**,** 1140.

SERRANO, M., CRAWSHAW, A. D., DEMBEK, M., MONTEIRO, J. M., PEREIRA, F. C., DE PINHO, M. G., FAIRWEATHER, N. F., SALGADO, P. S. & HENRIQUES, A. O. (2015) The SpoIIQ-SpoIIIAH complex of *Clostridium difficile* controls forespore engulfment and late stages of gene expression and spore morphogenesis. *Mol Microbiol*.

SHAM, L.-T., JENSEN, K. R., BRUCE, K. E. & WINKLER, M. E. (2013) Involvement of FtsE ATPase and FtsX extracellular loops 1 and 2 in FtsEX-PcsB complex function in cell division of *Streptococcus pneumoniae* D39. *MBio,* 4**,** e00431-13.

SIEGRIST, M. S., WHITESIDE, S., JEWETT, J. C., ADITHAM, A., CAVA, F. & BERTOZZI, C. R. (2013) D-amino acid chemical reporters reveal peptidoglycan dynamics of an intracellular pathogen. *ACS chemical biology,* 8**,** 500-505.

SILHAVY, T. J., KAHNE, D. & WALKER, S. (2010) The bacterial cell envelope. *Cold Spring Harb Perspect Biol,* 2**,** a000414.

SINGH, A., MAI, D., KUMAR, A. & STEYN, A. J. (2006) Dissecting virulence pathways of *Mycobacterium tuberculosis* through protein-protein association. *Proc Natl Acad Sci U S A,* 103**,** 11346-51.

SINGH, S. K., PARVEEN, S., SAISREE, L. & REDDY, M. (2015) Regulated proteolysis of a cross-link-specific peptidoglycan hydrolase contributes to bacterial morphogenesis. *Proc Natl Acad Sci U S A,* 112**,** 10956-61.

SINGH, S. K., SAISREE, L., AMRUTHA, R. N. & REDDY, M. (2012) Three redundant murein endopeptidases catalyse an essential cleavage step in peptidoglycan synthesis of *Escherichia coli* K12. *Mol Microbiol,* 86**,** 1036-51.

SINGH, V., DHAR, N., PATO, J., KOLLY, G. S., KORDULAKOVA, J., FORBAK, M., EVANS, J. C., SZEKELY, R., RYBNIKER, J., PALCEKOVA, Z., ZEMANOVA, J., SANTI, I., SIGNORINO-GELO, F., RODRIGUES, L., VOCAT, A., COVARRUBIAS, A. S., RENGIFO, M. G., JOHNSSON, K., MOWBRAY, S., BUECHLER, J., DELORME, V., BRODIN, P., KNOTT, G. W., AINSA, J. A., WARNER, D. F., KERI, G., MIKUSOVA, K., MCKINNEY, J. D., COLE, S. T., MIZRAHI, V. & HARTKOORN, R. C. (2016) Identification of aminopyrimidine-sulfonamides as potent modulators of Wag31-mediated cell elongation in mycobacteria. *Mol Microbiol*.

SONI, V., UPADHAYAY, S., SURYADEVARA, P., SAMLA, G., SINGH, A., YOGEESWARI, P., SRIRAM, D. & NANDICOORI, V. K. (2015) Depletion of *Mycobacterium tuberculosis* GlmU from Infected Murine Lungs Effects the Clearance of the Pathogen. *PLoS Pathog,* 11**,** e1005235.

SPENCER, J., MURPHY, L. M., CONNERS, R., SESSIONS, R. B. & GAMBLIN, S. J. (2009) Crystal structure of the LasA virulence factor from *Pseudomonas aeruginosa*: substrate specificity and mechanism of M23 metallopeptidases. *J Mol Biol,* 396**,** 908-23.

SQUEGLIA, F., ROMANO, M., RUGGIERO, A., VITAGLIANO, L., DE SIMONE, A. & BERISIO, R. (2013) Carbohydrate recognition by RpfB from *Mycobacterium tuberculosis* unveiled by crystallographic and molecular dynamics analyses. *Biophysical Journal,* 104**,** 2530-2539.

STOHL, E. A., CHAN, Y. A., HACKETT, K. T., KOHLER, P. L., DILLARD, J. P. & SEIFERT, H. S. (2012) *Neisseria gonorrhoeae* virulence factor NG1686 is a bifunctional M23B family metallopeptidase that influences resistance to hydrogen peroxide and colony morphology. *J Biol Chem,* 287**,** 11222-33.

SULIS, G., ROGGI, A., MATTEELLI, A. & RAVIGLIONE, M. C. (2014) Tuberculosis: epidemiology and control. *Mediterr J Hematol Infect Dis,* 6**,** e2014070.

SYCURO, L. K., PINCUS, Z., GUTIERREZ, K. D., BIBOY, J., STERN, C. A., VOLLMER, W. & SALAMA, N. R. (2010) Peptidoglycan crosslinking relaxation promotes *Helicobacter pylori*'s helical shape and stomach colonization. *Cell,* 141**,** 822-33.

TIDHAR, A., FLASHNER, Y., COHEN, S., LEVI, Y., ZAUBERMAN, A., GUR, D., AFTALION, M., ELHANANY, E., ZVI, A., SHAFFERMAN, A. & MAMROUD, E. (2009) The NlpD lipoprotein is a novel *Yersinia pestis* virulence factor essential for the development of plague. *PLoS One,* 4**,** e7023.

TURNER, R. D., HURD, A. F., CADBY, A., HOBBS, J. K. & FOSTER, S. J. (2012) Cell wall elongation mode in Gram-negative bacteria is determined by peptidoglycan architecture. *Nat Commun,* 4**,** 1496.

UEHARA, T., DINH, T. & BERNHARDT, T. G. (2009) LytM-domain factors are required for daughter cell separation and rapid ampicillin-induced lysis in Escherichia coli. *J Bacteriol,* 191**,** 5094-107.

UEHARA, T., PARZYCH, K. R., DINH, T. & BERNHARDT, T. G. (2010) Daughter cell separation is controlled by cytokinetic ring-activated cell wall hydrolysis. *EMBO J,* 29**,** 1412-22.

UHIA, I., WILLIAMS, K. J., SHAHREZAEI, V. & ROBERTSON, B. D. (2015) Mycobacterial Growth. *Cold Spring Harb Perspect Med,* 5.

VAN KESSEL, J. C. & HATFULL, G. F. (2007) Recombineering in *Mycobacterium tuberculosis*. *Nat Methods,* 4**,** 147-52.

VOLLMER, W., JORIS, B., CHARLIER, P. & FOSTER, S. (2008) Bacterial peptidoglycan (murein) hydrolases. *FEMS Microbiol Rev,* 32**,** 259-86.

WADE, M. M. & ZHANG, Y. (2004) Mechanisms of drug resistance in Mycobacterium tuberculosis. *Front Biosci,* 9**,** 975-94.

WAKAMOTO, Y., DHAR, N., CHAIT, R., SCHNEIDER, K., SIGNORINO-GELO, F., LEIBLER, S. & MCKINNEY, J. D. (2013) Dynamic persistence of antibiotic-stressed mycobacteria. *Science,* 339**,** 91-5.

WHO (2015) Global tuberculosis report 2015.

WIVAGG, C. N., BHATTACHARYYA, R. P. & HUNG, D. T. (2014) Mechanisms of beta-lactam killing and resistance in the context of *Mycobacterium tuberculosis*. *J Antibiot (Tokyo),* 67**,** 645-54.

WIVAGG, C. N. & HUNG, D. T. (2012) Resuscitation-promoting factors are required for beta-lactam tolerance and the permeability barrier in *Mycobacterium tuberculosis*. *Antimicrob Agents and Chemotherapy,* 56**,** 1591-1594.

YAHASHIRI, A., JORGENSON, M. A. & WEISS, D. S. (2015) Bacterial SPOR domains are recruited to septal peptidoglycan by binding to glycan strands that lack stem peptides. *Proc Natl Acad Sci U S A,* 112**,** 11347-11352.

YAKHNINA, A. A., MCMANUS, H. R. & BERNHARDT, T. G. (2015) The cell wall amidase AmiB is essential for *Pseudomonas aeruginosa* cell division, drug resistance and viability. *Mol Microbiol,* 97**,** 957-73.

YANG, D. C., PETERS, N. T., PARZYCH, K. R., UEHARA, T., MARKOVSKI, M. & BERNHARDT, T. G. (2011) An ATP-binding cassette transporter-like complex governs cell-wall hydrolysis at the bacterial cytokinetic ring. *Proc Natl Acad Sci USA,* 108**,** E1052-60.

YANG, D. C., TAN, K., JOACHIMIAK, A. & BERNHARDT, T. G. (2012) A conformational switch controls cell wall-remodelling enzymes required for bacterial cell division. *Mol Microbiol,* 85**,** 768-81.

ZASTROW, M. L. & PECORARO, V. L. (2014) Designing hydrolytic zinc metalloenzymes. *Biochemistry,* 53**,** 957-78.

ZHANG, Y., HEYM, B., ALLEN, B., YOUNG, D. & COLE, S. (1992) The catalase-peroxidase gene and isoniazid resistance of *Mycobacterium tuberculosis*. *Nature,* 358**,** 591-3.

ZUMLA, A., KIM, P., MAEURER, M. & SCHITO, M. (2013a) Zero deaths from tuberculosis: progress, reality, and hope. *Lancet Infect Dis,* 13**,** 285-7.

ZUMLA, A., NAHID, P. & COLE, S. T. (2013b) Advances in the development of new tuberculosis drugs and treatment regimens. *Nat Rev Drug Discov,* 12**,** 388-404.

ZUMLA, A., RAVIGLIONE, M., HAFNER, R. & VON REYN, C. F. (2013c) Tuberculosis. *N Engl J Med,* 368**,** 745-55.